REPORT NO. DOT-TSC-FAA-72-7

THE ILS SCATTERING PROBLEM AND SIGNAL DETECTION MODEL

G. CHIN, L. JORDAN, D. KAHN
S. MORIN,
TRANSPORTATION SYSTEMS CENTER
55 BROADWAY
CAMBRIDGE, MA. 02142

FEBRUARY 1972
TECHNICAL REPORT

transpo 72
U.S. International Transportation Exposition
Dulles International Airport
Washington, D.C.
May 27-June 4, 1972

Prepared for:

DEPARTMENT OF TRANSPORTATION
FEDERAL AVIATION ADMINISTRATION
WASHINGTON, D.C. 20590

1. Report No.	2. Government Accession No.	3. Recipient's Catalog No.
DOT-TSC-FAA-72-7		

4. Title and Subtitle	5. Report Date
THE ILS SCATTERING PROBLEM AND SIGNAL DETECTION MODEL	February 1972
	6. Performing Organization Code
7. Author(s)	8. Performing Organization Report No.
G. Chin, L. Jordan, D. Kahn *	
9. Performing Organization Name and Address	10. Work Unit No.
Department of Transportation Transportation Systems Center 55 Broadway, Cambridge, MA. 02142	R 2103
	11. Contract or Grant No.
	FA207
	13. Type of Report and Period Covered
12. Sponsoring Agency Name and Address	Technical Report
Department of Transportation Federal Aviation Systems Washington, D.C. 20590	14. Sponsoring Agency Code

15. Supplementary Notes

*S. Morin

16. Abstract

The construction of a mathematical model of The Instrument Landing System (ILS) multipath problem has been undertaken. This report presents the theoratical basis for any such model, a critique of previous models and newly achieved developments in ILS model construction.

17. Key Words

ILS, scattering theory, current deviation indication, derogation, receiver model, Doppler Shift, DDM

19. Security Classif. (of this report)	20. Security Classif. (of this page)	21. No. of Pages	22. Price
Unclassified	Unclassified	105	

TABLE OF CONTENTS

LIST OF ILLUSTRATIONS

LIST OF ILLUSTRATIONS (CONTINUED)

LIST OF ILLUSTRATIONS (CONTINUED)

ACKNOWLEDGMENT

We gratefully acknowledge the important and invaluable research efforts of Dr. P. Yoh who contributed especially to our understanding of the Ohio University programs. We also gratefully acknowledge the help received from Mr. S. Lam and Mr. R. Silva who contributed their scientific talents to the success of this research effort. Finally, we would also like to thank Mr. A. Robb and Mr. D. Newsom for their excellent programming work on this project.

PREFACE

The use of a mathematical computer model to parametrically determine the effect of different antennas as well as the effect of hangers, terrain and other scattering objects on ILS performance is very appealing. A complete scenario of parametric variations can be written to have the computer output the derogation associated with each variation of building positions building heights, terrain irregularities and different types of antennas. Unfortunately, it is a good deal easier to write the scenario than it is to obtain realistic equations of ILS scattering on which the scenario must be based.

In studying previous attempts to develop such a math model we find a need to examine very carefully the theoretical foundation of the models. What began as a simple critique of existing models has in the process been expanded into a careful analysis of the electromagnetic theory on which the math model is based. Thus, in addition to a critique we present in this report a study of many of the underlying assumptions of the math model and how the scattering theory is to be integrated with the ILS signal detection system.

Our aim, then, in this first major report, is to lay the foundation, through an in depth study of the physics of the scattering problem, for the generation of a user oriented computer model which will be used by the FAA to predict ILS performance under a variety of conditions such as those listed in the first paragraph above.

SECTION 1. SUMMARY

In the first part of this report, the basic ILS scattering problem is investigated starting from first principles. Maxwell's equations are first formally integrated using the vector Green's theorem. The resulting integral equations express the electric and magnetic fields at an observation point P inside a volume V in terms of volume integrals over the charge and current distributions inside V and surface integrals of the electric and magnetic fields over the surfaces bounding V. The surface integrals represent contributions to the electromagnetic fields at P from radiation sources located outside of the volume V and are identically zero if there are no such external sources.

These integral equations are then applied to the general problem of electromagnetic scattering. The volume of integration V is made multiply connected with an interior and an exterior boundary. The source of the incident radiation (e.g., an ILS antenna) is located inside V while the scatterer is enclosed by the interior boundary of V. Consequently, the charge and current distributions which constitute the source of the incident radiation are the only radiation sources interior to V. Under the assumption that the perturbations in the current and charge distributions of the primary source due to the presence of the scatterer can be neglected (Approx. No. 1), the integral equations for the electric and magnetic fields at an interior point of V are applied. The electromagnetic fields are represented as sums of the incident fields produced by the primary source and the scattered fields produced by the induced currents and charges in the scatterer. It is shown that the scattered electric and magnetic fields at the observation point P can be represented as surface integrals of the scattered fields over the surface of the scatterer.

To obtain approximate solutions to these surface integral equations for the scattered fields at P, an iterative approach is adopted. Specifically, from a knowledge of the boundary conditions which must be satisfied at the surface of the scatterer, approximate functional relationships among the scattered fields and the known incident fields are developed and then substituted into the surface integral equations. The integrals, which are now expressed in terms of the known incident fields, are then evaluated to produce approximate expressions for the scattered fields at the observation point. The functional relationships among the scattered and incident fields at the surface of the scatterer are extremely complicated in the case of certain structures, for example, for hollow dielectric buildings with various internal structure, but very simple in the case of perfect conductors or buildings with

metal walls (or, to a good approximation, metal rod reinforced concrete walls). Because of the difficulties of pursuing the analysis further with non-metal structures and because typical airport scattering objects are well approximated by perfect conductors, we assume for this report, that the scattering objects are perfect conductors (Approx. No. 2).

Application of the boundary conditions for perfect conductors yields a relationship between the scattered magnetic field at the observation point and the surface integral over the scatterer of the tangential component of the total (incident plus scattered) magnetic field. To approximate the total magnetic field on the surface of the conducting scatterer, we first employ the principles of ray optics. Specifically, we assume as a first approximation that the total magnetic field is zero on the side of the scatterer not directly illuminated by the primary source (Approx. No. 3). This is a good approximation when diffraction effects may be considered as second order effects. Diffraction effects may safely be considered second order when the wavelength of the incident radiation is small compared with the dimensions of the scatterer. This is the case for scattering from hangers, however, it is not the case for scattering from aircraft where the localizer wavelength and fuselage radius are comparable. To treat this case, special care would have to be taken to check that diffraction remains small; for if it does not, Approximation Number 3 could not be made and an alternative method for relating incident and scattered fields would be needed.

Having assumed that the tangential component of the magnetic field is zero on the unilluminated portion of the scatterer, it is next necessary to specify it on the illuminated side. This is done by assuming plane wave reflection (Approx. No. 4). For distances generally encountered in the ILS problem this approximation is valid (unless the scatterer dimensions are comparable to the wavelength in which case, Approximations 3 and 4 will have to be modified).

Since we are interested in the values of the scattered fields in the far field of the scatterer (the approaching aircraft being between the outer marker and the far end of the runway), the integral equations for the fields may be expanded asymptotically for large values of the distance between scatterer and observer (Approx. No. 5); a similar far field approximation is made for the antenna to scatterer distance. The Fraunhoffer version of this approximation is used in this report though the Fresnel approximation which is more accurate (particularly so for the new very tall hanger structures) has been obtained and will be used in the computer program.

The application of the above approximations in the analysis leads to the final expressions shown in Section 2.4, APPROXIMATE SOLUTIONS TO THE INTEGRAL EQUATIONS OF SCATTERING THEORY, Equations (2.47) and (2.48) for the scattered electromagnetic field. These differ from those used by IBM but are basically the same as the Ohio University expressions. The differences between the theory presented here and IBM's are discussed in Sections 2.5 and 2.6, LOCALIZER SIGNAL SCATTERING and COMPARISON WITH PREVIOUS WORK, where the theory is carefully applied to localizer signal scattering by a rectangular wall. By means of this application of the theory to scattering from a rectangular wall, it is shown how our results reduce to Ohio's if certain additional approximations relating to reflections from the ground plane are made in our equations. The differences between our formulation of the scattering problem and the IBM formulation are of a fundamental nature. The practical consequences of these differences are shown in an accompanying graph in which the example used by IBM for scattering from a vertical rectangular wall is used and the predicted DDM's compared. It is shown that the differences may often be significant.

In addition to the analysis of rectangular wall scattering, we present (Appendix A) the new scattering formula for vertical triangles and show how to use these when the triangles are elevated as in the case of triangular roof structures and tail sections of aircraft. [We have also obtained a closed form solution to the slanted rectangular wall (not previously obtained in the IBM formulation) which should be useful for calculating reflection from hangers with slanted roofs]. We also present new closed form solutions for double reflection between two vertical walls, (Appendix B).

In Section 3, MODELING OF ILS SIGNAL DETECTION, we go from the scattering problem to the signal detection problem, in which we try to understand how the DDM must be defined in the presence of multipath, and to develop a reasonable model of the ILS signal detection system. It is felt that the IBM and Ohio University expressions for DDM are inadequate for strong multipath environments since their expressions are strictly valid only for single carrier signals when the relative phases of the received carrier and sidebands are the same. We, therefore, present a unified model of ILS signal reception which includes the dephasing of carrier and sideband signals, Doppler effects, different receiving antenna gain patterns and capture effect systems.

To do this, a general expression for the receiver input current is written down which includes the polarization and gain vector of the antenna (the gain vector for a small circular loop receiving antenna is derived in Appendix C). This

is used to help represent the amplified signal, which appears at the output of the IF stage of the receiver, in terms of the different transmitted modulation waveforms and the gains and phase delays associated with the different radiation paths. This IF signal is then passed to a second detector which generates an audio frequency signal which is passed through a set of filters to obtain the relative 90 Hz and 150 Hz amplitudes, from which the course deviation indication (CDI) may be determined.

Since the second detector (amplitude modulation detector) is a nonlinear device, its output reflects interactions between the intended ILS signal and the spurious signals received due to multipathing or due to transmission of a secondary carrier. In order to estimate the relative passage of this output through the selective 90 Hz and 150 Hz tone filters, Fourier analysis is used to express the detected audio signal in terms of discrete frequency components for which well defined transmissivities by each filter are assumed. The interaction between the course and clearance signals in the general case of a dual carrier frequency system gives rise to the much-utilized "capture effect". Advantage is taken of the large separation between the ILS signal modulation frequencies and the intercarrier beat (8kHz) to find an approximate linear expression for the total detected audio signal in terms of independent course and clearance audio signals.

The isolated course and clearance signals have the character of audio outputs from an AM detector generated by standard single carrier ILS signals, distorted by multipathing. For this single carrier case, a simple relation is found for the principal components of the detected audio signal lying within the passbands of the modulation frequency filters. The analysis in this case is valid in the approximation that the aggregate of interfering signals is somewhat weaker than the direct carrier signal - a reasonable condition for any marginally flyable course.

Doppler modifications of detected signals arise as a consequence of the variation of multipath phase delays which is implicit with the motion of an airborne receiver. In the approximation stated immediately above, each received component of multipath interference may be characterized by the relative Doppler shift of its carrier to the direct path carrier. Sum and difference combinations of modulation and Doppler frequencies can under certain circumstances give net frequencies near the filter center frequencies resulting in possible false signals being passed by the 90 Hz or 150 Hz filters. With the aircraft approach speeds used today, the Doppler may, for example, increase the 90 Hz signal to the

point where it passes through the 150 Hz filter, or it may increase the 150 Hz to the extent that it is excluded from the 150 Hz filter. These possibilities are investigated by studying the frequency response of a narrowband modulation filter and calculating all significant contributions in each filter output. Thus, values are obtained for the two detected modulation amplitudes from which the apparent DDM and CDI are conventionally determined. As a practical matter, it appears that the Doppler contributions to signal derogation cannot be neglected for aircraft speeds in the vicinity of 200 feet/sec. and filter bandwidths around 15 cps.

Thus the new model is capable of calculating the detected audio frequency signal, including Doppler and capture effects, in the presence of any moderately strong multipath interference. It may therefore be applied to determination of the apparent CDI for any conventional localizer or glide slope system.

Possible depolarization of the electromagnetic field also had to be investigated. This was done and we found (Appendix D) that for omni-directional antennas the original horizontal polarization of the electric field vector is retained, though the magnetic field vector does undergo a small amount of depolarization. However, for dipole antennas, we find depolarization in both the magnetic and electric field vectors which, for some orientations, cannot be neglected (this is of particular importance for the glide slope system).

Finally, in Appendix E we append some additional comments on previous ILS modelling. These include comments on the Ohio University expression for DDM which assumed no scattered carrier signal and assumed that both the direct and scattered fields have identical polarization and phase. We also comment briefly on IBM's use of diffraction theory (Appendix E) and on a shortcoming of their experimental verification program (Appendix E).

SECTION 2. THE ILS SCATTERING PROBLEM

2.1 INTRODUCTION

Electromagnetic scattering is one of the most important and most complex topics in classical mathematical physics. Basically, the problem is to determine the field perturbations (scattered fields) which result when various obstacles (the scatterers) are placed in known (incident) electromagnetic fields. To solve a given scattering problem, one attempts to find a solution of Maxwell's equations which has the property that when it is added to the known or incident electromagnetic field the resulting total field satisfies the appropriate boundary conditions at the surfaces of the scattering obstacles. Unfortunately, exact solutions to scattering problems have been obtained in only a limited number of cases. In this report, integral equations for the scattered fields will be developed by directly integrating the electromagnetic field equations. Approximate solutions to these integral equations for the case of perfectly conducting scatterers will then be applied to investigate localizer signal scattering by a flat, vertical wall. Comparisons will be made with previous work.

2.2 INTEGRATION OF MAXWELL's EQUATIONS

Maxwell's equations in M.K.S. units for a homogeneous, isotropic medium with permittivity ε and permeability μ are given below.

$$\vec{\nabla} \times \vec{E} = i\omega\mu\vec{H} \tag{2.1}$$

$$\vec{\nabla} \times \vec{H} = \vec{J} - i\omega\varepsilon\vec{E} \tag{2.2}$$

$$\vec{\nabla} \cdot \vec{H} = 0 \tag{2.3}$$

$$\vec{\nabla} \cdot \vec{E} = \rho/\varepsilon \tag{2.4}$$

In Equations (2.1) through (2.4), it has been assumed that all fields vary harmonically in time as $e^{-i\omega t}$. The quantities $\vec{E}$, $\vec{H}$, $\vec{J}$, and ρ are, respectively, the electric field, the magnetic field, the current distribution, and the charge distribution. Taking the curls of Equations (2.1) and (2.2) we find that $\vec{E}$ and $\vec{H}$ satisfy the following field equations:

$$\vec{\nabla} \times (\vec{\nabla}\times\vec{E}) - k^2\vec{E} = i\omega\mu\vec{J} \quad , \tag{2.5}$$

$$\vec{\nabla} \times (\vec{\nabla}\times\vec{H}) - k^2\vec{H} = \vec{\nabla}\times\vec{J} \quad , \tag{2.6}$$

where $k^2 = \omega^2 \varepsilon\mu$.

Let V be a closed volume in the medium bounded by a regular surface S. Let $\vec{Q}$ and $\vec{P}$ be vector fields defined at each point in the medium. The vector Green's theorem for $\vec{P}$ and $\vec{Q}$ has the following form:

$$\int_V (\vec{Q}\cdot\vec{\nabla}\times\vec{\nabla}\times\vec{P} - \vec{P}\cdot\vec{\nabla}\times\vec{\nabla}\times\vec{Q})\,dv$$

$$= \int_S (\vec{P}\times\vec{\nabla}\times\vec{Q} - \vec{Q}\times\vec{\nabla}\times\vec{P})\cdot\hat{n}\,ds \quad , \tag{2.7}$$

where $\hat{n}$ is the unit normal to the surface S and is directed outward from the volume V.

The integral identity given by Equation (2.7) can be used to directly integrate the field Equations (2.5) and (2.6). To begin with, we define the function $\Psi(\vec{r}',\vec{r})$ as follows:

$$\Psi(\vec{r}',\vec{r}) = \frac{e^{ik|\vec{r}'-\vec{r}|}}{|\vec{r}'-\vec{r}|} \quad . \tag{2.8}$$

The two point function Ψ is just the Green's function of the Helmholtz equation. That is to say, Ψ satisfies the equation

$$(\nabla^2+k^2)\Psi = -4\pi\delta(\vec{r}'-\vec{r}) \quad , \tag{2.9}$$

where $\delta(\vec{r}'-\vec{r})$ is the Dirac delta function. The vector $\vec{r}'$ can be thought of as the position vector relative to some origin 0 of an observation point P inside V while $\vec{r}$ is the position vector relative to the origin of any source point in V or on S. Following Stratton,[1] we first define the vectors $\vec{P}$ and $\vec{Q}$ appearing in Equation (2.7) as follows:

$$\vec{P} = \vec{E}(\vec{r}) \qquad \vec{Q} = \hat{a}\,\Psi(\vec{r}',\vec{r}) \tag{2.10}$$

where $\hat{a}$ is a unit vector in some arbitrary, fixed direction. Referring to Equations (2.5), (2.9), and (2.10), the following vector relations hold:

$$\vec{\nabla}x\vec{Q} = \vec{\nabla}\Psi x\hat{a}$$

$$\vec{\nabla}x(\vec{\nabla}x\vec{Q}) = +\hat{a}k^2\psi + 4\pi\hat{a}\,\delta(\vec{r}'-\vec{r}) + \vec{\nabla}(\hat{a}\cdot\vec{\nabla}\Psi) \qquad (2.11)$$

$$\vec{\nabla}x(\vec{\nabla}x\vec{P}) = k^2\vec{E} + i\omega\mu\vec{J}$$

Substituting these various expressions into the integral relation (2.7) and integrating with respect to the unprimed source coordinates, we obtain after a few trivial vector manipulations the following expression for $\vec{E}(\vec{r}')$.

$$\vec{E}(\vec{r}') = \frac{1}{4\pi}\int_V (i\omega\mu\vec{J}\Psi + \frac{1}{\epsilon}\rho\vec{\nabla}\Psi)\,dv \qquad (2.12)$$
$$-\frac{1}{4\pi}\int_S \left[i\omega\mu(\hat{n}x\vec{H})\Psi + (\hat{n}x\vec{E})x\vec{\nabla}\Psi + (\hat{n}\cdot\vec{E})\vec{\nabla}\Psi\right]ds$$

The unit vector $\hat{a}$ has been dropped from (2.12) since its orientation is arbitrary and it would simply scalar multiply both sides of (2.12). Repeating this analysis with $\vec{P}$ defined as $\vec{H}(\vec{r})$, the following expression for $\vec{H}(\vec{r}')$ is obtained:

$$\vec{H}(\vec{r}') = \frac{1}{4\pi}\int_V (\vec{J}x\vec{\nabla}\Psi)\,dv \qquad (2.13)$$
$$+\frac{1}{4\pi}\int_S \left[i\omega\vec{\epsilon}(\hat{n}x\vec{E})\Psi - (\hat{n}x\vec{H})x\vec{\nabla}\Psi - (\hat{n}\cdot\vec{H})\vec{\nabla}\Psi\right]ds$$

Equations (2.12) and (2.13) express the electric and magnetic field intensities at any point P inside the volume V in terms of volume integrals over the charges and currents inside V and surface integrals of the fields over the bounding surface S. The surface integrals represent the contributions to $\vec{E}$ and $\vec{H}$ from sources located outside V. These two equations will be the basis for our treatment of electromagnetic scattering.

2.3 INTEGRAL EQUATIONS IN THE THEORY OF ELECTROMAGNETIC SCATTERING

To begin our discussion of electromagnetic scattering, consider the geometry depicted in Figure 1. Figure 1 depicts a multiply connected volume V containing a localized source of electromagnetic radiation which occupies a volume V_i in V. This source might, for example, be a glide slope or localizer antenna. The charge and current distributions within V_i will be denoted by ρ_i and $\vec{J}_i$ respectively. Elsewhere in V, $\vec{J}$ and ρ are assumed to be identically zero. Note that the volume V is bounded by an interior boundary surface S_1 and an outer boundary surface S_o. The volume V_1 bounded by S_1 is not included in V. The volume V consists of the region bounded by S_o, excluding the interior of S_1. To apply Equations (2.12)

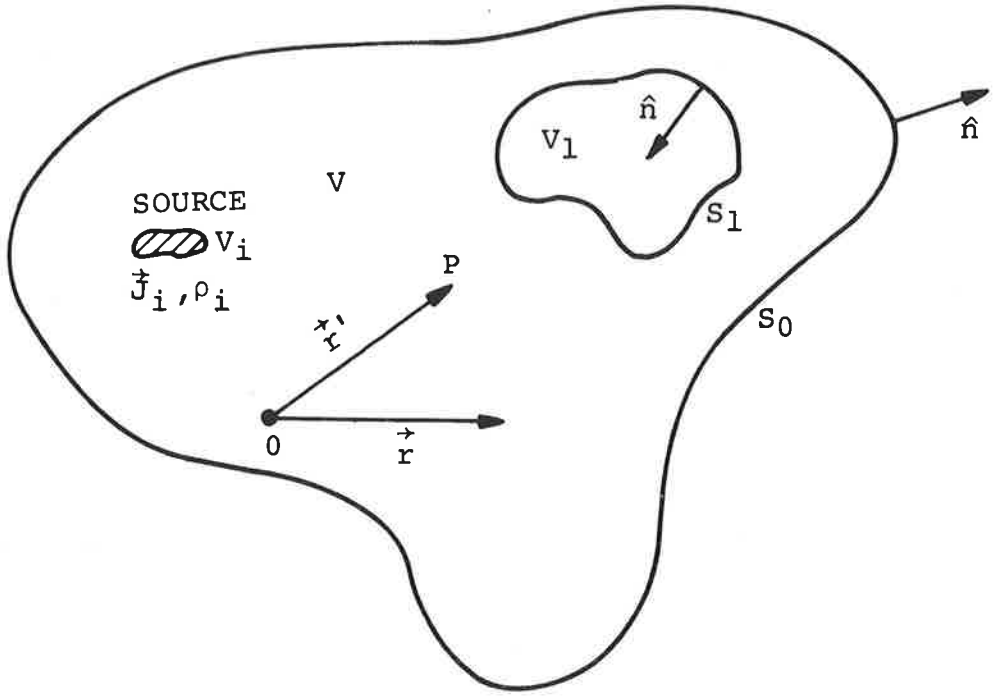

Figure 2.1 - Multiply Connected Region Containing Source

and (2.13) to such a multiply connected region, the surface integrals must be carried out over both bounding surfaces.

Let us assume that the source occupying the volume V_i in V is the only source of radiation. Let $\vec{E}_i(\vec{r})$ and $\vec{H}_i(\vec{r})$ denote, respectively, the electric and magnetic field intensities produced by this source. The subscript "i" is used to denote incident field. The values of $\vec{E}_i$ and $\vec{H}_i$ at a point P inside V are given by the following equations (Eqs. (2.12) and (2.13).

$$\vec{E}_i(\vec{r}') = \frac{1}{4\pi}\int_{V_i}(i\omega\mu\vec{J}_i\psi + \frac{1}{\varepsilon}\rho_i\vec{\nabla}\psi)dv$$

$$- \frac{1}{4\pi}\sum_{j=o}^{1}\int_{S_j}\left[i\omega\mu(\hat{n}x\vec{H}_i)\psi + (\hat{n}x\vec{E}_i)x\vec{\nabla}\psi + (\hat{n}\cdot\vec{E}_i)\vec{\nabla}\psi\right]ds \quad (2.14)$$

and

$$\vec{H}_i(\vec{r}') = \frac{1}{4\pi}\int_{V_i} (\vec{J}_i \times \vec{\nabla}\psi)\, dv$$

$$+ \quad \frac{1}{4\pi}\sum_{j=o}^{1} \int_{S_j}\left[i\omega\epsilon(\hat{n}\times\vec{E}_i)\psi - (\hat{n}\times\vec{H}_i)\times\vec{\nabla}\psi - (\hat{n}\cdot\vec{H}_i)\vec{\nabla}\psi\right] ds. \qquad (2.15)$$

Note that in Equations (2.14) and (2.15), the volume integrals are extended only over the volume V_i occupied by the localized source since $\vec{J}$ and ρ are zero elsewhere in V. Note also that each equation contains two surface integrals because of the two surfaces which bound V.

Equations (2.14) and (2.15) represent solutions to the field Equations (2.5) and (2.6) for the electric and magnetic field distributions inside the multiply connected region due to the localized source occupying the volume V_i in V depicted in Figure 2.1. Since this localized source is assumed to be the only source of radiation in the universe, the surface integrals appearing in Equations (2.14) and (2.15) are in fact identically zero. To see that this must be so, consider first the surface integrals, in Equations (2.14) and (2.15) of $\vec{E}_i$ and $\vec{H}_i$ over the interior boundary S_1. Since S_1 encloses no sources ($\vec{J} \equiv 0$ and $\rho \equiv 0$ in V_1), we can contract the surface S_1 down to a new boundary surface $\bar{S}_1$ which is enclosed by S_1 without adding any new charges or currents to the volume of integration. Consequently, the only changes in Equations (2.14) and (2.15) which result from shrinking S_1 down to $\bar{S}_1$ is that the surface integrals of $\vec{E}_i$ and $\vec{H}_i$ over S_1 are now carried out over $\bar{S}_1$. Since the electric and magnetic field intensities at P do not change as a result of this contraction, we must conclude that the surface integrals over $\bar{S}_1$ equal the corresponding surface integrals over S_1. But, the values of the surface integrals in (2.14) and (2.15) of $\vec{E}_i$ and $\vec{H}_i$ over $\bar{S}_1$ can be made arbitrarily small by simply allowing the surface area of $\bar{S}_1$ to go to zero. Consequently, we can conclude that the surface integrals of $\vec{E}_i$ and $\vec{H}_i$ over S_1 appearing in Equations (2.14) and (2.15) are identically zero. That is to say,

$$\int_{S_1}\left[i\omega\mu(\hat{n}\times\vec{H}_i)\psi + (\hat{n}\times\vec{E}_i)\times\vec{\nabla}\psi + (\hat{n}\cdot\vec{E}_i)\vec{\nabla}\psi\right] ds \equiv 0 \qquad (2.16)$$

and

$$\int_{S_1}\left[i\omega\varepsilon\,(\hat{n}\times\vec{E}_i)\psi-(\hat{n}\times\vec{H}_i)\times\vec{\nabla}\psi-(\hat{n}\cdot H_i)\vec{\nabla}\psi\right]ds \equiv 0 \qquad (2.17)$$

A similar argument can be made regarding the surface integrals of $\vec{E}_i$ and $\vec{H}_i$ over the outer boundary S_o. Since no new sources of radiation are added to the volume of integration by expanding S_o to some new surface $\bar{S}_o$ ($\vec{J}\equiv o$ and $\rho\equiv o$ outside S_o); the surface integrals over $\bar{S}_o$ must equal the corresponding integrals over S_o. But if the surface $\bar{S}_o$ is allowed to recede to infinity, the surface integrals over $\bar{S}_o$ go to zero because of the following asymptotic properties of electromagnetic fields produced by localized sources.[1,2]

$$\left.\begin{aligned}&\lim_{r\to\infty} r\vec{E} \text{ is finite}\\ &\lim_{r\to\infty} r\left[(\hat{r}\times\vec{H})+\left(\frac{\varepsilon}{\mu}\right)^{1/2}\vec{E}\right]=0\end{aligned}\right\}. \qquad (2.18)$$

$$\left.\begin{aligned}&\lim_{r\to\infty} r\vec{H} \text{ is finite}\\ &\lim_{r\to\infty} r\left[\left(\frac{\varepsilon}{\mu}\right)^{1/2}(\hat{r}\times\vec{E})-\vec{H}\right]=0\end{aligned}\right\}. \qquad (2.19)$$

where $\hat{r}=\vec{r}/r$ is a unit vector in the direction of $\vec{r}$. Consequently, we can conclude that the surface integrals of $\vec{E}_i$ and $\vec{H}_i$ over S_o appearing in Equations (2.14) and (2.15) are identically zero. That is to say,

$$\int_{S_o} i\omega\mu\,(\hat{n}\times\vec{H}_i)\psi+(\hat{n}\times\vec{E}_i)\times\vec{\nabla}\psi+(\hat{n}\cdot\vec{E}_i)\vec{\nabla}\psi\;ds\equiv 0, \qquad (2.20)$$

and

$$\int_{S_o}\left[i\omega\varepsilon\,(\hat{n}\times\vec{E}_i)\psi-(\hat{n}\times\vec{H}_i)\times\vec{\nabla}\psi-(\hat{n}\cdot\vec{H}_i)\vec{\nabla}\psi\right]ds\equiv 0. \qquad (2.21)$$

Substituting Equations (2.16), (2.17), (2.20) and (2.21) into Equations (2.14) and (2.15), we obtain the following expressions for $\vec{E}_i(\vec{r}')$ and $\vec{H}_i(\vec{r}')$:

$$\vec{E}_i(\vec{r}') = \frac{1}{4\pi}\int_{V_i}(i\omega\mu\vec{J}_i\psi+\frac{1}{\varepsilon}\rho_i\vec{\nabla}\psi)\,dv, \qquad (2.22)$$

$$\vec{H}_i(\vec{r}') = \frac{1}{4\pi} \int_{V_i} (\vec{J}_i x \vec{\nabla}\Psi) dv \quad . \qquad (2.23)$$

Equations (2.22) and (2.23) are the familiar expressions for the electric and magnetic field intensities produced by localized sources of radiation in the absence of boundaries.

Suppose now that a scattering object is placed inside the interior boundary S_1. The situation is depicted in Figure 2.2.

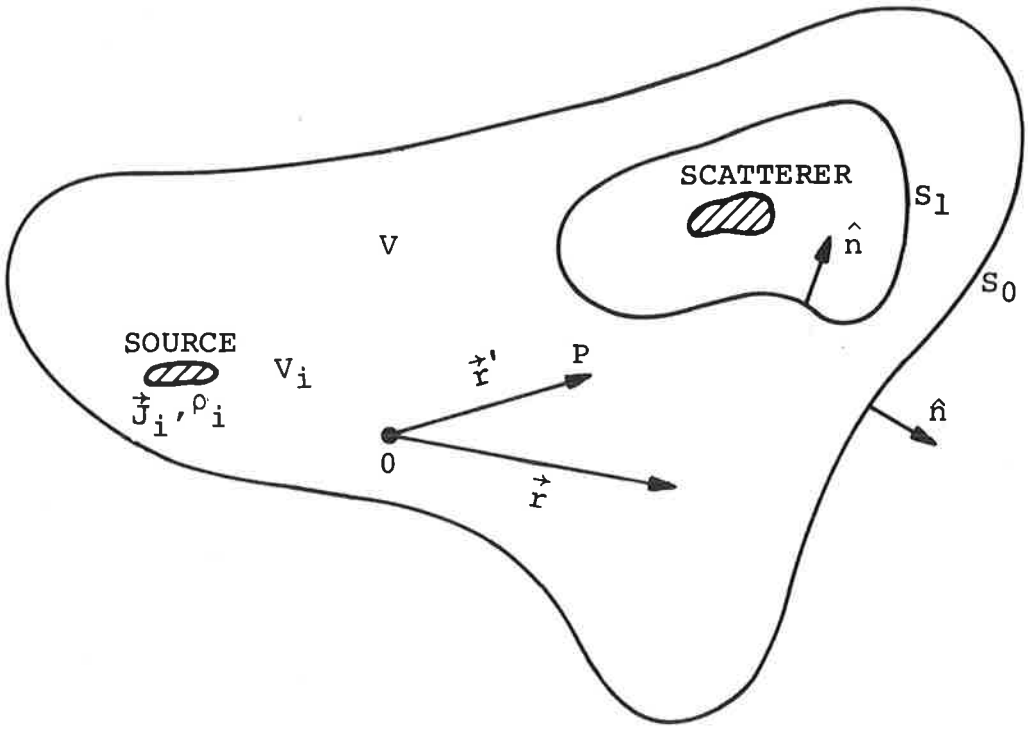

Figure 2.2 - Geometry Illustrating the Arrangement of Source and Scatterer

The scatterer could be composed of a conducting or dielectric material or a combination of the two. Charges and currents will be induced in the scatterer by the incident fields $\vec{E}_i$ and $\vec{H}_i$ generated by the primary source of radiation occupying the volume V_i in V. These secondary sources will in turn radiate electromagnetic waves. Let $\vec{E}_s(\vec{r})$ and $\vec{H}_s(\vec{r})$ denote, respectively, the electric and magnetic fields generated by the charges and currents induced in the scatterer. The subscript "s" is used to denote scattered field. The total electric and magnetic fields can be represented as follows:

$$\vec{E}(\vec{r}) = \vec{E}_i(\vec{r}) + \vec{E}_s(\vec{r})$$
$$\vec{H}(\vec{r}) = \vec{H}_i(\vec{r}) + \vec{H}_s(\vec{r}) \qquad (2.24)$$

The scattered fields $\vec{E}_s$ and $\vec{H}_s$ will of course exert forces on the charges and currents of the primary source. As a result, the charge distribution ρ_i and the current distribution $\vec{J}_i$ will assume new values which we will denote by ρ_i' and $\vec{J}_i'$ respectively. However, we will assume that the perturbations of $\vec{J}_i$ and ρ_i due to the presence of the scatterer are second order effects and that they can be ignored. That is to say, we will assume that

$$\vec{J}_i' = \vec{J}_i$$
$$\rho_i' = \rho_i \qquad (2.25)$$

These approximations should be very good for scatterers in the far field of the primary radiator.[2]

To calculate the total electric and magnetic fields at a point P inside V, we simply apply Equations (2.12) and (2.13). For example the electric field is given by

$$\vec{E}(\vec{r}') = \frac{1}{4\pi}\int_{V_i}\left(i\omega\mu\vec{J}_i\psi + \frac{1}{\epsilon}\rho_i\vec{\nabla}\psi\right)dv$$

$$-\frac{1}{4\pi}\sum_{j=o}^{1}\int_{S_j} i\omega\mu(\hat{n}\times\vec{H})\psi + (\hat{n}\times\vec{E})\times\vec{\nabla}\psi + (\hat{n}\cdot\vec{E})\vec{\nabla}\psi\, ds \qquad (2.26)$$

where $\vec{E} = \vec{E}_i + \vec{E}_s$ and $\vec{H} = \vec{H}_i + \vec{H}_s$ (Eq. (2.24)). Notice that the localized source occupying the volume V_i is still the only source of radiation inside V since the scatterer lies in the volume V_1 bounded by S_1 and this region is excluded from V. Notice also that we have made use of the approximation (2.25). According to Equation (2.22), the volume integral appearing in Equation (2.26) equals $\vec{E}_i(\vec{r}')$. Consequently, since $\vec{E} = \vec{E}_i + \vec{E}_s$, the scattered electric field at P is given by

$$\vec{E}_s(\vec{r}') = -\frac{1}{4\pi}\sum_{j=o}^{1}\int_{S_j}\left[i\omega\mu(\hat{n}\times\vec{H}_i)\psi + (\hat{n}\times\vec{E}_i)\times\vec{\nabla}\psi + (\hat{n}\cdot\vec{E}_i)\vec{\nabla}\psi\right]ds$$

$$-\frac{1}{4\pi}\sum_{j=o}^{1}\int_{S_j}\left[i\omega\mu(\hat{n}\times\vec{H}_s)\psi + (\hat{n}\times\vec{E}_s)\times\vec{\nabla}\psi + (\hat{n}\cdot\vec{E}_s)\vec{\nabla}\psi\right]ds \qquad (2.27)$$

where we have made use of Equation (2.24) and have separated the surface integrals involving the incident and scattered fields. But the integrals of $\vec{E}_i$ and $\vec{H}_i$ over the surfaces S_o and S_1 have already been shown to be identically zero (Eqs. (2.16) and (2.20)). Furthermore, if the surface S_o is allowed to recede to infinity, the surface integral over S_o of the scattered fields will go to zero since $\vec{E}_s$ and $\vec{H}_s$ have the same asymptotic properties as $\vec{E}_i$ and $\vec{H}_i$ (Eqs. (2.18) and (2.19)). Consequently, we finally arrive at the following expression for $\vec{E}_s(\vec{r}')$:

$$\vec{E}_s(\vec{r}') = -\frac{1}{4\pi}\int_{S_1}\left[i\omega\mu(\hat{n}\times\vec{H}_s)\psi+(\hat{n}\times\vec{E}_s)\times\vec{\nabla}\psi+(\hat{n}\cdot\vec{E}_s)\vec{\nabla}\psi\right]ds \tag{2.28}$$

Since the surface S_o has been allowed to recede to infinity, Equation (2.28) is valid for any point P lying outside the surface S_1. The analogous expression for $\vec{H}_s(\vec{r}')$ is

$$\vec{H}_s(\vec{r}') = \frac{1}{4\pi}\int_{S_1}\left[i\omega\varepsilon(\hat{n}\times\vec{E}_s)\psi-(\hat{n}\times\vec{H}_s)\times\vec{\nabla}\psi-(\hat{n}\cdot\vec{H}_s)\vec{\nabla}\psi\right]ds. \tag{2.29}$$

In fact, the surface S_1 can be collapsed down onto the surface of the scatterer itself so that Equations (2.28) and (2.29) become valid for all points P outside the body of the scatterer. This situation is depicted below.

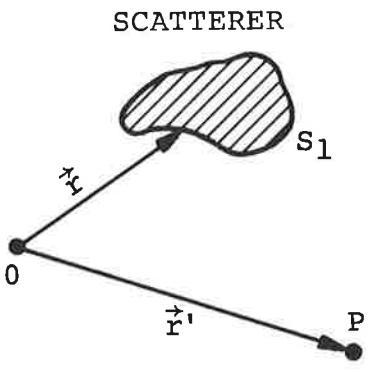

Figure 2.3. Collapsing Surface S_1 onto Scatterer

Henceforth then, it will be understood that the surface S_1 is the actual surface of the scatterer. The unit normal $\hat{n}$ which appears in Equations (2.28) and (2.29) points into the body of the scatterer.

The integral Equations (2.28) and (2.29) express the scattered electromagnetic fields at an observation point P in terms of integrals of the

scattered fields over the surface of the scatterer. These equations represent first order solutions to the scattering problem in that they are based upon the approximation that the charge and current distributions of the primary source are not changed by the fields generated by the scatterer (Equation (2.25)). In the next section, useful approximate solutions to Equations (2.28) and (2.29) will be developed for the case of perfectly conducting scatterers.

2.4 APPROXIMATE SOLUTIONS TO THE INTEGRAL EQUATIONS OF SCATTERING THEORY

Approximate solutions to the integral Equations (2.28) and (2.29) can be obtained by using interative methods. Specifically, from a knowledge of the boundary conditions which must be satisfied on the surface of the scatterer S_1, approximate functional relationships among $\vec{E}_s$ and $\vec{H}_s$ on S_1 and the known incident fields $\vec{E}_i$ and $\vec{H}_i$ on S_1 are developed and then substituted into the integrals in Equations (2.28) and (2.29). The integrals are then evaluated to produce approximate expressions for $\vec{E}_s$ and $\vec{H}_s$ at an observation point P. This procedure is particularly straightforward for the case of perfectly conducting scatterers because of the relative simplicity of the boundary conditions. Henceforth, we will concentrate exclusively upon perfectly conducting scatterers.

Consider the integral Equation (2.29) for the scattered magnetic field intensity:

$$\vec{H}_s(\vec{r}') = \frac{1}{4\pi}\int_{S_1}\left[i\omega\epsilon(\hat{n}\times\vec{E}_s)\psi-(\hat{n}\times\vec{H}_s)\times\vec{\nabla}\psi-(\hat{n}\cdot\vec{H}_s)\vec{\nabla}\psi\right]ds \qquad (2.29)$$

For convenience, Equation (2.29) will be modified by making use of the fact that, as shown earlier the surface integral appearing in (2.29) of the incident fields $\vec{E}_i$ and $\vec{H}_i$ is identically zero (Eq. (2.17)). That is to say,

$$0 \equiv \frac{1}{4\pi}\int_{S_1}\left[i\omega\epsilon(\hat{n}\times\vec{E}_i)\psi-(\hat{n}\times\vec{H}_i)\times\vec{\nabla}\psi-(\hat{n}\cdot\vec{H}_i)\vec{\nabla}\psi\right]ds. \qquad (2.30)$$

Adding Equation (2.30) to (2.29) and recalling that $\vec{E}=\vec{E}_i+\vec{E}_s$ and $\vec{H}+\vec{H}_i+\vec{H}_s$, we obtain the following equation:

$$\vec{H}_s(\vec{r}') = \frac{1}{4\pi}\int_{S_1}\left[i\omega\varepsilon(\hat{n}\times\vec{E})\Psi - (\hat{n}\times\vec{H})\times\vec{\nabla}\Psi - (\hat{n}\cdot\vec{H})\vec{\nabla}\Psi\right]ds, \qquad (2.31)$$

where $\vec{E}$ and $\vec{H}$ are the total fields on S_1. At the surface of a perfect conductor, the tangential component of the total electric field and the normal component of the total magnetic field are identically zero. Mathematically, these boundary conditions can be expressed as follows:

$$\hat{n} \times \vec{E} \equiv 0; \quad (\hat{n}\times\vec{E}_s = -\hat{n}\times\vec{E}_i)$$

$$\hat{n} \cdot \vec{H} \equiv 0; \quad (\hat{n}\cdot\vec{H}_s = -\hat{n}\cdot\vec{H}_i) \qquad (2.32)$$

Consequently, for a perfect conductor, Equation (2.31) takes the following simple form:

$$\vec{H}_s(\vec{r}') = -\frac{1}{4\pi}\int_{S_1}(\hat{n}\times\vec{H}) \times \vec{\nabla}\Psi \, ds \; . \qquad (2.33)$$

To approximate $(\hat{n}\times\vec{H})$ on the surface of the scatterer, we first employ the principles of geometrical or ray optics. According to ray optics, there is a deep shadow region (no illumination) on the side of the scatterer not directly exposed to the incident radiation from the primary source. In the shadow region, $\vec{E}$ and $\vec{H}$ are identically zero ($\vec{E}_s = -\vec{E}_i$ and $\vec{H}_s = -\vec{H}_i$). the surface S_1 is thus divided up into an illuminated side S_+ and a shadow side S_-, the two sides being separated by a sharp shadow boundary Γ. This situation is depicted below.

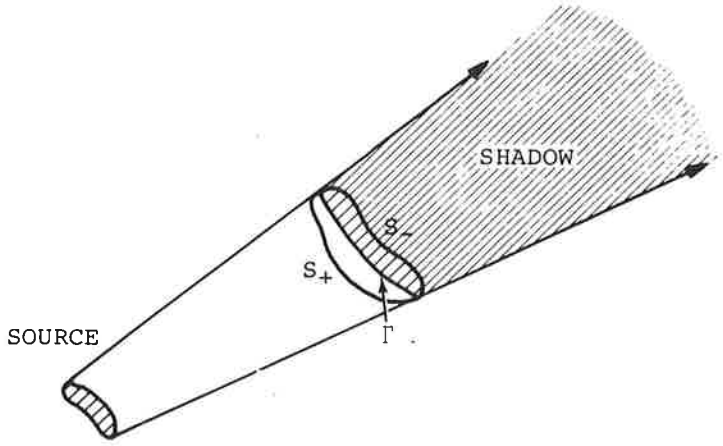

Figure 2.4. Shadow and Illuminated Regions of Scatterer

If it is assumed that $\vec{E}$ and $\vec{H}$ are identically zero on S_-, then Equation (2.33) becomes

$$\vec{H}_s(\vec{r}') = -\frac{1}{4\pi}\int_{S_+} (\hat{n}\times\vec{H}) \times \vec{\nabla}\Psi \, ds \quad , \tag{2.34}$$

where the integral is performed only over the illuminated side of the scatterer. Finally, to specify $(\hat{n}\times\vec{H})$ on S_+, the assumption of plane wave reflection from the local infinite tangent plane is made. That is to say, at each point Q on S_+, it is assumed that $\vec{E}_s(Q)$ and $\vec{H}_s(Q)$ have the values of the reflected fields which would exist if a plane electromagnetic wave with amplitudes $\vec{E}_i(Q)$ and $\vec{H}_i(Q)$ were incident upon an infinite, plane perfectly conducting boundary tangent to S_+ at Q. The boundary condition satisfied by the tangential components of the incident and reflected magnetic fields when a plane wave is incident upon an infinite , plane , perfectly conducting boundary is

$$\hat{n} \times \vec{H}_s = \hat{n} \times \vec{H}_i \quad , \tag{2.35}$$

or equivalently,

$$\hat{n} \times \vec{H} = \hat{n} \times (\vec{H}_i + \vec{H}_s) = 2(\hat{n}\times\vec{H}_i) \quad . \tag{2.36}$$

Assuming that Equation (2.36) is valid at each point on S_+, Equation (2.34) becomes

$$\vec{H}_s(\vec{r}') = -\frac{1}{2\pi}\int_{S_+} (\hat{n}\times\vec{H}_i) \times \vec{\nabla}\Psi \, ds \quad . \tag{2.37}$$

The analogous expression for $\vec{E}_s(\vec{r}')$ can be obtained by applying Equation (2.2) which, in the absence of currents, takes the form

$$\vec{\nabla} \times \vec{H} = -i\omega\varepsilon \vec{E} \tag{2.38}$$

Substituting (2.37) into (2.38) the following expression for $\vec{E}_s(\vec{r}')$ is obtained:

$$\vec{E}_s(\vec{r}') = -\frac{i}{2\pi\omega\varepsilon}\vec{\nabla}' \times \int_{S_+} (\hat{n}\times\vec{H}_i) \times \vec{\nabla}\Psi \, ds \quad , \tag{2.39}$$

where $\vec{\nabla}'$ acts upon the primed or field point coordinates. Equation (2.39) can be rewritten by taking the operator $\vec{\nabla}'$x inside the integral and noting that $\vec{\nabla}\Psi$ is the only function under the integral which depends upon r':

$$\vec{E}_s(\vec{r}') = -\frac{i}{2\pi\omega\varepsilon}\int_{S_+}\left[(\hat{n}x\vec{H}_i)\vec{\nabla}'\cdot(\vec{\nabla}\Psi) - \left\{(\hat{n}x\vec{H}_i)\cdot\vec{\nabla}'\right\}\vec{\nabla}\Psi\right]ds \tag{2.40}$$

Since $\vec{\nabla}\Psi$ is a function of $|\vec{r}'-\vec{r}|$, the following relationships hold true:

$$\vec{\nabla}'\cdot(\vec{\nabla}\Psi) = -\vec{\nabla}\cdot(\vec{\nabla}\Psi) = -\nabla^2\Psi$$

$$\left[(\hat{n}x\vec{H}_i)\cdot\vec{\nabla}'\right]\vec{\nabla}\Psi = -\left[(\hat{n}x\vec{H}_i)\cdot\vec{\nabla}\right]\vec{\nabla}\Psi \tag{2.41}$$

Substituting the relations (2.41) into (2.40) and noting that for $\vec{r}'\neq\vec{r}$, $-\nabla^2\Psi = k^2\Psi$ (Eq. (2.9)), we obtain the following equation for $\vec{E}_s(\vec{r}')$:

$$\vec{E}_s(\vec{r}') = -\frac{ik}{2\pi}\left(\frac{\mu}{\varepsilon}\right)^{1/2}\int_{S_+}\left[(\hat{n}x\vec{H}_i)\Psi + \frac{1}{k^2}\left\{(\hat{n}x\vec{H}_i)\cdot\vec{\nabla}\right\}\vec{\nabla}\Psi\right]ds \tag{2.42}$$

where we have made use of the fact that $k=\omega\sqrt{\mu\varepsilon}$.

We will be primarily concerned with the distributions of $\vec{E}_s$ and $\vec{H}_s$ in the far field or Fraunhofer zone of the scatterer. To obtain expressions for $\vec{E}_s$ and $\vec{H}_s$ in the Fraunhofer zone, Equations (2.37) and (2.42) are expanded asymptotically for large values of $r'=|\vec{r}'|$. For convenience, let the origin of coordinates, 0, lie on the surface of the scatterer. Let L denote some characteristic linear dimension of the scatterer. The Green's function Ψ is given in Equation (2.8):

$$\Psi = \frac{e^{ik|\vec{r}'-\vec{r}|}}{|\vec{r}'-\vec{r}|}\,. \tag{2.8}$$

Suppose that r'>>L. Then in the denominator of (2.8), $|\vec{r}'-\vec{r}|$ can be approximated very accurately by r'. That is, the variations in the amplitude of Ψ as $\vec{r}$ varies over the surface of the scatterer can be ignored if r'>>L. More care must be exercised in approximating the phase of Ψ because of the oscillatory behavior of the exponential. If r'>>L, then $|\vec{r}'-\vec{r}|$ can be written approximately as follows:

$$|\vec{r}'-\vec{r}| \approx r' - \hat{r}'\cdot\vec{r} + \frac{r^2}{2r'} - \frac{(\hat{r}'\cdot\vec{r})^2}{2r'} , \quad (2.43)$$

where $\hat{r}'=\vec{r}'/r'$ is a unit vector in the direction of $\vec{r}'$. In the Fraunhofer zone, $L^2/2r'$ is very small compared to the wavelength $\lambda=2\pi/k$ of the incident radiation so that the quadratic terms in Equation (2.43) can be ignored in comparison with the other two terms:

$$|\vec{r}'-\vec{r}| \approx r' - \hat{r}'\cdot\vec{r} \quad \text{(Fraunhofer approximation)}. \quad (2.44)$$

Combining these amplitude and phase approximations, we may write down the following asymptotic expression for Ψ for field points in the radiation zone of the scatterer:

$$\Psi \approx \frac{e^{ikr'}}{r'} e^{-ik(\hat{r}'\cdot\vec{r})} \quad (2.44)$$

A similar analysis of $\vec{\nabla}\Psi$ and $(\vec{A}\cdot\vec{\nabla})\vec{\nabla}\Psi$ where $\vec{A}$ is an arbitrary vector leads to the following asymptotic expressions:

$$\vec{\nabla}\Psi \approx - ik \frac{e^{ikr'}}{r'} \cdot e^{-ik(\hat{r}'\cdot\vec{r})}\hat{r}' , \quad (2.45)$$

$$(\vec{A}\cdot\vec{\nabla})\vec{\nabla}\Psi \approx (\vec{A}\cdot\hat{r}')\hat{r}'k^2 \frac{e^{ikr'}}{r'} e^{-ik(\hat{r}'\cdot\vec{r})} . \quad (2.46)$$

Substituting the asymptotic forms (2.44), (2.45), and (2.46) into Equations (2.37) and (2.42), we obtain the following asymptotic or far field expressions for $\vec{H}_s$ and $\vec{E}_s$:

$$\vec{H}_s(\vec{r}') = - \frac{ik}{2\pi} \frac{e^{ikr'}}{r'} \cdot \hat{r}' \times \int_{S_+} (\hat{n}\times\vec{H}_i) e^{-ik(\hat{r}'\cdot\vec{r})} ds, \quad (2.47)$$

$$\vec{E}_s(\vec{r}') = \frac{ik}{2\pi}\left(\frac{\mu}{\epsilon}\right)^{1/2} \frac{e^{ikr'}}{r'} \cdot \hat{r}' \times \left[\hat{r}'\times \int_{S_+} (\hat{n}\times\vec{H}_i) e^{-ik(\hat{r}'\cdot\vec{r})} ds\right], \quad (2.48)$$

where we have made use of the identity $\vec{a} \times (\vec{a}\times\vec{b}) = (\vec{a}\cdot\vec{b})\vec{a} - a^2\vec{b}$ in Equation (2.48). Notice that the asymptotic expressions for $\vec{H}_s$ and $\vec{E}_s$ in Equations (2.47) and (2.48) are related as follows:

$$\hat{r}' \times \vec{H}_s + \left(\frac{\varepsilon}{\mu}\right)^{1/2} \vec{E}_s = 0$$

$$\left(\frac{\varepsilon}{\mu}\right)^{1/2} \hat{r}' \times \vec{E}_s - \vec{H}_s = 0 \qquad (2.49)$$

These results are in agreement with the asymptotic relations given in Equations (2.18) and (2.19).

Equations (2.47) and (2.48) are the basic equations used by the Ohio University researchers and the TSC group for studying localizer signal scattering from metallic airport structures. However, caution must be exercised in applying these equations since the assumptions upon which they are based are unrealistic for many applications. Generally speaking, Equations (2.47) and (2.48) can be applied with some confidence in situations in which the wavelength $\lambda=2\pi/k$ of the incident radiation is small compared with the dimensions of the scatterer. When λ is comparable to or greater than the dimensions of the scatterer (length, radius of curvature, etc.), the assumption of a sharp boundary on the surface of the scatterer separating the illuminated side (S_+) from the shadow side (S_-) breaks down because of diffraction. The assumption of local plane wave reflection from the infinite tangent plane also breaks down when λ is comparable to or greater than the radius of curvature of the scatterer. It would for example, be unwise to attempt to use Equations (2.47) and (2.48) to study localizer signal scattering from the fuselages of aircraft since at localizer frequencies, $\lambda \approx 10$ ft which is comparable to or greater than the radii of curvature of all aircraft presently in use. Another fact to be borne in mind is that Equations (2.47) and (2.48) apply to the Fraunhofer zone of the scatterer. That is to say, these equations are based upon the assumption that $L^2/2r'$ is very small compared to a wavelength where L is same characteristic linear dimension of the scatterer. For very large scatterers, and for observation points relatively close to the scatterer, this condition may not be satisfied. One way of circumventing this difficulty is to divide up the illuminated surface S_+ into smaller subsections, apply Equations (2.47) and (2.48) to each subsection, and then add up the contributions from the various subsections to get the total scattered fields. A more direct approach is to simply retain the quadratic terms in the expansion (2.43) and to express the scattered fields in terms of Fresnel integrals. This approach is in fact presently being undertaken at TSC.

In spite of these various restrictions upon the applicability of Equations (2.47) and (2.48), they can provide a great deal of useful information about scattering phenomena. In the next section, these equations will be used to treat the problem of localizer signal scattering by a flat, vertical wall.

2.5 LOCALIZER SIGNAL SCATTERING

To illustrate the techniques developed in the preceding section, we will treat the important problem of localizer signal scattering by a flat, vertical, rectangular wall. The geometry of the problem is depicted below.

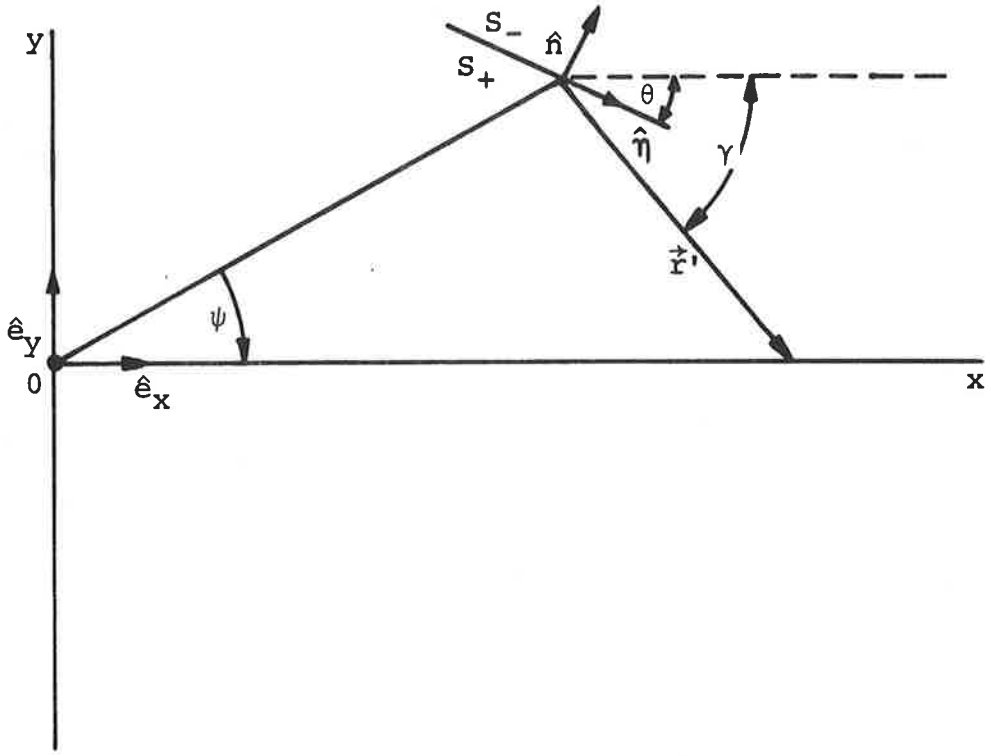

Figure 2.5. Scattering From a Vertical Wall, Ground Plane Shown

The x-y plane is the ground plane. For simplicity, it is assumed that the ground is perfectly flat and perfectly conducting. The x-axis represents the center line of the runway. The z-axis is perpendicular to the ground and points out of the page. The unit vectors in the x, y, and z directions are denoted by $\hat{e}_x$, $\hat{e}_y$, and $\hat{e}_z$ respectively. The localizer antenna is located a distance H above the ground and has coordinates (0,0,H) relative to the x, y, z coordinate system. H is typically on the order of 10 feet for the localizer.

In the far field of the localizer antenna, the electric field can be written as follows:

$$\vec{E} = \hat{u}\, E_o\, f(\phi)\, \frac{e^{ikR}}{R}\,, \qquad (2.50)$$

where $\hat{u}$ is a unit polarization vector, E_o is an amplitude, R is the distance from the localizer to the field point, and $f(\phi)$ is the horizontal field pattern of the antenna. For an arbitrary field point with coordinates (x,y,z), R and ϕ are defined as follows:

$$R = \sqrt{x^2+y^2+(z-H)^2}$$

$$\phi = \tan^{-1}\left(\frac{y}{x}\right) \qquad (2.51)$$

The electric field generated by the localizer is assumed to be polarized parallel to the ground so that $\hat{u}$ is given by

$$\hat{u} = \frac{y\,\hat{e}_x - x\,\hat{e}_y}{D_p} \quad , \qquad (2.52)$$

where $D_p = \sqrt{x^2+y^2}$ is the horizontal distance from the antenna to the field point.

To account for reflections from the perfectly conducting ground plane, an image antenna located at (0,0,-H) is included in the formulation to cancel the E field of the antenna on the ground (z=0). The total incident electric field (direct plus ground reflected) is given by

$$\vec{E}_i = \hat{u}\, E_o\, f(\phi) \left[\frac{e^{ikR}}{R} - \frac{e^{ikR_i}}{R_i}\right] \quad , \qquad (2.53)$$

where $R_i = \sqrt{x^2+y^2+(z+H)^2}$ is the distance from the image antenna to the field point.

Equation (2.53) can be rewritten as follows:

$$\vec{E}_i = \hat{u}\, E_o\, f(\phi)\, \frac{e^{ikR}}{R}\left[1 - \frac{R\, e^{ik(R_i-R)}}{R_i}\right] . \qquad (2.54)$$

We now make the assumption of small elevation angles. That is to say, we will assume that $D_p = \sqrt{x^2+y^2}$ is much greater than the magnitudes of (z-H) and (z+H). If $D_p >> |z-H|$ and $|z+H|$, then $D_p \approx R \approx R_i$ and the factor R/R_i in Equation (2.54) can be set approximately equal to 1. However, the path length difference (R_i-R) in the exponential must be approximated more accurately because of the oscillatory behavior of the exponential. To this end, we expand R and R_i in power series retaining only the two leading terms:

$$R \approx D_p + \frac{(z-H)^2}{2D_p} \quad , \tag{2.55}$$

$$R_i \approx D_p + \frac{(z+H)^2}{2D_p} \quad . \tag{2.56}$$

Consequently, the path length difference (R_i-R) is given approximately by

$$R_i - R \approx \frac{2zH}{D_p} \quad . \tag{2.57}$$

Incorporating these various approximations into Equation (2.54), we obtain the following expression for $\vec{E}_i$ at field points with small elevation angles:

$$\vec{E}_i = \hat{u}\, E_o\, f(\phi)\, \frac{e^{ikR}}{R} \left[1 - e^{2ikzH/D_p}\right] \quad . \tag{2.58}$$

The corresponding incident magnetic field $\vec{H}_i$ can be derived from Equation (2.58) by recalling that $\vec{E}$ and $\vec{H}$ have the following asymptotic relationship in the far field of a localized source (Eq. (2.19)):

$$\vec{H} = \left(\frac{\varepsilon}{\mu}\right)^{1/2} (\hat{r} \times \vec{E}) \quad . \tag{2.59}$$

Consequently, $\vec{H}_i$ is given by

$$\vec{H}_i = \left(\frac{\varepsilon}{\mu}\right)^{1/2} E_o\, f(\phi)\, \frac{e^{ikR}}{R} \left[1 - e^{2ikzH/D_p}\right] (\hat{R} \times \hat{u}) \quad , \tag{2.60}$$

where $\hat{R}=\vec{R}/R$ and $\vec{R}=x\hat{e}_x+y\hat{e}_y+(z-H)\hat{e}_z$. The magnetic polarization vector $(\hat{R}\times\hat{u})$ is given by

$$\hat{R} \times \hat{u} = \frac{\left[x\hat{e}_x+y\hat{e}_y+(z-H)\hat{e}_z\right]}{R} \times \frac{\left[y\hat{e}_x-x\hat{e}_y\right]}{D_p} \quad ,$$

$$\hat{R} \times \hat{u} = -\frac{D_p}{R}\,\hat{e}_z + (z-H)\,\frac{\left(x\hat{e}_x+y\hat{e}_y\right)}{RD_p} \quad . \tag{2.61}$$

The magnitude of the second term in Equation (2.61) is $|z-H|/R \approx |z-H|/D_p$ which we are assuming is very small compared to 1. The magnitude of the first term on the other hand is approximately equal to 1 when $D_p >> |z-H|$. Consequently $\hat{R} \times \hat{u}$

approximately equals $(-\hat{e}_z)$ for small angles of elevation. Making this approximation, Equation (2.60) can be rewritten as follows:

$$\vec{H}_i = - \hat{e}_z \left(\frac{\varepsilon}{\mu}\right)^{1/2} E_o \, f(\phi) \, \frac{e^{ikR}}{R} \left[1 - e^{2ikzH/D_p} \right] . \quad (2.62)$$

It will be assumed that for any point on the vertical wall, $D_p >> |z-H|$ so that Equation (2.62) can be used to accurately describe the variation of $\vec{H}_i$ over the surface of the scatterer.

The length and height of the vertical wall depicted in Figure 2.5 will be denoted by L and h respectively. The coordinates of the midpoint of the base of the wall will be denoted by (x_1, y_1, o). If

$$D_{p1} = \sqrt{x_1^2+y_1^2}$$

is much greater than L, then the angle subtended by the wall at the origin of coordinates will be very small. Assuming that this is the case, $f(\phi)$ in Equation (2.62) can be replaced by $f(\psi)$ where $\psi=\tan^{-1}(y_1/x_1)$ to a very good approximation. In other words, we can ignore the variation of the horizontal antenna pattern over the surface of the wall when $D_{p1}>>L$, assuming of course the $f(\phi)$ does not vary too rapidly with ϕ.

Let R_1 denote the distance from the antenna to the mid point of the base of the wall:

$$R_1 = \sqrt{x_1^2 + y_1^2 + H^2} \quad (2.63)$$

When R_1 is much greater than the dimensions of the wall, the distance R from the antenna to any point P on the wall can be represented approximately as follows:

$$R = R_1 + \hat{R}_1 \cdot \vec{r} \quad (2.64)$$

where $\hat{R}_1=\vec{R}_1/R_1$, $\vec{R}_1=x_1\hat{e}_x+y_1\hat{e}_y-H\hat{e}_z$, and $\vec{r}$ is a vector in the plane of the wall drawn from the mid point of the base to the point P. In Equation (2.64), the quadratic path length difference terms have been neglected. Let $\hat{\eta}$ denote a unit vector parallel to the wall and parallel to the x-y plane (Fig. 2.5). Using the point $(x_1,y_1,0)$ as a new origin of coordinates, the vector $\vec{r}$ can be represented as follows:

$$\vec{r} = \eta \, \hat{\eta} + z \, \hat{e}_z \quad , \quad (2.65)$$

where η is variable ranging from -L/2 t_o +L/2 and z is just the elevation of the point P on the wall above the ground. The vector $\hat{\eta}$ can be expressed in terms of $\hat{e}_x$ and $\hat{e}_y$ as follows:

$$\hat{\eta} = \cos\theta\ \hat{e}_x - \sin\theta\ \hat{e}_y \qquad (2.66)$$

where θ is the angle between $\hat{\eta}$ and the x-axis (Fig. 2.5). Substituting (2.66) in (2.65), we obtain the following expression for $\vec{r}$:

$$\vec{r} = \eta\cos\theta\ \hat{e}_x - \eta\sin\theta\ \hat{e}_y + z\ \hat{e}_z \quad . \qquad (2.67)$$

The path length difference $\hat{R}_1 \cdot \vec{r}$ can now be calculated:

$$\hat{R}_1 \cdot \vec{r} = \eta\left(\frac{x_1}{R_1}\cos\theta - \frac{y_1}{R_1}\sin\theta\right) - \frac{zH}{R_1} \quad . \qquad (2.68)$$

Since $R_1 \approx D_{p1}$ ($H << D_{p1}$), $x_1/R_1 \approx x_1/D_{p1} = \cos\psi$ and $y_1/R_1 \approx y_1/D_{p1} = \sin\psi$. Making these approximations, Equation (2.68) becomes:

$$\hat{R}_1 \cdot \vec{r} = \eta\cos(\theta+\psi) - \frac{zH}{D_{p1}} \quad . \qquad (2.69)$$

Substituting Equation (2.69) into Equation (2.64), we obtain the following approximate expression for the distance R:

$$R = R_1 + \eta\cos(\theta+\psi) - \frac{zH}{D_{p1}} \quad . \qquad (2.70)$$

In the denominator of Equation (2.62) R can be simply replaced by R_1 and in the factor $[1 - e^{2ikzH/D_p}]$, D_p can be replaced by D_{p1}. Incorporating all of these approximations into Equation (2.62), we obtain the following expression for $\vec{H}_i$ on the surface of the wall:

$$\vec{H}_i = \hat{e}_z\left(\frac{\varepsilon}{\mu}\right)^{1/2} E_o\, f(\psi)\, \frac{e^{ikR_1}}{R_1}\, e^{ik\eta\cos(\theta+\psi)} \cdot \left[2i\sin k\left(\frac{zH}{D_{p1}}\right)\right] \qquad (2.71)$$

The expression for $\vec{H}_i$ given in Equation (2.71) can now be substituted into Equation (2.48) to calculate the scattered electric field $\vec{E}_s$ produced by the wall. The origin of coordinates for this integration will be the mid point of the base of the wall (x_1, y_1, o).

Equation (2.48) is reproduced here for ease of reference

$$\vec{E}_s(\vec{r}') = \frac{ik}{2\pi}\left(\frac{\mu}{\epsilon}\right)^{1/2} \frac{e^{ikr'}}{r'} \cdot \hat{r}' \times \left[\hat{r}' \times \int_{S_+} (\hat{n}\times\vec{H}_i)\, e^{-ik(\hat{r}'\cdot\vec{r})}\, ds.\right] \tag{2.48}$$

The unit normal vector $\hat{n}$ points <u>into</u> S_+(Fig. 2.5). In terms of the unit vectors $\hat{e}_x$, $\hat{e}_y$, and $\hat{e}_z$, $\hat{n}$ is given by

$$\hat{n} = \sin\theta\, \hat{e}_x + \cos\theta\, \hat{e}_y \tag{2.72}$$

Clearly, $\hat{n} \times \hat{H}_i$ is parallel to $\hat{n}$ since $\vec{H}_i$ is parallel to $\hat{e}_z$ (Eq. (2.71)).

The vector $\vec{r}'$ is drawn from the point (x_1,y_1,o) to the observation point which is of course the location of the receiving antenna on the aircraft. Let x_2, y_2, z_2 denote the coordinates of the receiver relative to the x, y, and z axes respectively. Then $\vec{r}'$ is given by

$$\vec{r}' = (x_2-x_1)\, \hat{e}_x + (y_2-y_1)\, \hat{e}_y + z_2\, \hat{e}_z\ . \tag{2.73}$$

The magnitude r' of the vector $\vec{r}'$ is denoted by R_2:

$$r' \equiv R_2 = \sqrt{(x_2-x_1)^2 + (y_2-y_1)^2 + z_2^2} \tag{2.74}$$

The horizontal distance of the receiver from the point (x_1,y_1,o) is denoted by D_{p2}:

$$D_{p2} = \sqrt{(x_2-x_1)^2 + (y_2-y_1)^2}\ . \tag{2.75}$$

It is assumed that the elevation angle of $\vec{r}'$ is very small. That is to say, it is assumed that $D_{p2} >> z_2$. The phase term $\hat{r}'\cdot\vec{r}$ appearing in the integral in Equation (2.48) is given by

$$\hat{r}'.\vec{r} = \eta\cos\theta\, \frac{(x_2-x_1)}{R_2} - \eta\sin\theta\, \frac{(y_2-y_1)}{R_2} + \frac{z\, z_2}{R_2}\ , \tag{2.76}$$

where use has made of Equation (2.67). Since $D_{p2} >> z_2$, $D_{p2} \approx R_2$. Consequently, the following approximate relationships hold:

$$\frac{(x_2-x_1)}{R_2} \approx \frac{(x_2-x_1)}{D_{p2}} = \cos\gamma$$

$$\frac{(y_2-y_1)}{R_2} \approx \frac{(y_2-y_1)}{D_{p2}} = -\sin\gamma \quad , \tag{2.77}$$

where γ is the angle between the projection of the vector $\vec{r}'$ onto the x-y plane and the x-axis (Fig. 2.5). Consequently, Equation (2.76) can be rewritten as follows:

$$\hat{r}'\cdot\vec{r} = \eta \cos(\gamma-\theta) + \frac{z\, z_2}{D_{p2}} \quad . \tag{2.78}$$

The integral in Equation (2.48) can now be evaluated quite easily. It should be noted that the range of integration of the variable z is $-h \leq z \leq +h$. This range of integration must be used in order to take into account the image of the wall in the ground plane. Carrying out the integrations in η $(-L/2 \leq \eta \leq +L/2)$ and z $(-h \leq z \leq +h)$, we obtain the following expression for the total scattered field $\vec{E}_s$ (direct plus ground reflected):

$$\vec{E}_s = (\hat{r}'x(\hat{r}'x\hat{\eta}))\, i\frac{kLh}{\pi} E_o f(\psi) \frac{e^{ik(R_1+R_2)}}{R_1R_2} \cdot \operatorname{sinc}\left[\frac{kL}{2}(\cos(\theta+\psi)-\cos(\gamma-\theta))\right]$$

$$\cdot \left\{ \operatorname{sinc}\left[kh\left[\frac{H}{D_{p1}} - \frac{z_2}{D_{p2}}\right]\right] - \operatorname{sinc}\left[kh\left[\frac{H}{D_{p1}} + \frac{z_2}{D_{p2}}\right]\right] \right\} . \tag{2.79}$$

where $\operatorname{sinc}(x) = \sin x/x$.

For the low angles of elevation which we are assuming, the triple vector product $\hat{r}'$ x $(\hat{r}'x\hat{\eta})$ can be simplified greatly. We first expand the triple vector product as follows:

$$\hat{r}' \text{ x } (\hat{r}'x\hat{\eta}) = (\hat{r}'\cdot\hat{\eta})\ \hat{r}' - \hat{\eta} \tag{2.80}$$

The unit vector $\hat{r}'$ is given by

$$\hat{r}' = \frac{(x_2-x_1)}{R_2}\hat{e}_x + \frac{(y_2-y_1)}{R_2}\hat{e}_y + \frac{z_2}{R_2}\hat{e}_z \quad . \tag{2.81}$$

For small angles of elevation ($R_2 \approx D_{p2} >> z_2$), we can ignore the z-component of $\hat{r}'$ and use Equation (2.77) to obtain the following expression for $\hat{r}'$.

$$\hat{r}' \approx \cos\gamma\ \hat{e}_x - \sin\gamma\ \hat{e}_y \tag{2.82}$$

Consequently, $\hat{r}'\cdot\hat{\eta} \approx \cos\theta\cos\gamma + \sin\theta\sin\gamma = \cos(\gamma-\theta)$ (Eq. (2.66)). Making these approximations in Equation (2.80), we obtain the

following approximate expression for the polarization vector $\hat{r}' \times (\hat{r}' \times \hat{\eta})$:

$$\hat{r}' \times (\hat{r}' \times \hat{\eta}) = - \sin(\gamma-\theta)\left[\sin\gamma\ \hat{e}_x + \cos\gamma\ \hat{e}_y\right] \quad (2.83)$$

which is of course parallel to the ground plane. The magnitude of the vector given in Equation (2.83) is just $\sin(\gamma-\theta)$. Consequently, the magnitude of the scattered field is given by

$$E_s = \frac{ikLh}{\pi} f(\psi) \frac{e^{ik(R_1+R_2)}}{R_1 R_2} \sin(\gamma-\theta)\ \mathrm{sinc}\ \frac{kL}{2}\left[\cos(\theta+\psi) - \cos(\gamma-\theta)\right]$$

$$\cdot \mathrm{sinc}\left[kh\left[\frac{H}{D_{p1}} - \frac{z_2}{D_{p2}}\right]\right] - \mathrm{sinc}\left[kh\left[\frac{H}{D_{p1}} + \frac{z_2}{D_{p2}}\right]\right] \quad (2.84)$$

For an omnidirectional receiving antenna, the expression given in Equation (2.84) is the appropriate one to use for calculating perturbations in the difference in depth of modulation.

2.6 COMPARISON WITH PREVIOUS WORK

The result obtained in the preceding section for the scattered electric field produced by a flat vertical wall will now be compared with the solutions to the same problem obtained by the Ohio University and I.B.M. researchers.

Our Equation (2.84) for E_s does not differ significantly from the expression obtained by the Ohio University group. This comes as no surprise since our methods of approach are almost identical. Their solution is somewhat simpler in that it does not contain the sinc functions which depend upon the height of the localizer antenna (H), the height of wall (h), and the height of the receiver (z_2) that appear in Equation (2.84). Instead, their expression for E_s is simply proportional to $h^3\ H\ z_2$. The fact that the Ohio University solution has a simpler dependence upon the parameters h, H, and z_2 than does our solution is due to the fact that the Ohio University researchers used a linear approximation to describe ground reflections. Specifically, instead of multiplying the antenna field pattern by the factor $[1 - e^{2ikzH/D_p}]$ to account for ground reflections (Eq. (2.58)), as we did, the Ohio University researchers multiplied the antenna field pattern by $(2kzH/D_p)$. That is, they assumed that $(2KzH/D_p) << 1$, and essentially expanded $[1 - e^{2ikzH/D_p}]$ in a power series in $(2kzH/D_p)$ retaining only the first two terms. They made a similar approximation to describe the reflections of the scattered fields from the

ground plane. Our expression for E_s in fact reduces to the Ohio University expression if the sinc functions involving H, h, and z_2 appearing in Equation (2.84) are approximated by the first two terms in their power series expansions. In essence then, there are no fundamental differences between our treatment of the scattering problem and the Ohio University treatment.

On the other hand, the I.B.M. approach to the problem of localizer signal scattering by a vertical wall differs fundamentally from our approach and that of Ohio University. For convenience, their approach to the problem will be illustrated using our equations and notation.

For ease of reference, Equations (2.28) and (2.29) are reproduced here:

$$\vec{E}_s(\vec{r}') = -\frac{1}{4\pi}\int_{S_1}\left[i\omega\mu(\hat{n}x\vec{H}_s)\psi+(\hat{n}x\vec{E}_s)x\vec{\nabla}\psi+(\hat{n}\cdot\vec{E}_s)\vec{\nabla}\psi\right]ds, \tag{2.28}$$

$$\vec{H}_s(\vec{r}') = \frac{1}{4\pi}\int_{S_1}\left[i\omega\varepsilon(\hat{n}x\vec{E}_s)\psi-(\hat{n}x\vec{H}_s)x\vec{\nabla}\psi-(\hat{n}\cdot\vec{H}_s)\vec{\nabla}\psi\right]ds \quad . \tag{2.29}$$

Equations (2.28) and (2.29) express the scattered fields outside a scatterer in terms of integrals of the scattered fields over the surface S_1 of the scatterer. For treating perfectly conducting scatterers, we chose to work with Equation (2.29) since the integral simplies greatly for a perfect conductor. The integral in (2.29) was first modified by adding to the right hand side of (2.29) the corresponding integral of the incident fields $\vec{E}_i$ and $\vec{H}_i$. Since the surface integral in (2.28) and (2.29) of $\vec{E}_i$ and $\vec{H}_i$ over S_1 are identically zero, the left hand side of (2.29) was unchanged by this addition and we obtained the following modified expression for $\vec{H}_s(\vec{r}')$:

$$\vec{H}_s(\vec{r}') = \frac{1}{4\pi}\int_{S_1}\left[i\omega\varepsilon(\hat{n}x\vec{E})\psi-(\hat{n}x\vec{H})x\vec{\nabla}\psi-(\hat{n}\cdot\vec{H})\vec{\nabla}\psi\right]ds, \tag{2.31}$$

where $\vec{E}$ and $\vec{H}$ are the total fields on S_1 ($\vec{E}=\vec{E}_i+\vec{E}_s$, $\vec{H}=\vec{H}_i+\vec{H}_s$). The analogous expression for the scattered electric field is:

$$\vec{E}_s(\vec{r}') = -\frac{1}{4\pi}\int_{S_1}\left[i\omega\mu(\hat{n}x\vec{H})\Psi+(\hat{n}x\vec{E})x\vec{\nabla}\Psi+(\hat{n}\cdot\vec{E})\vec{\nabla}\Psi\right]ds \quad (2.85)$$

For a perfectly conducting scatterer, the surface S_1 is divided into an illuminated side S_+ and a shadow side S_-. On the shadow side, it is assumed as a first approximation that $\vec{E}\equiv\vec{H}\equiv 0$ ($\vec{E}_s=-\vec{E}_i$ and $\vec{H}_s=-\vec{H}_i$ on S_-). With this approximation, the integrals in (2.31) and (2.85) are extended only over the illuminated side S_+ of S_1. That is to say, $\vec{E}_s(\vec{r}')$ and $\vec{H}_s(\vec{r}')$ are expressed in terms of surface integrals of the total fields over S_+.

Had we chosen to work directly with Equations (2.28) and (2.29) rather than (2.31) and (2.85) the same result would have been obtained. For example, assuming that $\vec{E}_s = -\vec{E}_i$ and $\vec{H}_s = -\vec{H}_i$ on S_-, Equation (2.28) becomes:

$$\vec{E}_s(\vec{r}') = -\frac{1}{4\pi}\int_{S_+}\left[i\omega\mu(\hat{n}x\vec{H}_s)\Psi+(\hat{n}x\vec{E}_s)x\vec{\nabla}\Psi+(\hat{n}\cdot\vec{E}_s)\vec{\nabla}\Psi\right]ds$$

$$+\frac{1}{4\pi}\int_{S_-}\left[i\omega\mu(\hat{n}x\vec{H}_i)\Psi+(\hat{n}x\vec{E}_i)x\vec{\nabla}\Psi+(\hat{n}\cdot\vec{E}_i)\vec{\nabla}\Psi\right]ds\ . \quad (2.86)$$

However, we know that the surface integral of $\vec{E}_i$ and $\vec{H}_i$ over the total surface S_1 is identically zero. Consequently, the surface integral in (2.86) of $\vec{E}_i$ and $\vec{H}_i$ over S_- is the negative of the corresponding surface integral of $\vec{E}_i$ and $\vec{H}_i$ over S_+. Therefore, Equation (2.86) can be rewritten as follows:

$$\vec{E}_s(\vec{r}') = -\frac{1}{4\pi}\int_{S_+}\left[i\omega\mu(\hat{n}x\vec{H}_s)\Psi+(\hat{n}x\vec{E}_s)x\vec{\nabla}\Psi+(\hat{n}\cdot\vec{E}_s)\vec{\nabla}\Psi\right]ds$$

$$-\frac{1}{4\pi}\int_{S_+}\left[i\omega\mu(\hat{n}x\vec{H}_i)\Psi+(\hat{n}x\vec{E}_i)x\vec{\nabla}\Psi+(\hat{n}\cdot\vec{E}_i)\ \vec{\nabla}\Psi\right]ds \quad (2.87)$$

Combining these two integrals over S_+ and recalling that $\vec{E}=\vec{E}_i+\vec{E}_s$ and $\vec{H}=\vec{H}_i+\vec{H}_s$, we are left with a surface integral over S_+ of the total fields $\vec{E}$ and $\vec{H}$.

The I.B.M. researchers essentially use the same integral Equations (2.28) and (2.29) to treat the problem of localizer signal scattering. To obtain an expression for the scattered electric field produced by a vertical wall, they simply carry out the integral appearing in (2.28) over the illuminated surface of the wall. That is to say, they use the following expression for $\vec{E}_s(r')$:

$$\vec{E}_s(\vec{r}') = -\frac{1}{4\pi}\int_{S_+}\left[i\omega\mu(\hat{n}x\vec{H}_s)\psi+(\hat{n}x\vec{E}_s)x\vec{\nabla}\psi+(\hat{n}\cdot\vec{E}_s)\vec{\nabla}\Psi\right]ds \quad .(2.88)$$

That is to say, instead of integrating the total fields over S_+ as we did, they just integrate the scattered fields. In effect, they ignore the integral of $\vec{E}_s$ and $\vec{H}_s$ over S_-, the shadow side of S_1. Instead of setting $\vec{E}_s$ and $\vec{H}_s$ equal to $-\vec{E}_i$ and $-\vec{H}_i$ respectively on the shadow side S_-, they in effect assume that $\vec{E}_s$ and $\vec{H}_s$ are identically zero on S_- which is not true.

Comparing our result for the magnitude E_s of the scattered field produced by a vertical wall with the I.B.M. results, we find that the only real difference between the two expressions is that whereas our Equation (2.84) contains a factor $[2\sin(\gamma-\theta)]$ to describe the horizontal field pattern of the wall, their Equation (2.43) contains a corresponding factor M_G which is given in our angle notation by:

$$M_G = \left[\sin(\theta+\psi)+\sin(\gamma-\theta)\right]\cos\left[\gamma-\psi-2\theta\right] . \qquad (2.89)$$

The effects of this difference on perturbations in the difference in depth of modulation predicted by the two models can be very pronounced as can be seen in some of the accompanying comparative graphs. Figures 2.6 and 2.7 (static and dynamic) show the difference between the new and old (I.B.M.) formulations. Also, as examples of the dependence of the derogation on the building size, location and orientation, we show in Figures 2.8 to 2.18 the microamp deviation of a localizer V-ring signal that would be received by an aircraft flying the centerline of the runway in level flight, 50 feet above the ground as predicted by the new math model for scattering off a vertical wall.

These Cal Comp generated figures are presented here as examples of typical output obtained from the computer model and as examples of one way in which this output can be presented. In all figures the x-distance is measured from the Localizer as origin and the y-distance from the centerline of the runway.

In Figure 2.8, the microampere deviation calculated along the runway centerline caused by a 100 foot by 50 foot rectangular wall situated behind the Localizer and 470 feet from the runway centerline is shown to increase markedly as the wall is moved closer to the Localizer. This is expected as more energy is reflected back onto the runway in these cases.

Figure 2.9 shows a similar marked increase in the derogation for buildings located closer to, but in front of the Localizer.

Figures 2.10 and 2.11 show the derogation due to a larger building, 500 feet by 50 feet, which is located further from the runway centerline (1000 feet instead of 470 feet). Well beyond the Localizer in either direction, (-2000 feet or +8250 feet), there is only negligible derogation, while closer in, at -1000 feet and at +500 feet, the derogation is significant.

The explicit variation of the derogation on the building's position relative to the runway centerline is shown in Figures 2.12 and 2.13. There is a dramatic increase in the amount of derogation when the building is placed close to the runway centerline (e.g., when y=470 feet).

Figures 2.14 and 2.15 show the derogation for different orientations of the building, both in terms of the magnitude and the location of the derogation on the runway centerline. As indicated in the accompanying sketches, the different locations of the derogation along the runway centerline occur because of the different specular reflection directions of the various building orientations.

Finally, in Figures 2.16-2.18, the increase in the derogation with the increase of building size is shown.

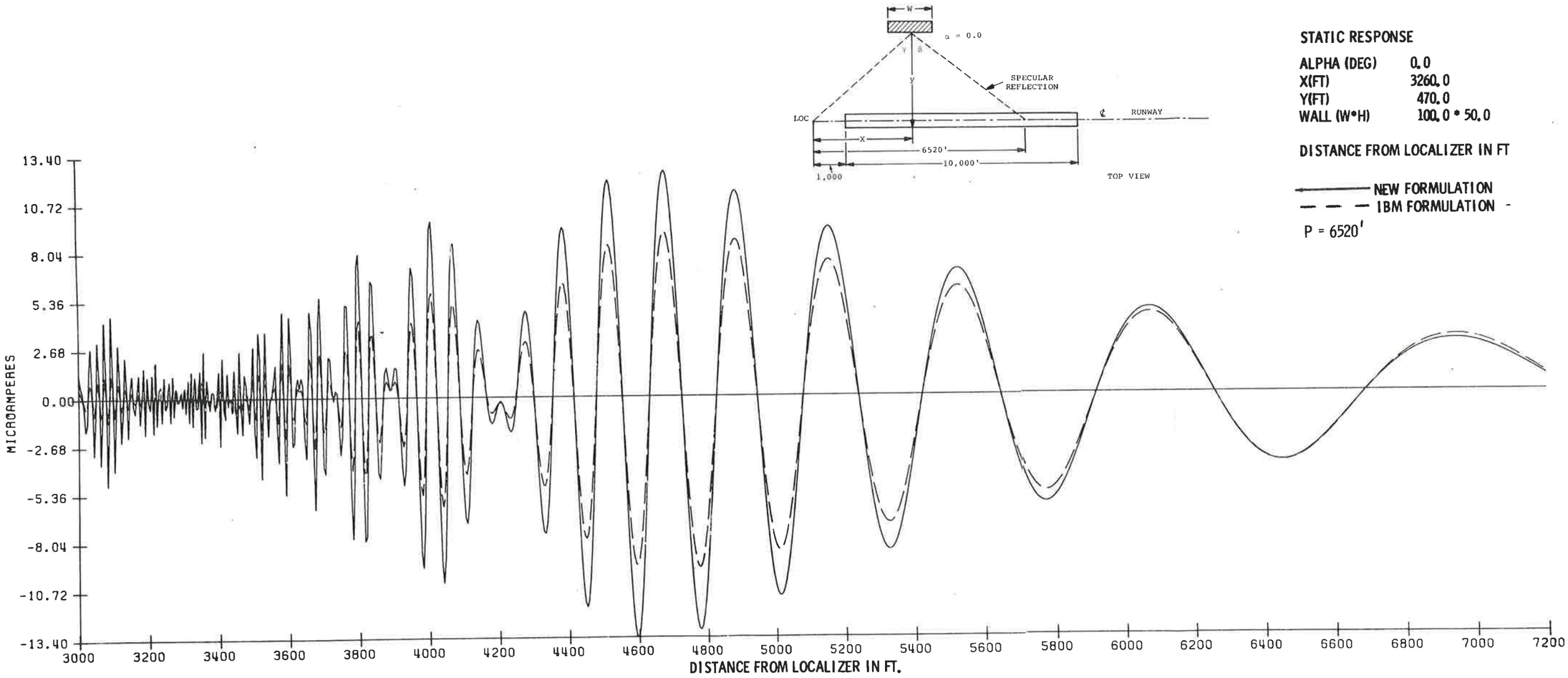

Figure 2.6. Comparison between the I.B.M. and the new formulation, in the static case for a vertical flat wall parallel to the runway.

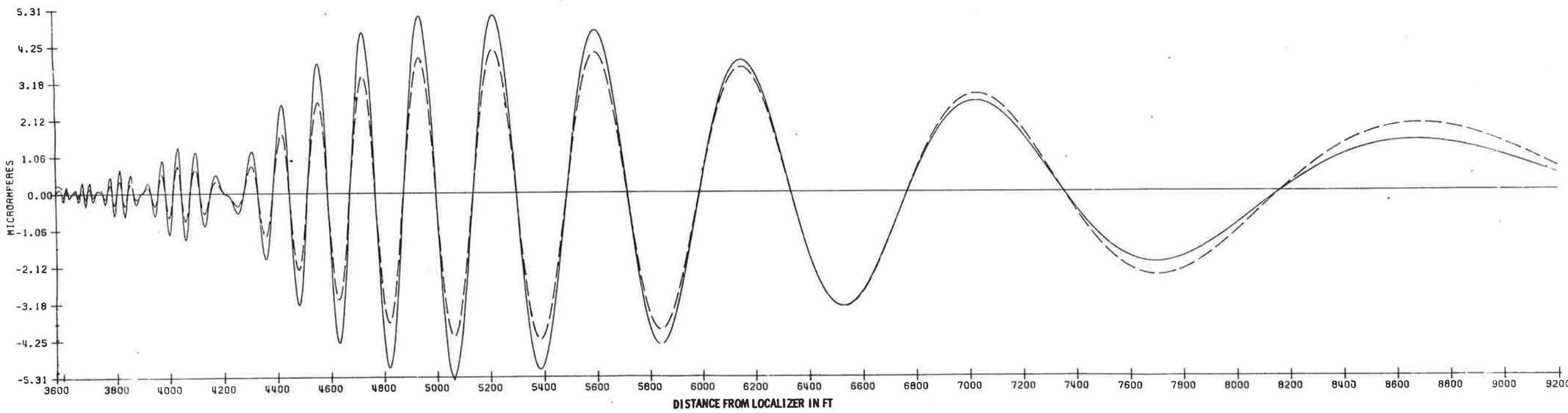

Figure 2.7. Same as Figure 2.6 except the dynamic cases are compared.

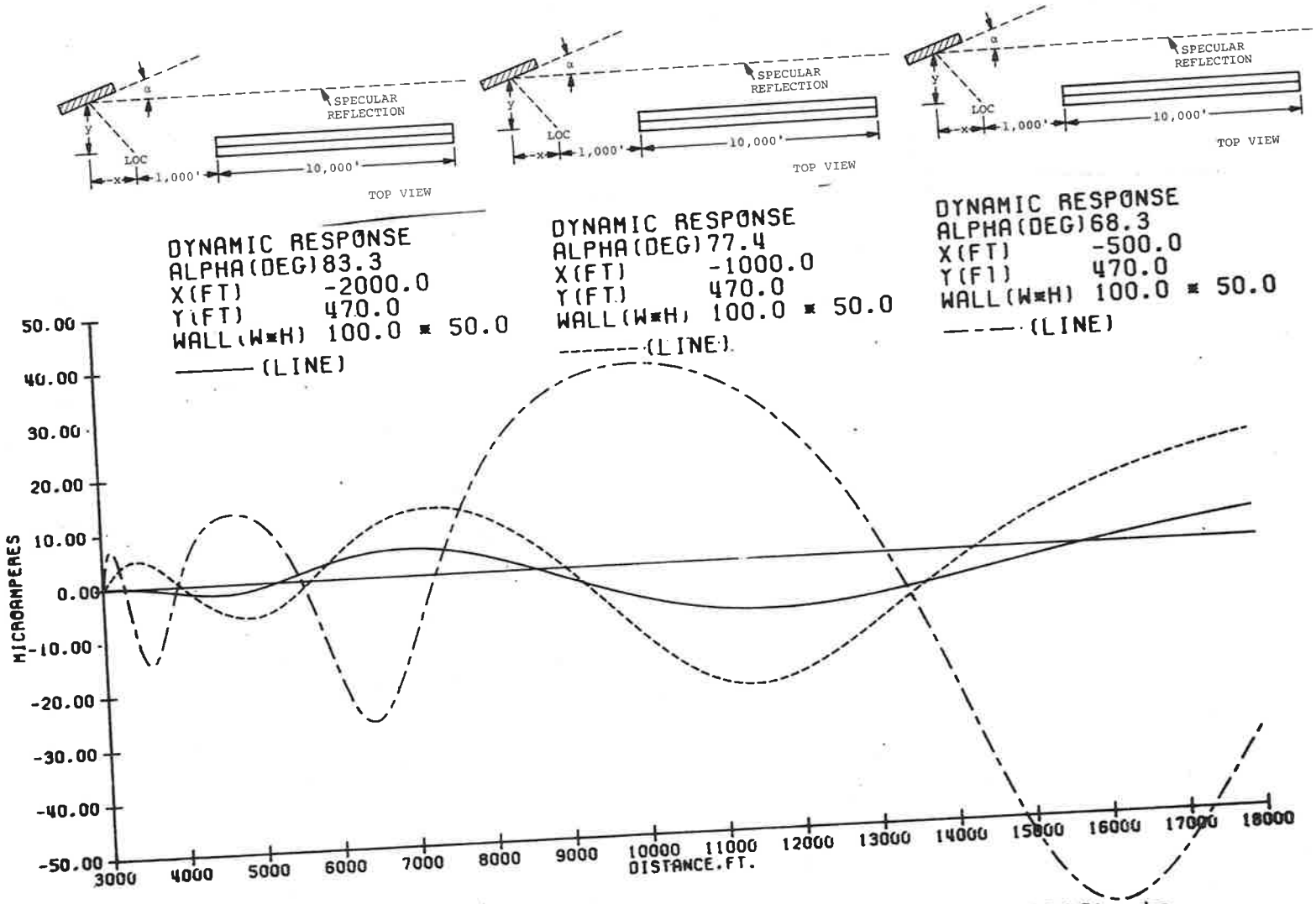

Figure 2.8. The wall's "X" position is changed from -2000ft. to -1000ft. to -500ft. while the "Y" position of 470ft. and the dimensions of the wall are held constant. The angle alpha is varied to give specular reflection parallel to the runway.

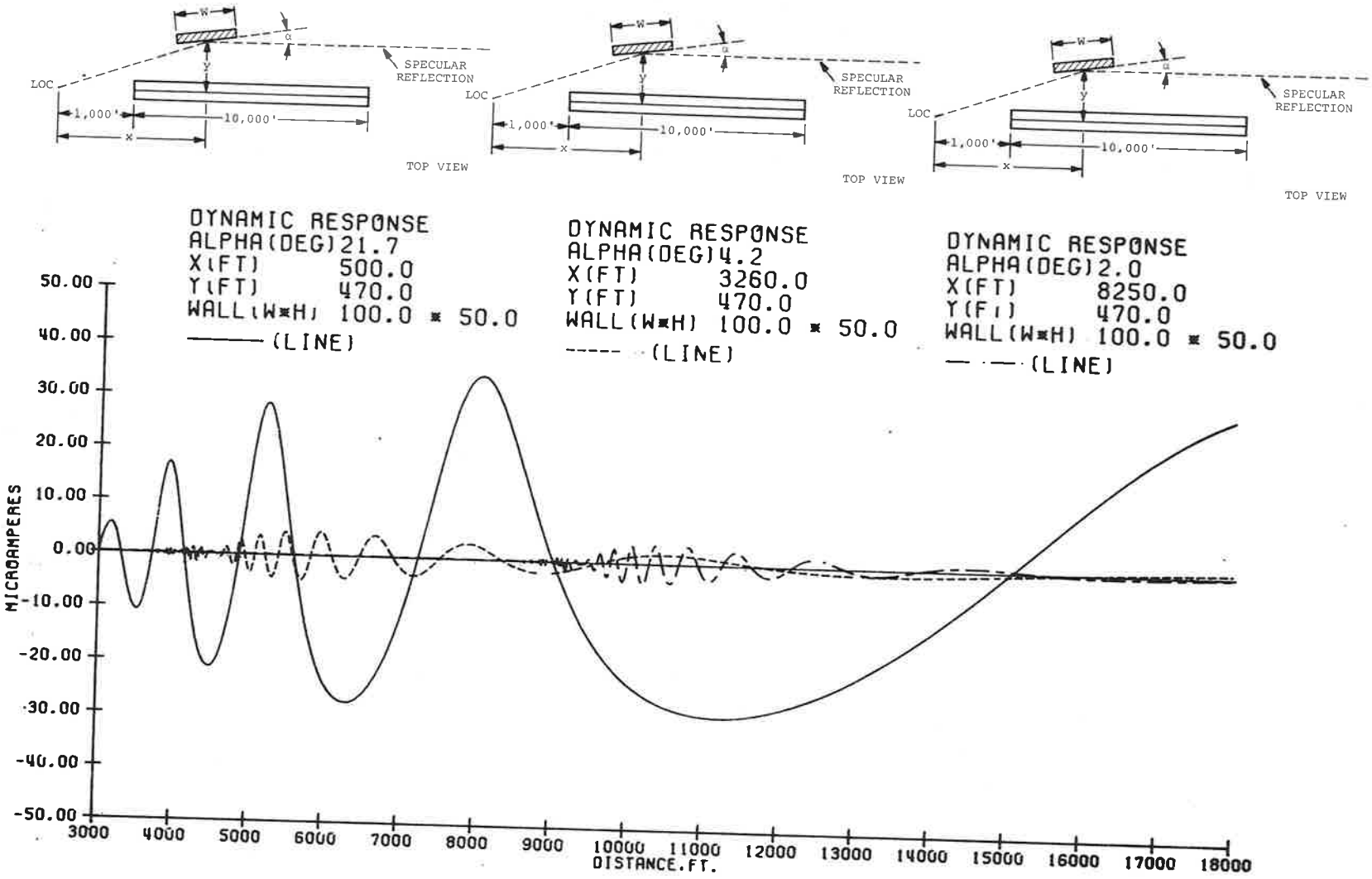

Figure 2.9. The wall's "X" position is changed from 500ft., to 3260ft. and to 8250ft. while the "Y" position of 470ft. and the dimensions of the wall are held constant. The angle alpha is selected so that specular reflection is parallel to the runway.

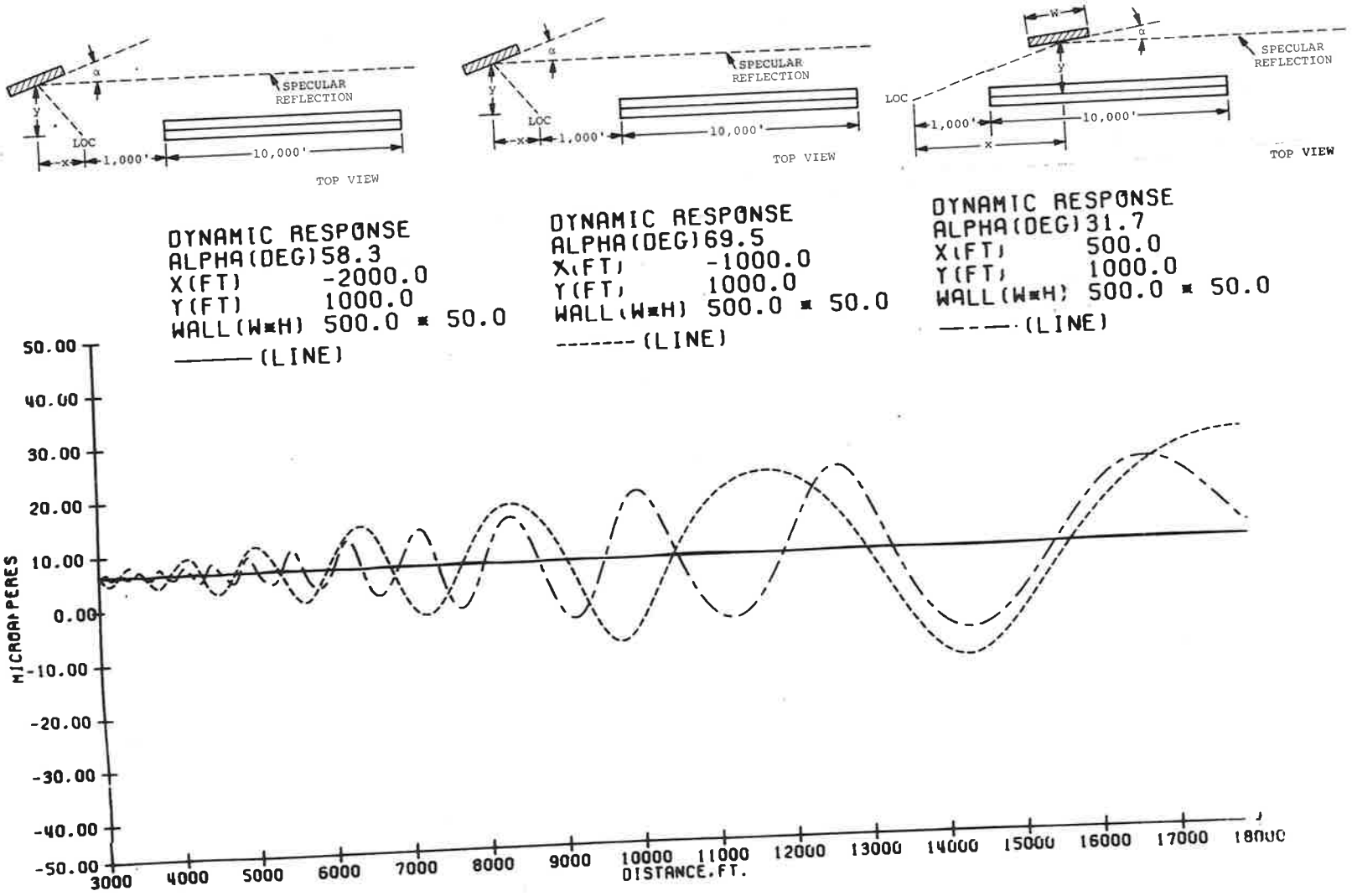

Figure 2.10. The wall's "Y" position is now 1000ft. while the walls "X" position is changed from -2000ft., to -1000 ft. and to 500ft. and the dimensions of the wall are held constant. The angle alpha is varied to give specular reflection parallel to the runway.

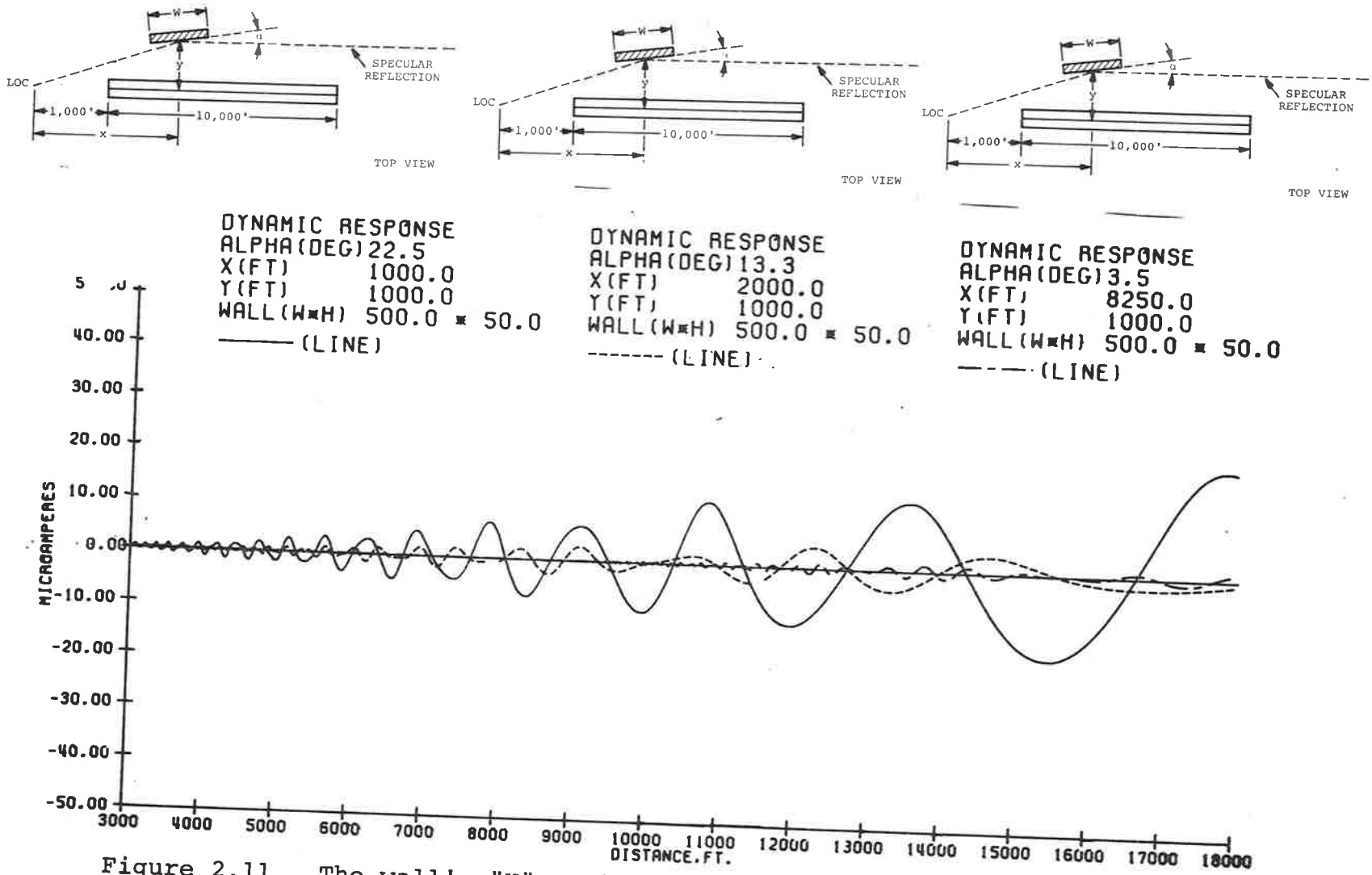

Figure 2.11. The wall's "X" position is changed from 1000ft. to 2000ft. and to 8250ft. while the "Y" position of 1000 ft. and the dimensions of the wall are held constant. The angle alpha is varied to give specular reflection parallel to the runway.

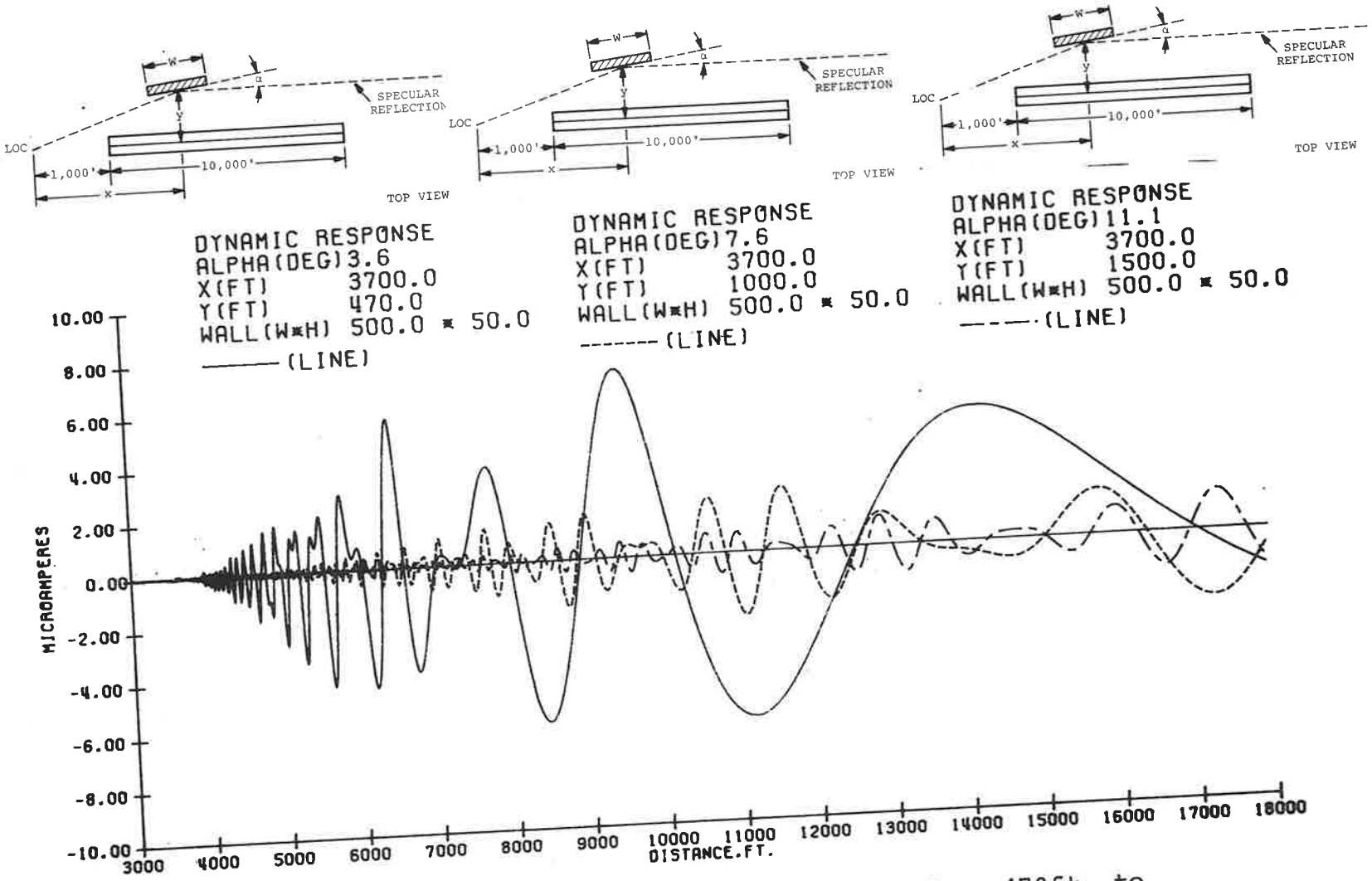

Figure 2.12. The wall's "Y" position is changed from 470ft. to 1000ft. and to 1500ft. while the "X" position and the dimensions of the wall are held constant. The angle alpha is varied to give specular reflection parallel to the runway.

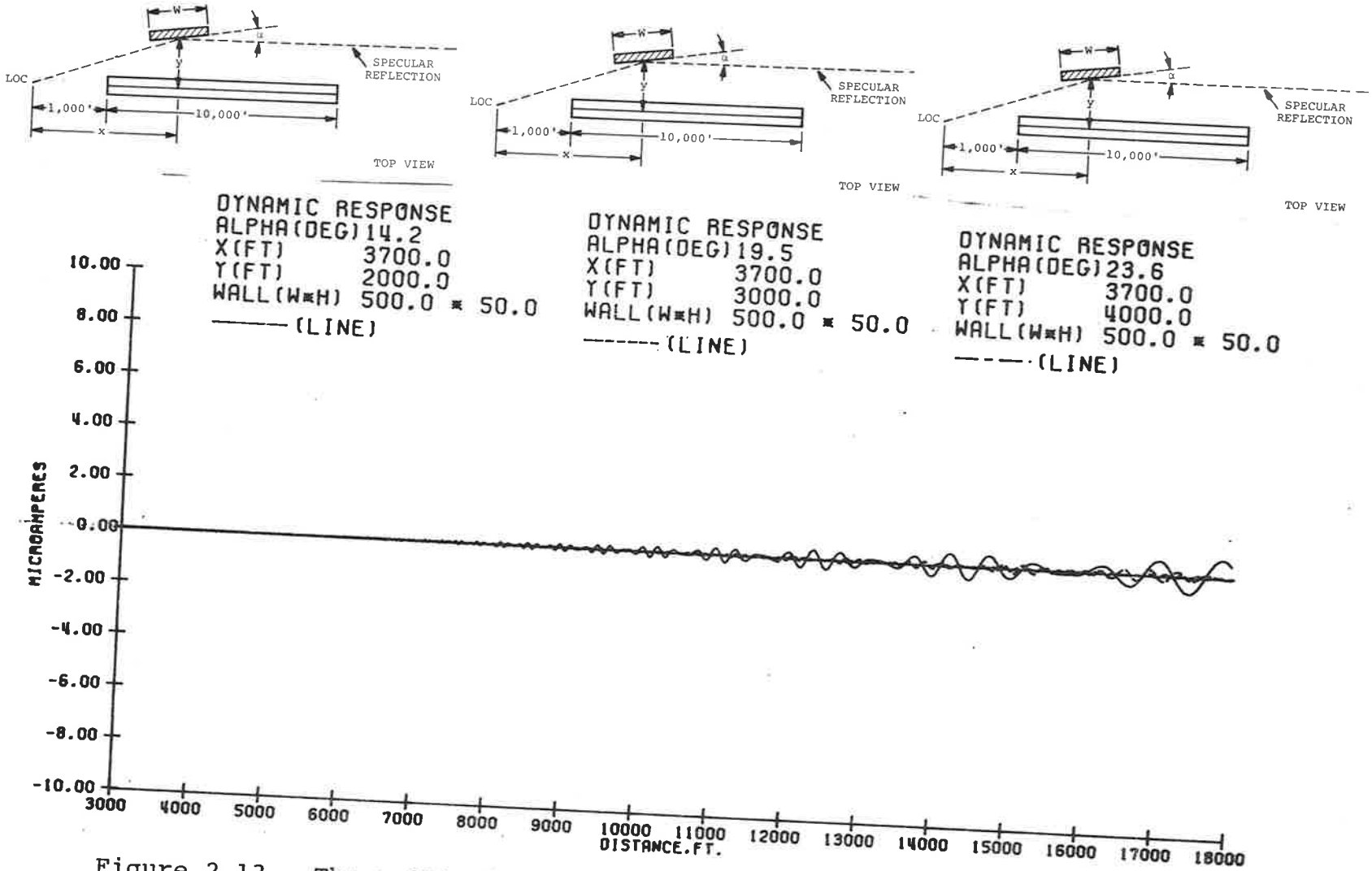

Figure 2.13. The wall's "Y" position is changed from 2000ft. to 3000ft. and to 4000ft. while the "X" position and the dimension of the wall are held constant. The angle alpha is varied to give specular reflection parallel to the runway.

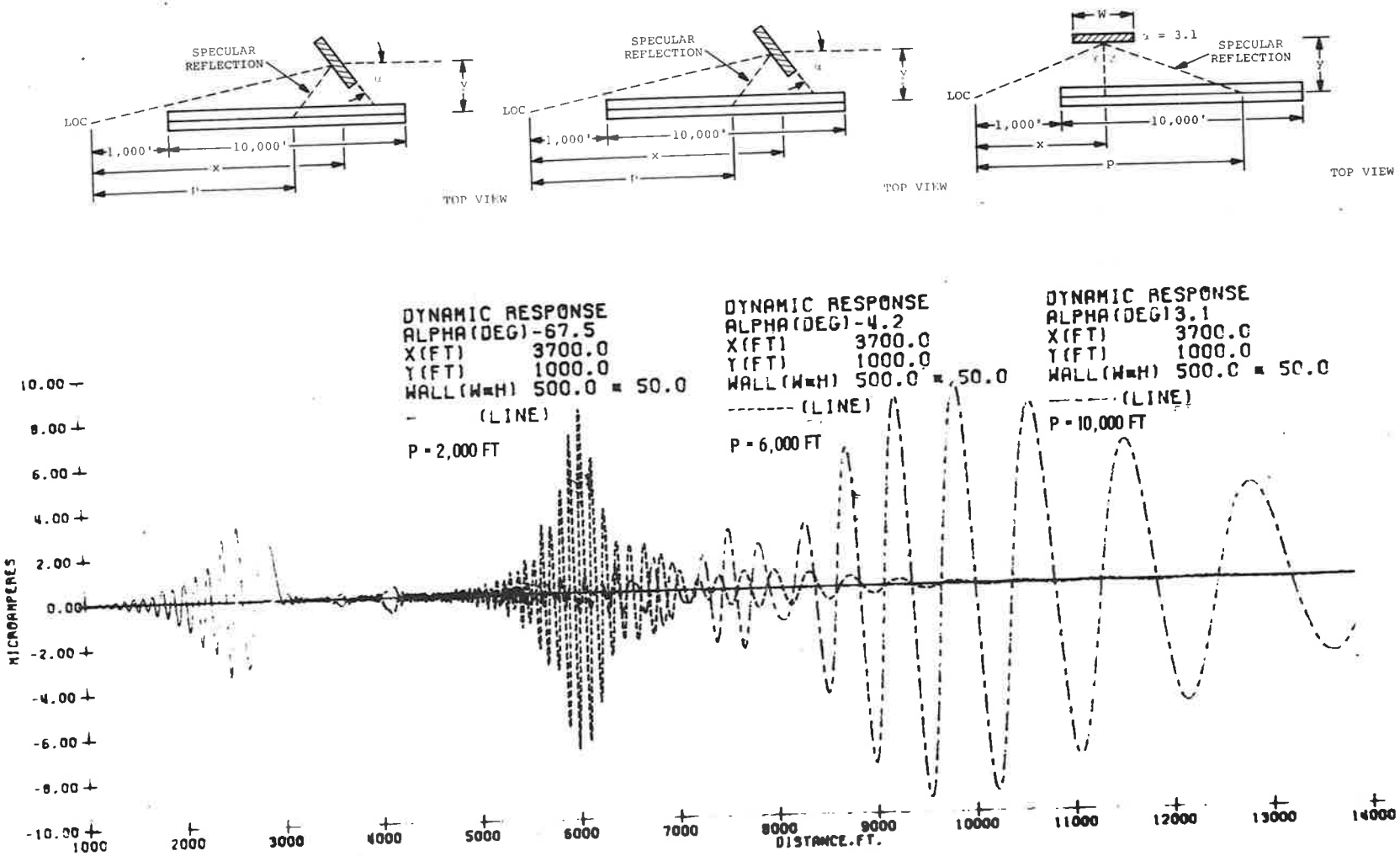

Figure 2.14. Different angles of alpha, -67.5°, -4.2° and 3.1° are used to place specular reflection at different points along the runway. The "X" and "Y" positions and the dimensions of the wall are held constant.

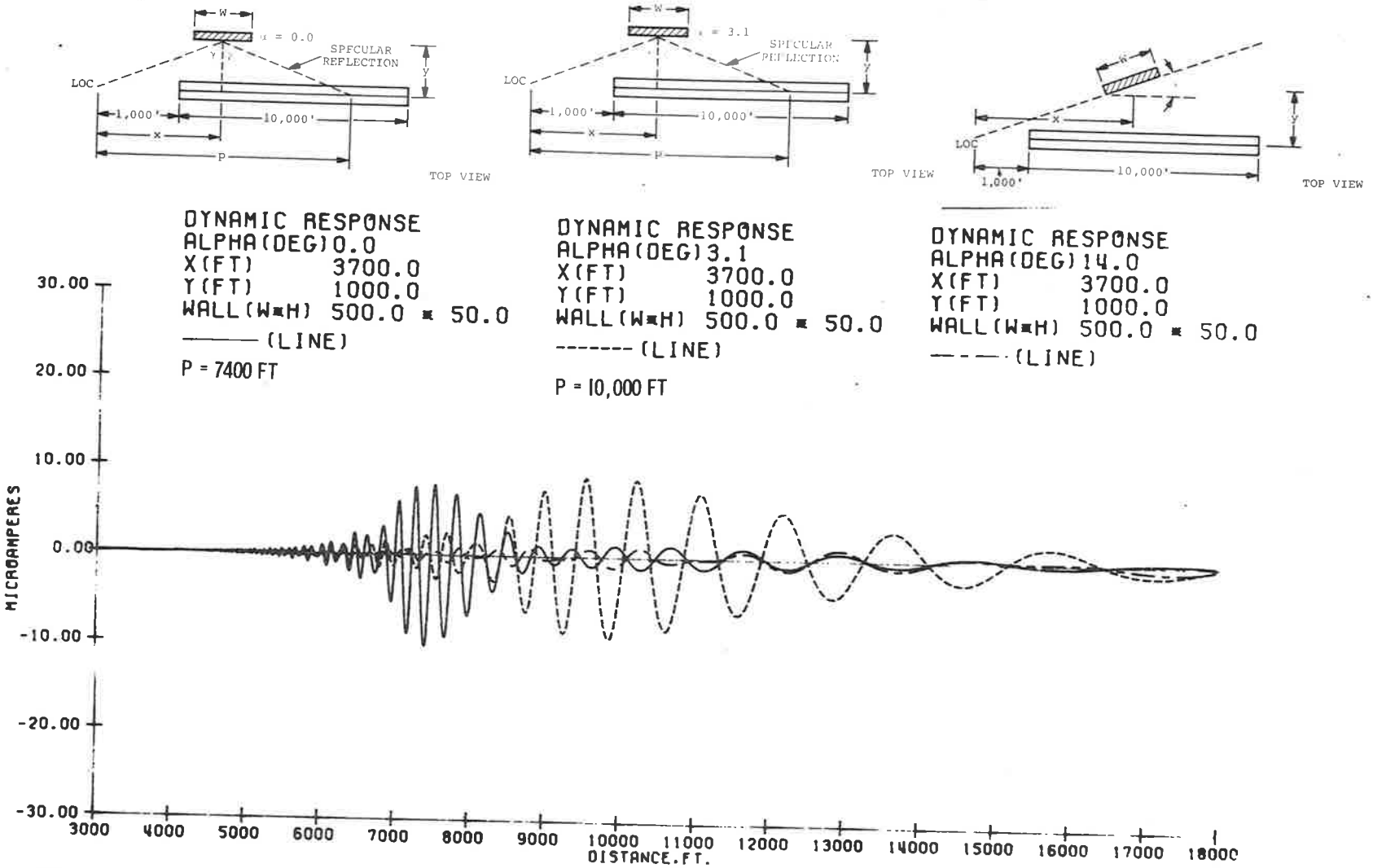

Figure 2.15. Different angles of alpha, 0.0°, 3.1° and 14.0° are used to position the specular reflection at different areas indicated by the sketch. The "X" and "Y" positions and the dimensions of the wall are held constant.

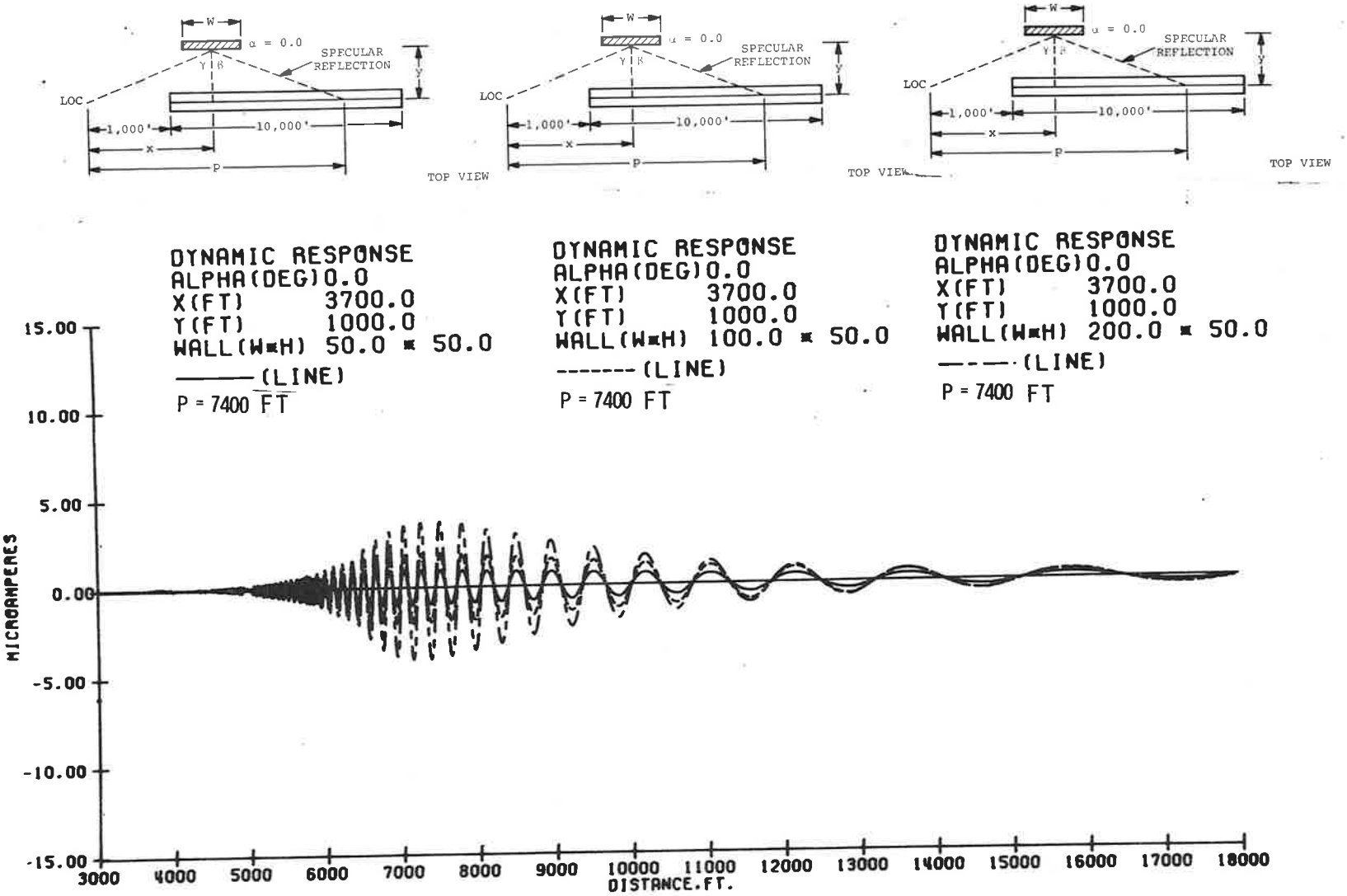

Figure 2.16. Different lengths of the wall, 50ft., 100ft. and 200ft. are used while the "X" and "Y" positions and the height of the wall are held constant.

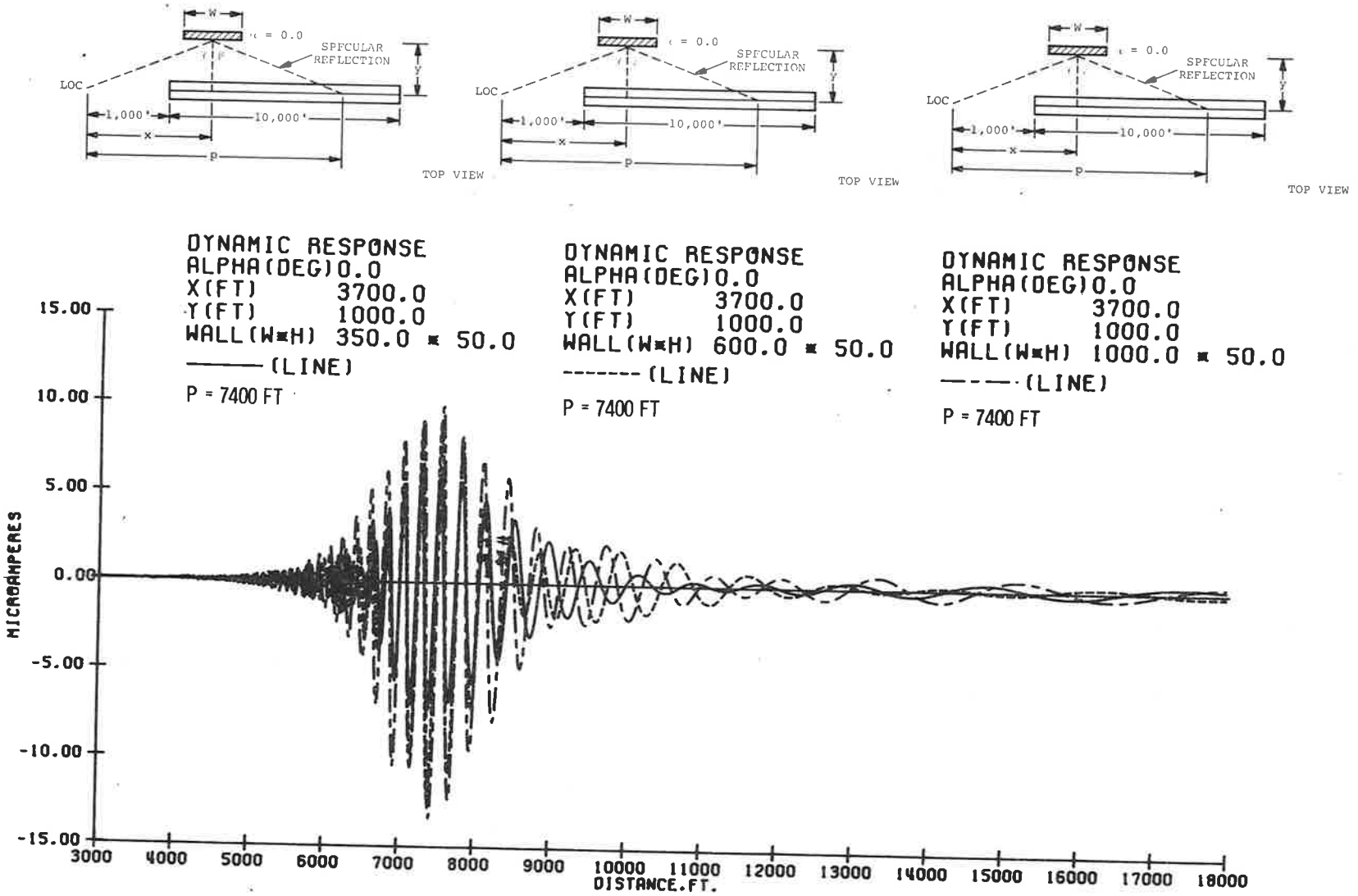

Figure 2.17. Different lengths of the wall, 350ft., 600ft. and 1000ft. are used while the "X" and "Y" position and the height of the wall are held constant.

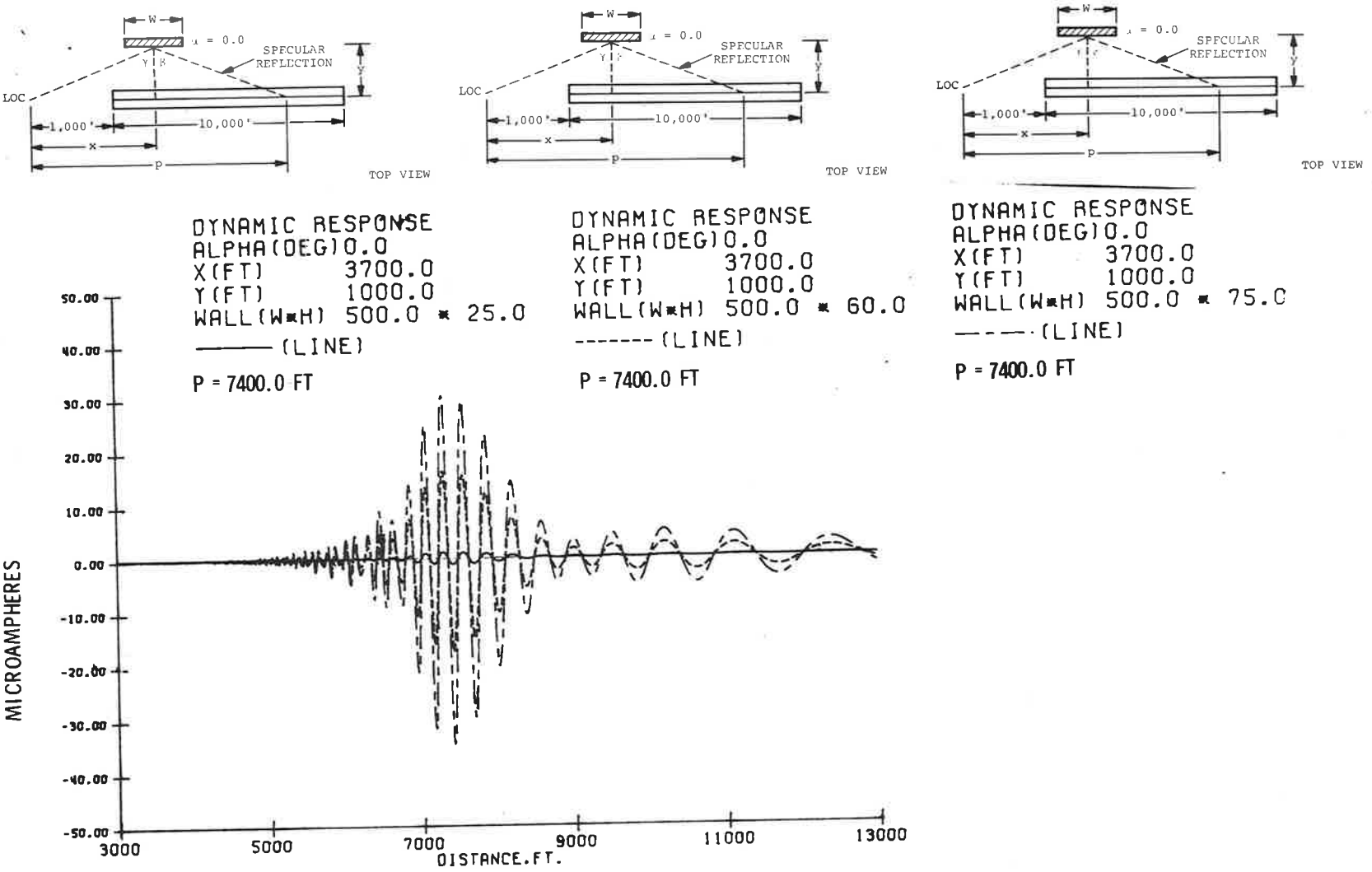

Figure 2.18. Different heights of the wall, 25ft. 60ft. and 75ft. are used while the "X" and "Y" position and the height of the wall are held constant.

SECTION 3. MODELLING OF ILS SIGNAL DETECTION

3.1 INTRODUCTION

In implementing computer prediction of the course deviation indication (CDI) for complex derogating environments and arbitrary selection of the localizer and/or glide slope signal transmitting system, it is desirable to have a unified approach to the modelling of DDM detection by standard aircraft ILS receivers. To effectively treat any existing or future ILS system, a detection model must adequately account for systems utilizing one or two carrier frequencies, for arbitrary relative phasing between different signal components, variation of receiving antenna gain patterns and effects of aircraft speed. The models presently in use fall short of this objective. The I.B.M. code is developed only for the localizer null reference system; the Ohio glide slope programs incorporate null reference, sideband reference and capture effect, but in the latter case the auxilliary carrier signal is ignored.[3] The Ohio codes are further restricted in applicability to moderate derogations near or on the glide course centerline, and none of the foregoing models takes any account of relative Doppler effects.

All in all, the approaches that have been taken in dealing with signal detection have been somewhat simplistic. The DDM concept is easily defined in an ideal signal transmission environment, but is much less easily defined in the presence of strong multipath interference. In the general case, i.e. in a complex multipath environment, it is possible to represent the radio frequency signal derived by an aircraft receiver from the total incident radiation field of a single carrier ILS system by the form:

$$E(t) = \mathrm{Re}\left[(E_c+E_{90}\cos(2\pi 90t)+E_{150}\cos(2\pi 150t)e^{-i\omega_c t}\right] ,$$

where $\omega_c/2\pi$ is the carrier frequency and E_c, E_{90}, and E_{150} are the complex amplitudes of the carrier and respective sidebands in the received signal. One may define the difference in depth of modulation as

$$DDM = (|E_{150}| - |E_{90}|)/|E_c| ,$$

but it cannot be assumed (as it has been by I.B.M. and Ohio U) that it is this quantity that is detected by actual receivers

operating in complex multipath environments. In fact, the above defined DDM is detected by receivers of standard design only when the relative phases of E_C, E_{90}, and E_{150} are all the same. This is in general not true when any significant amount of multipath interference is present.

Below we develop a unified model of ILS signal reception that attempts to reach a higher level of completeness and correctness for actual receivers than the previously used models. In the course of the derivation, a number of approximations are inevitably taken. While it is felt that these are all reasonably justified, the overall consequences of the model should be verified by empirical data. The treatment does illuminate the relative significance for the detected ILS signal of carrier and sideband dephasing and of Doppler effects on receiver dynamic response.

3.2 RECEIVER MODEL

Localizer and glide slope signals are assumed to be detected by heterodyne AM receivers similar in basic design to the schematic diagram shown in Figure 3.1. The figure indicates generally how the 90 and 150 Hz modulations are amplified, detected, and separated and the difference applied to one of the movements of a cross pointer indicator. The sum of the 90 and 150 Hz outputs is held constant by an AGC feedback loop, so that once calibrated, the instrument gives a faithful readout of the apparent CDI (course deviation indication) whenever the incident signal radiation exceeds a minimum level.

The guidance radiation field (localizer or glide slope) is coupled to the receiver input via an antenna which may be assumed to have specified directional and polarization characteristics. Any antenna used in practice may be treated as a linear system. This fact allows us to consider the scalar current transmitted to the receiver input load as the resultant of individual currents generated by various electromagnetic field components incident on the antenna. We shall assume that all incident component fields are transverse and harmonic, and so are adequately described by an electric vector $\vec{E}$ and a unit vector $\hat{k}$ in the direction of propagation. For a number of such component fields incident on a specified antenna, the receiver input current can be expressed in the form:

$$I_{in} = \Sigma\, I_j = \Sigma\, \vec{g}(\hat{k}_j) \cdot \vec{E}_j \qquad (3.1)$$

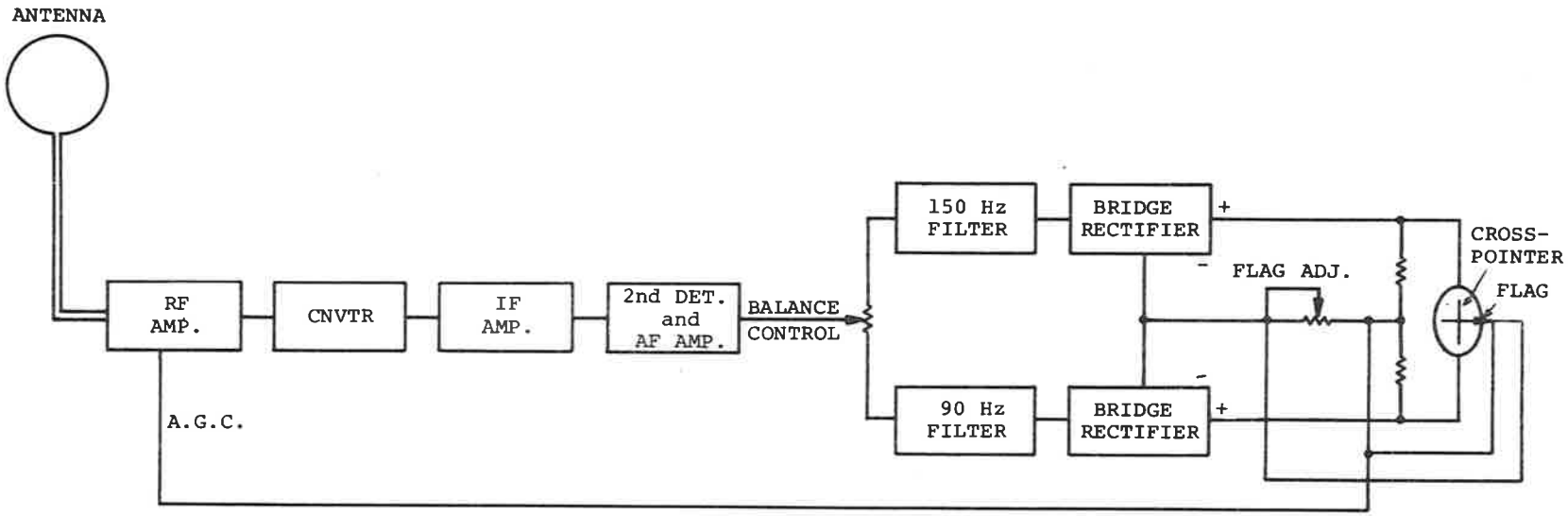

Figure 3.1. Schematic Diagram of Typical ILS Receiver

where $\vec{g}(\hat{k})$ conveys both the "gain" and polarization characteristics of the antenna for plane waves incident in the direction $\hat{k}$.

As an example, it is shown in Appendix C that the gain vector for a small horizontal circular loop antenna (which is a reasonable approximation to many aircraft localizer receiving antennae) takes the form

$$\vec{g}(\hat{k}) = c_a \hat{n} \times \hat{k}, \tag{3.2}$$

where the unit vector $\hat{n}$ is normal to the plane of the loop and the maximum gain c_a depends on the area of the loop, the carrier wavelength, and the impedance of the input circuit.

The ILS radiation fields to be considered may be generated by multiple element antennae and/or waveguide radiators operating on one or two carrier frequencies. In every case a number of distinct carrier modulations are radiated, each in a specific spatial pattern. To assure computational accuracy, it will be necessary in some instances to compute the direct and scattered radiation reaching the receiver from each source independently; in other cases, combinations of elements may be treated as point sources giving rise to certain directional radiation patterns. In any event, we will consider the individually computed components of the received field to represent radiation travelling approximately by specific point to point paths between the transmitting antenna and the aircraft. Let a specific modulation waveform be denoted by $u_m(t)$ and a specific propagation path be denoted by the subscript p. Then to each component field computed at the receiving antenna, there corresponds a component of the amplified signal at the output of the I.F. stage of the receiver, which can be suitably represented by the complex form:

$$V_{IFp}(t) = \sum_m a_{mp} u_m(t) e^{-i\omega_m t} e^{i\phi_p}. \tag{3.3}$$

Here the terms a_{mp} include as factors the relative values of the initially radiated amplitudes of the particular modulation components m, the antenna gain factor $\vec{g}(\hat{k}_p)\cdot\vec{E}_p$, and the path attenuation due to field divergence, reflections, etc. The phase delay of the path p is denoted by ϕ_p and the carrier frequency associated with the modulation m is $\omega_m/2\pi$.

In practice, it is only necessary to consider two distinct carrier frequencies, ω_c and $\omega_c - \Delta_c$. Grouping together

all the modulations of a specific carrier, we may express Equation (3.3) in the equivalent form:

$$V_{IFp}(t) = e^{i\phi p}\left(e^{-i\omega ct}\sum_m a_{mp}u_{1m}(t)+e^{-i(\omega c-\Delta c)t}\sum_n b_{np}u_{2n}(t)\right) \quad (3.4)$$

Here the b_{np} factors associated with the secondary carrier terms are exactly analogous to the a_{mp}. Summing this equation over all multipath modes p gives a complex representation of the total I.F. output signal. This is passed to the second detector which generates an audio frequency signal

$$V_{AF}(t) = \left|\sum_p V_{IFp}(t)\right|. \quad (3.5)$$

Determination of the C.D.I. is based on the relative amplitudes of 90 Hz and 150 Hz components found in this audio signal by passing it through selective filters. Denoting the action of these filters symobolically by the operators H_{90} and H_{150} (to be defined presently), we may represent the outputs of an ILS receiver as

$$V_{90}(t) = H_{90}\ [V_{AF}(t)] \quad (3.6a)$$

$$V_{150}(t) = H_{150}\ [V_{AF}(t)]\ ; \quad (3.6b)$$

$$CDI_{static} = s_m \frac{\overline{V_{150}}-\overline{V_{90}}}{\overline{V_{150}}+\overline{V_{90}}} \text{ microamperes.} \quad (3.7)$$

In Equation (3.7) the factor s_m is the cross-pointer sensitivity which has the standard values 387.0 for localizer signals and 676.0 for glide slope signals. The magnitudes $\overline{V_{150}}$ and $\overline{V_{90}}$ are obtained by rectification of the detected modulation tone signals $V_{150}(t)$ and $V_{90}(t)$.

3.3 ANALYSIS OF THE AUDIO SIGNAL $V_{AF}(t)$-CAPTURE EFFECT

We now seek a reasonably accurate estimate of the received 90 Hz and 150 Hz modulations in the general multipath, capture effect situation. For this we need an expression for $V_{AF}(t)$ in the form of a Fourier series, and we need suitable definitions of the filter operators H_{90} and H_{150}.

It is the possible presence of many signal derogating scatterers in the glide slope environment that makes analytical derivation of $V_{AF}(t)$ from $V_{IF}(t)$ difficult. Because of the receiving aircraft's motion, each derogating signal is received with a possibly significant Doppler shift relative to the direct ILS transmission. The consequence is that a large range of frequencies may generally be present

in the audio output of the second detector, instead of solely the modulation tone frequencies. The action of the 90 and 150 Hz filters on such complex signals must be considered.

Additional spurious signals occur in reception of radiation from capture effect transmitting systems near all harmonics of the 8 kHz carrier separation frequency. This fact allows a convenient reduction of the audio signal analysis problem, if the capture effect of the detector is treated first. We follow a procedure suggested in part by Manney[4]. The total I.F. output signal may be written as:

$$V_{IF}(t) = \left[A_1(t)+e^{i\Delta ct}A_2(t)\right] e^{-i\omega ct} \tag{3.8}$$

where:

$$A_1(t) = \sum_m u_{1m}(t)\sum_p a_{mp}e^{i\phi p}$$

$$A_2(t) = \sum_n u_{2n}(t)\sum_p b_{np}e^{i\phi p} \tag{3.9}$$

The audio signal (Eq. 3.5) can now be expressed as

$$V_{AF}(t) = \left[|A_1(t)|^2+|A_2(t)|^2+2Re\left(A_1(t)A_2(t)^*e^{-i\Delta ct}\right)\right]^{1/2} \tag{3.10}$$

Now the scale of the time variation of the complex amplitudes A_1 and A2 is given by the modulation frequencies 90 Hz and 150 Hz or perhaps by the latter frequency shifted by the upper limit of observed Doppler displacement. In the worst case for glide slope signal reception, the frequency spectral range of A_1 and A2 is certainly less than 500 Hz, which can be considered small compared to $\Delta_c/2\pi$ = 8 kHz. Accordingly, we may expand the instantaneous value of $V_{AF}(t)$ in a power series in $\exp(i\Delta_c t)$, i.e.

$$V_{AF}(t) = \sum_{-\infty}^{+\infty} V_n(t)e^{ni\Delta ct} \tag{3.11}$$

In this expression, because of the spectral narrowness of the factors $V_n(t)$, the term primarily contributing frequencies within the passbands of the modulation filters is $V_o(t)$. This term can be defined by averaging the expression for $V_{AF}(t)$ (Eq. (3.10)) over the phase of $\exp(i\Delta_c t)$, i.e.

$$V_o(t) = \frac{1}{2\pi}\int_0^{2\pi}\left[|A_1(t)|^2+|A_2(t)|^2+2Re(A_1A_2^*e^{-i\psi})\right]^{1/2}d\psi \tag{3.12}$$

This integral is easily transformed to:

$$V_o(t) = \left[2(|A_1(t)|+|A_2(t)|)/\pi\right] \int_0^{\pi/2} (1-k^2\sin^2\theta)^{1/2} d\theta, \quad (3.13)$$

where:

$$k^2 = 4|A_1(t)|\ |A_2(t)|/\left[|A_1(t)|+|A_2(t)|\right]^2$$

$$\theta = (\psi+\delta_{12})/2$$

$$e^{i\delta 12} = A_1A_2^*/|A_1A_2|$$

The integral on the right of Equation (3.13) is a complete elliptic integral of the second kind and is commonly denoted by E(k):

$$E(k) = \frac{\pi}{2}\left(1 - \sum_{n=1}^{\infty}\left[\frac{(2n)!}{(2^n n!)^2}\right]^2 \frac{k^{2n}}{2n-1}\right) \quad (3.14)$$

Thus for the purpose of determining the detected 90 and 150 Hz modulations, the unfiltered audio signal is to a good approximation

$$V_{AF}(t) \approx \frac{2}{\pi}(|A_1(t)|+|A_2(t)|)E(k) \quad (3.15)$$

To put the above expression in usable form, we must carry the approximation somewhat further. Let the magnitude of amplitude $A_1(t)$ be the sum of a constant average value a_{01} and a zero-mean time varying function $a_1(t)$:

$$|A_1(t)| = a_{01} + a_1(t) \quad (3.16a)$$

The quantity $a_1(t)$ represents the total modulation that would be detected if the second carrier were completely absent. Similarly, let

$$|A_2(t)| = a_{02} + a_2(t) \quad (3.16b)$$

Inserting Equations (3.16) into (3.15) and treating $a_1(t)$ and $a_2(t)$ as small quantities, we obtain an expansion for V_{AF}:

$$V_{AF}(t) = a_o \sum_{n=0}^{\infty}\sum_{p=0}^{n}\sum_{q=0}^{n}\sum_{r=0}^{\infty} \Gamma^n_{pqr} k_o^{2n} \left(\frac{a_1}{a_{01}}\right)^p \left(\frac{a_2}{a_{02}}\right)^q \left(\frac{a}{a_o}\right)^r \quad (3.17)$$

Here:

$$a_o = a_{01} + a_{02}$$

$$
\begin{aligned}
a(t) &= a_1(t) + a_2(t) \\
k_o^2 &= 4a_{01}a_{02}/a_o^2 \\
\Gamma^n_{pqr} &= 1 \quad ; n=0,\ r=0,1 \\
&= 0 \quad ; n=0,\ r\geq 2 \\
&= (-1)^{r+1} \frac{2n(2n)!(r+2n-2)!}{2^{4n}(n!)^2(n-p)!p!(n-q)!q!r!} \ ; \qquad (3.18)
\end{aligned}
$$

$n \geq 1$.

After rearrangement we find that the series begins thus:

$$
\begin{aligned}
V_{AF}(t) &= a_{01} + a_{02} + a_1(t) + a_2(t) \\
&+ \sum_{n=1}^{\infty} \Gamma^n_{000} k_0^{2n} \left[a_{01} + a_{02} + \left(1 - n\frac{a_{01}-a_{02}}{a_{01}}\right) a_1(t) \right. \\
&+ \left(1 - n\frac{a_{02}-a_{01}}{a_{02}}\right) a_2(t) \\
&+ \left(n(n-1)(a_{01}-a_{02})^2/2 - na_{01}a_{02} \right) \\
&\left. \cdot (a_1(t)/a_{01} - a_2(t)/a_{02})^2/a_0 \right] \qquad (3.19) \\
&+ 0(k_0^4 a^3) \\
&\approx (a_{01}+a_{02})(1 - a_{01}a_{02}/a_0^2 - \cdots \\
&+ a_1(t)(1 - a_{02}^2/a_0^2 - \cdots \\
&+ a_2(t)(1 - a_{01}^2/a_0^2 - \cdots \\
&+ \cdots
\end{aligned}
$$

Summing a finite number of the terms constant and linear in $a_1(t)$ and $a_2(t)$ gives an accurate representation of the audio signal $V_{AF}(t)$ when the parameter $k_0 \ll 1$. The convergence of the series as $k \to 1$ is not easy to discuss because the modulations of ILS transmissions are quite high (40% in the case of localizer signals, 80% for glide slope signals). It is suggested that the accuracy of the model in this range be checked by comparing calculated receiver characteristics with data given by Manney[4].

3.4 MULTIPATH EFFECTS AND FOURIER EXPANSIONS FOR CARRIER ENVELOPES

It remains to find suitable Fourier expansions for the separate carrier envelopes $|A_1(t)|$ and $|A_2(t)|$. In a manner similar to the treatment above of the capture effect, we will obtain series expansions for the Fourier coefficients of the desired solution. Again we will not rigorously resolve questions of convergence, but will rely ultimately on the agreement found between model predictions and known receiver characteristics. With this attitude, we consider the "static" audio signal that would be detected at a specified point in space by a stationary receiver.

It is useful to transform the expression for the typical complex amplitude given by Equation (3.9). Advantage is taken of the fact that each transmitted modulation waveform $u_{nm}(t)$ can be written as the sum of three Fourier components:

$$u_{nm}(t) = u_{nmo}\, f_o + u_{nm90}\, f_{90}(t) + u_{nm150}\, f_{150}(t) \qquad (3.20)$$

$$= \sum_{\ell=0}^{2} u_{nm\ell}\, f_\ell(t),$$

where, for example $f_\ell(t) \equiv f_{90}(t) = \cos(2\pi 90t+\delta_1)$, etc. Thus the complex amplitude for each carrier can be written

$$A(t) = \sum_{\ell=0}^{2} f_\ell(t)\, \alpha_\ell\, e^{i\theta_\ell}. \qquad (3.21)$$

Here

$$\alpha_\ell e^{i\theta_\ell} = \sum_{m,}\sum_{p} u_{nm\ell}\, a_{mp}\, e^{i\phi_p}. \qquad (3.22)$$

To develop the most convenient expansion for the modulus of the right hand side of Equation (3.21) we introduce an arbitrary phase constant ϕ. Since

$$|A| = |Ae^{-i\phi}|\ ,$$

$$|A(t)| = \left[\left(\Sigma f_\ell(t)\alpha_\ell \cos(\theta_\ell-\phi)\right)^2 + \left(\Sigma f_\ell(t)\alpha_\ell \sin(\theta_\ell-\phi)\right)^2\right]^{1/2} \qquad (3.23)$$

At any particular instant of time it is possible to eliminate one or other of the squared quantities within the bracket by the proper choice of ϕ. The square root can then be taken exactly. The result, however, will have a complicated time

dependence through the implicit dependence of ϕ on time. We shall assume that the choice $\phi=\theta_0$, the phase of the constant term of (3.21), makes the average value of the second squared term small; on this basis we will use the approximation:

$$|A(t)| \simeq \alpha_0 + \alpha_1\cos(\theta_1-\theta_0)f_1(t) + \alpha_2\cos(\theta_2-\theta_0)f_2(t). \tag{3.24}$$

The required phase of the constant amplitude term for each carrier frequency is given by

$$\theta_0 = \mathrm{Tan}^{-1}\left[\frac{\Sigma\Sigma u_{nmo}\ a_{mp}\ \sin\phi_p}{\Sigma\Sigma_{mp} u_{nmo}\ a_{mp}\ \cos\phi_p}\right] = \phi[n] \tag{3.25}$$

In comparing with the notation of the capture effect treatment (Eq. 3.16) and the definitions of the f_n, we have for each carrier

$$a_0 = \alpha_0$$

$$a_1(t) = \alpha_1\cos(\theta_1-\theta_0)\cos(2\pi 90t+\delta_{90}) + \alpha_2\cos(\theta_2-\theta_0)\cos(2\pi 150t+\delta_{150}). \tag{3.26}$$

3.5 DOPPLER EFFECTS

As a landing aircraft moves there are relative changes in the phases of the various multipath radiation components of the ILS signals received. The amplitudes of the 90 Hz and 150 Hz terms of the detected modulation thus vary with time, and accordingly, each tone acquires a frequency spread. Since the relative Doppler frequency between direct and scattered radiation can be as much as 120 Hz in some cases for typical landing approach speeds, the bandwidth of the modulation filters becomes important in determining receiver dynamic response. The effect envisioned here is that certain greatly Doppler shifted signal components may either be severely damped by one filter or unexpectedly passed by the other depending on the circumstances of receiver design, aircraft speed, etc. This is independent of the intentional RC damping that is always introduced into the cross pointer indicator circuits.

To evaluate the possible magnitudes of such phenomena, we consider a particularly simple model for the frequency response of each modulation filter. Though the characteristics of this filter may differ markedly from those of filters

in actual receivers, the model is adequate for studying the general effect of filter bandwidth on receiver rejection of ILS interference.

The two detected tones which emerge from the modulation filters were earlier denoted by $V_{90}(t)$ and $V_{150}(t)$ (Eq. (3.6)). We now define these more precisely: Let

$$V_{\substack{90\\(150)}}(t) = \int_0^\infty h_{\substack{90\\(150)}}(\tau)\, V_{AF}(t-\tau)\,d\tau \ , \tag{3.27}$$

where $h_f(\tau)$ is the impulse response function of a narrowband filter corresponding to center frequency f. Following Middleton[5], we represent the narrowband filter by the response function

$$h_f(\tau) = h_0(\tau)\cos(2\pi f\tau+\psi) \tag{3.28}$$

and we select as the particular "window function"

$$\begin{aligned} h_0(\tau) &= 2/T \quad 0<\tau<T \\ &= 0 \quad \text{otherwise.} \end{aligned} \tag{3.28a}$$

The output of such a filter when driven by a sinusoidal input $A\cos(2\pi f_\ell t+\delta_\ell)$ is approximately

$$V_f(t) \approx \frac{A}{2}\mathrm{sinc}\left[\pi(f-f_\ell)T\right]\cos\left[2\pi ft+\delta_\ell+\psi+2\pi(f_\ell-f)(t-T/2)\right] \tag{3.29}$$

whenever $f+f_\ell >> T^{-1}$. The reciprocal of the integration time T is the nominal filter bandwidth. The phase ψ is purely additive and so may be dropped without loss of generality.

To derive results pertaining to the ILS audio signal (Eq. 3.5) from Equation (3.29), we assume that the phase shifts of individual multipath components due to aircraft motion lead to sinusoidal time variations, and we will neglect the time variation of amplitude coefficients. To this end we may write Eq. (3.19) as

$$V_{AF}(t) = C_0(a_{01}+a_{02}) + C_1a_1(t) + C_2a_2(t) \tag{3.30}$$

where the C's can be defined in terms of slowly varying amplitudes that will be considered constant and the a's (as defined by Equations (3.22 and 3.26)) will contain typical terms such as:

$$u_{nm\ell}a_{mp}\cos(\phi_p-\theta_0)f_\ell(t) = \frac{1}{2}u_{nm\ell}a_{mp}(\cos(2\pi f_\ell t+\delta_\ell+\phi_p(t)-\theta_0(t)) + \cos(2\pi f_\ell t+\delta_\ell-\phi_p(t)+\theta_0(t))).$$

This form shows that for each multipath component the audio modulation frequencies are modified by sum and difference combinations with the relative Doppler frequency $d/dt(\phi_p-\theta_0)$. Considering all combinations of input modulation frequency f_ℓ and Doppler shift which may give net frequencies near the filter center frequencies f, we find the following significant terms in the filter outputs $V_f(t)$ (notation will be detailed below):

1. The average carrier level received by paths with large Doppler shifts gives rise to a contribution from each filter

$$C_0\sum_m\sum_p a_{mp}(u_{1m0}+u_{2m0})\,\mathrm{sinc}\left[(2\pi f-\dot{\phi}+\dot{\phi}_p)T/2\right]\cos(2\pi fT/2+\phi-\phi_p),$$

2. The modulation at one frequency modified by a moderate Doppler shift gives rise to a contribution in the output of the opposite frequency filter

$$\frac{1}{2}\sum_{n=1}^{2} C_n\sum_m\sum_p a_{mp}u_{nm\ell}\,\mathrm{sinc}\left[(2\pi\Delta f\mp\dot{\phi}_p\pm\dot{\phi})T/2\right] \cdot \cos\left[2\pi f_\ell t+\delta_\ell+2\pi\Delta fT/2\pm\phi_p\mp\phi\right]$$

Here Δf is $f-f_\ell$, and upper and lower signs refer to filter frequency f=90 Hz and 150 Hz respectively.

3. In the case of equal modulation and filter frequencies the output contribution is

$$\sum_{n=1}^{2} C_n\sum_m\sum_p a_{mp}u_{nm\ell}\,\mathrm{sinc}\left[(\dot{\phi}-\dot{\phi}_p)T/2\right]\cos(\phi-\phi_p)\cos(2\pi ft+\delta_\ell)$$

The total detected signal at each modulation frequency f is the sum of the contributions 1, 2, and 3. It may be noted that only the phase of 3 is well defined in relation to the phase of the transmitted modulation. This confronts us with the final problem of this development: we must calculate the rectified signal derived from each $V_f(t)$ which is passed directly to the cockpit panel instruments to generate the CDI display. A reasonable approximation can be reached by ignoring the relative phases of contributions 1, 2, and 3 and defining the final ILS signals as being the r.m.s. envelope of the $V_f(t)$ obtained above. We thus arrive at the final formula:

$$V_f = \Bigg[C_o^2 \sum_m \sum_p a_{mp}^2 \sum_{n=1}^{2} u_{nmo}^2 \left(\operatorname{sinc}\left[(2\pi f - \dot{\phi} + \dot{\phi}_p) T/2\right]\right)^2$$

$$+ \frac{1}{4} \sum_{n=1}^{2} C_n^2 \sum_m \sum_p a_{mp}^2 u_{nm\ell}^2 \Bigg|_{f_\ell \neq f} \cdot \left(\operatorname{sinc}\left[(2\pi(f - f_\ell) \mp \dot{\phi}_p \pm \dot{\phi}) T/2\right]\right)^2$$

$$+ \left(\sum_{n=1}^{2} C_n \sum_m \sum_p a_{mp} u_{nm\ell} \Bigg|_{f_\ell = f} \cdot \cos(\phi_p - \phi) \operatorname{sinc}\left[(\dot{\phi}_p - \dot{\phi}) T/2\right] \right)^2 \Bigg]^{1/2} \qquad (3.31)$$

Again the upper and lower signs refer to filter frequencies of 90 Hz and 150 Hz respectively. As a practical consideration, each of the terms of Equation (3.31) can be accumulated as the individual path attenuation factors a_{mp} are calculated, <u>except</u> for the coefficients C_o^2, C_n^2, and C_n, the reference phases $\phi(\equiv \phi[n])$ and Doppler frequencies $\dot{\phi}(\equiv \dot{\phi}[n])$. To facilitate this method of computation we adopt the approximation

$$\dot{\phi}[n] = 2\pi \frac{dR}{dt} / \lambda \quad , \qquad (3.32)$$

where R is the instantaneous range of the receiving aircraft to the transmitting antenna and λ is the carrier wavelength. The remaining notation of Equation (3.31) is explained in the following tabulation:

f = modulation filter frequency 90 Hz or 150 Hz.

f_ℓ = transmitted modulation frequency, ℓ=1 for 90 Hz, ℓ=2 for 150 Hz, ℓ=0 for constant or unmodulated carrier terms.

ϕ_p = phase delay of a particular transmission path p between transmitting element and receiving antenna.

$\dot{\phi}_p$ = time derivative of ϕ_p.

$\phi[n]$ = approximate phase of the aggregate of direct and reflected carrier amplitudes at the receiver relative to the transmitted carrier phase (defined by Eq. (3.25)). For course signal n=1 and for clearance signal n=2.

$\dot{\phi}[n]$ = estimated time derivative of the aggregate phase $\phi[n]$ (defined by Eq. (3.32)).

T = filter integration time, equal to reciprocal of filter bandwidth.

$u_{nm\ell}$ = carrier (ℓ=0) or sideband (ℓ=1,2) strength in the modulated transmission from a particular element or set of elements m of the course (n=1) or clearance (n=2) signal.

a_{mp} = relative amplitude of radiation from antenna element or array m reaching receiver by a more or less specifically identified path p.

$$C_o = \sum_{n=0}^{\infty} \Gamma^n_{ooo}\, k_o^{2n}$$

$$C_1 = \sum_{n=0}^{\infty} \Gamma^n_{ooo}\, k_o^{2n}\left(1 - n\,\frac{a_{01}-a_{02}}{a_{01}}\right)$$

$$C_2 = \sum_{n=0}^{\infty} \Gamma^n_{ooo}\, k_o^{2n}\left(1 - n\,\frac{a_{02}-a_{01}}{a_{02}}\right)$$

Γ^n_{ooo}, k_o^2 = special coefficients (defined in Eqs. (3.18)).

$$a_{on} = \sum_m \sum_p u_{nmo} a_{mp} \cos(\phi_p - \phi[n])$$

The quantities V_{150} and V_{90} determined by Equation (3.31) are inserted in Equation (3.7) to obtain the undamped CDI which would be generated by a moving ILS receiver. The "dynamic" CDI, which incorporates the effect of the RC damping circuit, may be derived from the undamped CDI by the usual numerical techniques, which are perfectly adequate. A minor error in the I.B.M. localizer code is that the calculated ILS data is generated in the order of a takeoff sequence rather than a landing approach; this causes a slight shift in the "dynamic" course bends.

REFERENCES

1. Stratton, J. A., "Electromagnetic Theory," McGraw Hill Book Co., New York, 1941.

2. Silver, S., "Microwave Antenna Theory and Design," Dover Publications, New York, 1965.

3. McFarland, R. H., Hill, D., and Luttermoser, D., "Earth Cover and Contour Effects," Technical Report RD-65-30 for the Federal Aviation Agency under Contract FA64WA-5060, Department of Electrical Engineering, Ohio University, Athens, Ohio, May, 1965, p. 46.

4. Manney, C., "A Study of Two Frequency Capture Effects on ILS Receivers," Final Report RD-69-12 for the Federal Aviation Administration under contract FA66WA-1556, Wilcox Company, Kansas City, Missouri, March, 1969.

5. Middleton, D., An Introduction to Statistical Communication Theory, McGraw Hill, New York, 1960, p.98.

6. IBM, Federal Systems Division, "Multipath and Diffraction Effects of Structures on Localizer Systems," FAA-RD-70-20, Final Report, August 1970.

7. Abramowitz, M., and Stegun, I. A., Editors, Handbook of Mathematical Functions, National Bureau of Standards, U.S. Dept. of Commerce, Washington, D.C., 1966, p. 360, eq. 9.1.21, and p. 484, eq. 11.3.20.

8. Redlich, R. W., "Theory of Localized Signal Disturbance by Reflection from a Cylindrical Fuselage," T. M. Number 6A, Department of Electrical Engineering, Ohio University, March 1970.

9. Redlich, R. W., and Gorman, J. T., "Disturbance of ILS Localizer Signals by Reflection from Large Hangers," IEEE Transaction on Aerospace and Electronic System, November 1969, pp. 1001-1002.

10. Redlich, R. W., and Gorman, J. T., "Computation of Localizer Signal Disturbance by Reflections from Large Aircraft on the Ground," T.M. Number 10, Department of Electrical Engineering, Ohio University, April 1971.

REFERENCES

11. Gorman, J. T., "The Effects of Scattering from a 747 Aircraft Fuselage and Tail Fin on the Operation of the Glide Path Portion of an Instrument Landing System," T.M. Number 19, Department of Electrical Engineering, Ohio University, May 1971.

12. Avionics Research Group, "Earth Cover and Contour Effects on Image Glide Paths - Phase III," Final Report Number RD-68-60, Department of Electrical Engineering, Ohio University, September 1968.

13. Avionics Research Group, "Earth Cover and Contour Effects on Image Glide Path - Phase II," Report Number RD-66-39, Department of Electrical Engineering, Ohio University, July 1966.

14. Avionics Research Group, "Earth Cover and Contour Effects on Image Glide Path," Report Number 65-30, Department of Electrical Engineering, Ohio University, May, 1965.

15. Jordan, E. C., Electromagnetic Waves and Radiating Systems, Prentice-Hall Inc., 1950, pp. 563-565.

APPENDIX A

SCATTERING FROM A VERTICAL TRIANGLE,
NEW FORMULATION

We use the current distribution method to calculate the scattered field for an infinitely conductive triangular surface. The scattered electric far field is (with ground reflections included)

$$E_s = \frac{i\omega\mu}{4\pi}\frac{e^{ikR_2}}{R_2}\hat{R}_2 \times \hat{R}_2 \times \vec{I} \tag{A.1}$$

where

$$\vec{I} = 8\left(\frac{\varepsilon}{\mu}\right)^{1/2}\hat{\eta}E_o f(\psi)\frac{e^{ikR_1}}{R_1}\int d\xi \int d\eta e^{iAn}\sin(m\xi)\sin(n\xi) \tag{A.2}$$

where $A = k(\cos\gamma - \sin\beta)$

$m = kz_2/R_2$

$n = kh/D_{pl}$

For a right triangle with the base on the ground and the vertex to the left the integration $d\xi$ is from 0 to $h\eta/B + h/2$ and $d\eta$ is from $-B/2$ to $+B/2$. The following result is obtained (Fig. A-1):*

$$\begin{aligned}\vec{E}_s = \frac{k}{2\pi}BE_o f(\psi)\frac{e^{ik(R_1+R_2)}}{R_2R_1}(\hat{R}_2 x\hat{k})\cos\beta \\ \Bigg\{ \frac{1}{(m-n)}\Bigg[e^{i(m-n)h/2}\,\mathrm{sinc}\Bigg[\frac{1}{2}(AB+\sigma(m-n)h)\Bigg] \\ - e^{-i(m-n)h/2}\mathrm{sinc}\Bigg[\frac{1}{2}(AB-\sigma(m-n)h)\Bigg]\Bigg] \\ + \frac{1}{(m+n)}\Bigg[-e^{i(m+n)h/2}\mathrm{sinc}\Bigg[\frac{1}{2}(AB+\sigma(m+n)h)\Bigg] \\ + e^{-i(m+n)h/2}\mathrm{sinc}\Bigg[\frac{1}{2}(AB-\sigma(m+n)h)\Bigg]\Bigg]\Bigg\}\end{aligned} \tag{A.3}$$

For the vertex to the left $\sigma=1$.

For the case of the vertex to the right the integration $d\xi$ is from 0 to $-h\eta/B + h/2$. The scattered electric field

---

*Note that the angles γ and β defined in Fig. A-1 and used here for convenience correspond to the angles $\pi/2-(\theta+\psi)$ and $\pi/2-(\gamma-\theta)$, respectively, used in Part 2 Sections 5 and 6 of this report.

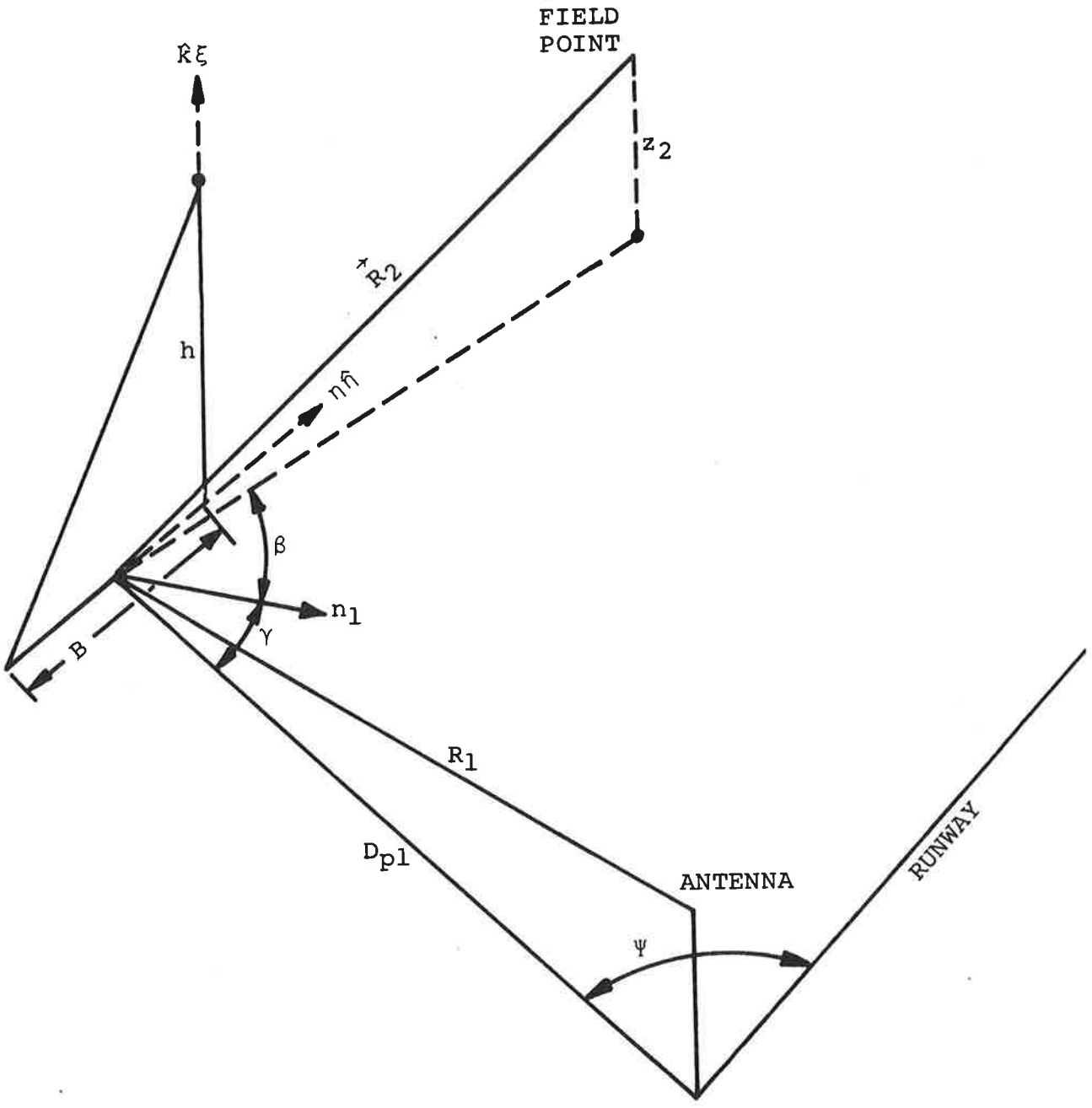

Figure A-1. Geometry for the Scattering from a Vertical Right Triangle

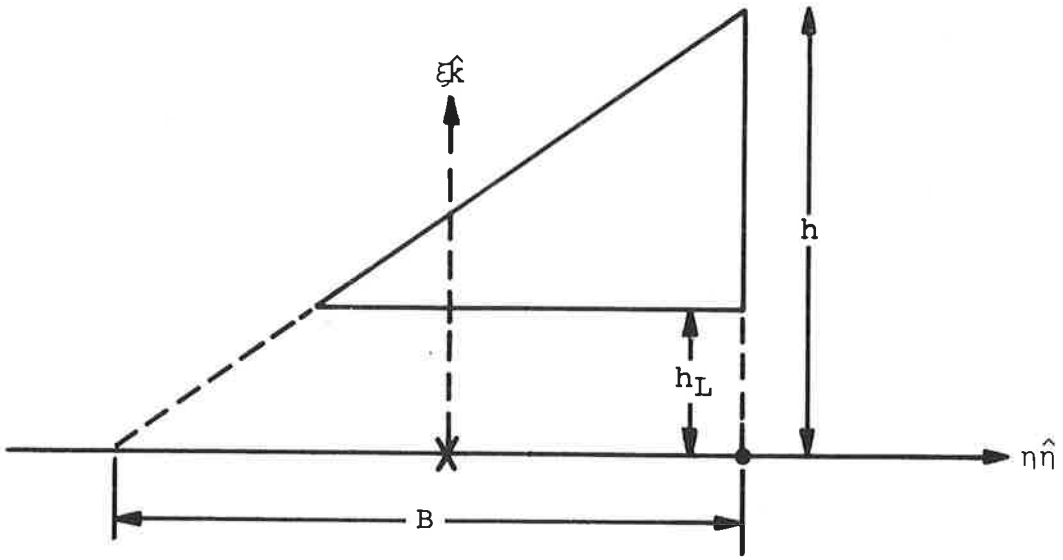

Figure A-2. Elevated Triangle

is given by Equation A.3 with $\sigma=-1$.

For the case of an elevated triangle (Fig. A-2) for the vertex to the left the integration $d\xi$ is from h_L to $h\eta/B + h/2$ and $d\eta$ is from $B(h_L/h - 1/2)$ to $B/2$. The result is then

$$\vec{E}_s = \frac{2k}{\pi} iE_o f(\psi) \frac{e^{ik(R_1+R_2)}}{R_2R_1} (\hat{R}_2 x \hat{k}) \cos\beta x I' \qquad (A.4)$$

where

$$I' = -\frac{1}{4}\left\{\frac{1}{(m-n)} \frac{e^{i(m-n)h/2}}{Y_1}\left[e^{iY_1B/2} - e^{iY_1BC}\right]\right.$$
$$- \frac{1}{(m-n)} \frac{e^{-i(m-n)h/2}}{Y_2}\left[e^{iY_2B/2} - e^{iY_2BC}\right]$$
$$- \frac{1}{(m+n)} \frac{e^{i(m+n)h/2}}{Y_3}\left[e^{iY_3B/2} - e^{iY_3BC}\right]$$
$$\left. + \frac{1}{(m+n)} \frac{e^{-i(m+n)h/2}}{Y_4}\left[e^{iY_4B/2} - e^{iY_4BC}\right]\right\}$$

$$+\left[-\frac{\sin(m-n)h_L}{2(m-n)}+\frac{\sin(m+n)h_L}{2(m+n)}\right]\frac{1}{iA}\left[e^{iAB/2}-e^{iABC}\right] \qquad (A.5)$$

where

$$\left.\begin{aligned} Y_1 &= A+\sigma(m-n)\frac{h}{B}\\ Y_2 &= A-\sigma(m-n)\frac{h}{B}\\ Y_3 &= A+\sigma(m+n)\frac{h}{B}\\ Y_4 &= A-\sigma(m+n)\frac{h}{B}\end{aligned}\right\} \qquad (A.6)$$

$$C = h_L/h - 1/2$$

For the vertex to the left $\sigma=1$.

For the case of the vertex to the right the integration $d\xi$ is from h_L to $-h\eta/B + h/2$ and $d\eta$ is from $-B/2$ to $B(-h_L/h + 1/2)$. The result is given by Equation A.4, with

$$\begin{aligned} I' = -\frac{1}{4}\Bigg\{ &\frac{1}{(m-n)}\frac{e^{i(m-n)h/2}}{Y_1}\left[e^{-iY_1BC}-e^{-iY_1B/2}\right]\\ &-\frac{1}{(m-n)}\frac{e^{-i(m-n)h/2}}{Y_2}\left[e^{-iY_2BC}-e^{-iY_2B/2}\right]\\ &-\frac{1}{(m+n)}\frac{e^{i(m+n)h/2}}{Y_3}\left[e^{-iY_3BC}-e^{-iY_3B/2}\right]\\ &+\frac{1}{(m+n)}\frac{e^{-i(m+n)h/2}}{Y_4}\left[e^{-iY_4BC}-e^{-iY_4B/2}\right]\Bigg\}\\ &+\left[-\frac{\sin(m-n)h_L}{2(m-n)}+\frac{\sin(m+n)h_L}{2(m+n)}\right]\frac{1}{iA}\left[e^{-iABC}-e^{-iAB/2}\right]\end{aligned} \qquad (A.7)$$

where Y_1, Y_2, Y_3 and Y_4 are given by Equation A.6 but with $\sigma=-1$. Note that Equation A.7 (with $\sigma=-1$) is just the complex conjugate of Equation A.5 with $\sigma=1$.

These are the new closed form solutions for scattering from triangular shapes that are to be incorporated into the computer program.

APPENDIX B

MULTIPLE SCATTERING FROM VERTICAL RECTANGULAR WALLS,
NEW FORMULATION

In this appendix we treat the multiple scattering of electromagnetic waves from a set of two vertical rectangular walls where infinite conductivity is assumed. In the double reflection study given by I.B.M.[6] only the reflected field was used in their equation (2.3). For reflection from a reflecting rectangular wall, the current distribution method yields the same result as given by I.B.M. if the total field is used instead of the reflected field and if the second line integral in the right side of their equation (2.3) is included. In the following calculation the current distribution method is used to obtain the new equations for double reflection.

The electric field at a point on the second wall is given by (Fig. B-1)*

$$E_p = i \frac{kL_1h_1E_of(\psi)}{\pi R_1R_2} \exp\left[ik(R_1+D_{p20}+\eta_2\sin\gamma_2)\right] \cdot \cos\beta_1 \left[\mathrm{sinc}\left[\frac{kL_1}{2}(\sin\gamma_1-\sin\beta_1)\right]\right] \cdot \left\{ \mathrm{sinc}\left[kh_1\left[\frac{H}{D_{p1}} - \frac{z_2}{R_2}\right]\right] - \mathrm{sinc}\left[kh_1\left[\frac{H}{D_{p1}} + \frac{z_2}{R_2}\right]\right]\right\} \quad (B.1)$$

where $\mathrm{sinc}(x) = \sin x/x$ and where $k = 2\pi/\lambda$

At the second wall the incident magnetic field is given by

$$\vec{H}_p \cong \sqrt{\varepsilon/\mu}\, E_p(-\hat{K}) \quad (B.2)$$

and the surface current on the wall is given by

$$\vec{J}_2 = 2\vec{H}_p x \hat{n}_2 \cong -2\sqrt{\varepsilon/\mu}\, E_p \hat{\eta}_2 \quad (B.3)$$

At the receiver the scattered field from the second wall is given by

$$\vec{E}_s = \frac{i\omega\mu}{4\pi} \frac{\exp[ikR_3]}{R_3} \hat{R}_3 x \hat{R}_3 x \int \vec{J}_2 \exp\left[-ik(\vec{\rho}\cdot\hat{R}_3)\right] d\eta_2 dz_2 \quad (B.4)$$

---

*Note that the angles γ_1 and β_1 defined in Fig. B-1 and used here for convenience correspond to the angles $\pi/2 - (\theta+\psi)$ and $\pi/2 - (\gamma-\theta)$, respectively, used in Sections 2.5 and 2.6.

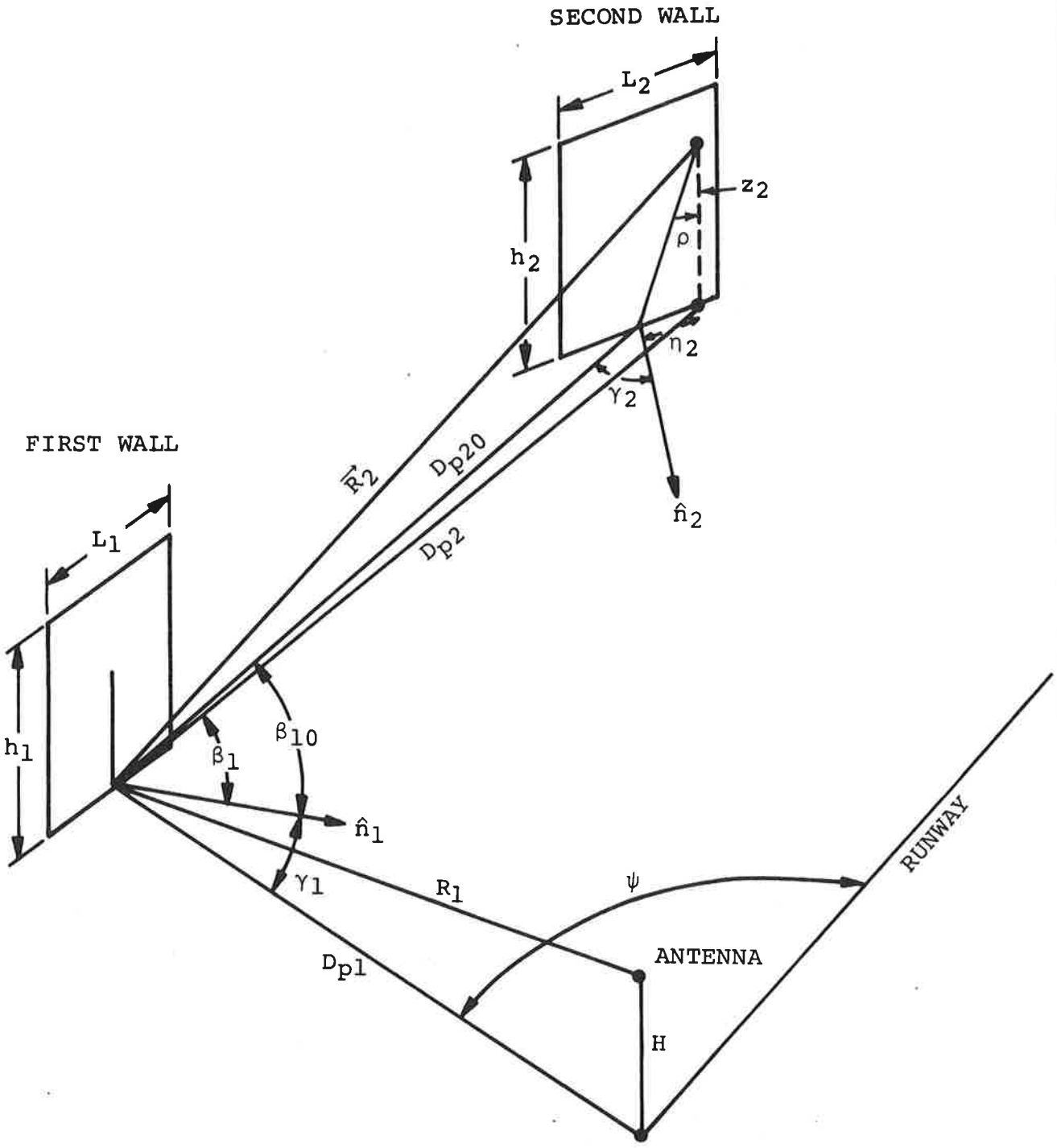

Figure B-1. Double Reflection from Rectangular Walls

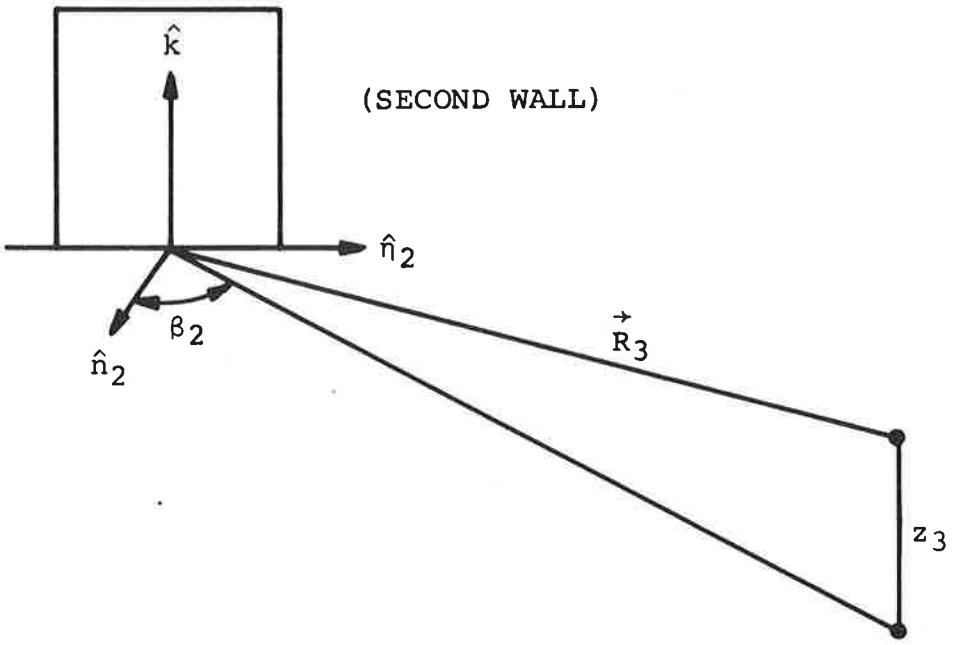

Figure B-2. Scattering from the Second Wall

where $\vec{\rho}\cdot\hat{R}_3 \cong \eta_2 \sin\beta_2 + z_2(z_3/R_3)$. (B.5)

Denoting the form with the integral by I we have

$$I = -2\sqrt{\varepsilon/\mu}\,\hat{\eta}_2 i\frac{kL_1h_1}{\pi}\,E_o f(\psi)\frac{\exp\left[ik(R_1+D_{p20})\right]}{R_1 D_{p20}} I_1 I_2 \qquad (B.6)$$

where (with ground reflection included)

$$I_1 \cong -2i\int_0^{h_2} \sin\left[kz_2(z_3/R_3)\right]\left\{\mathrm{sinc}\left(kh_1\left[\frac{H}{D_{p1}} - \frac{z_2}{D_{p2}}\right]\right)\right.$$

$$\left. - \mathrm{sinc}\left(kh_1\left[\frac{H}{D_{p1}} + \frac{z_2}{D_{p2}}\right]\right)\right\} dz_2 \qquad (B.7)$$

and where

$$I_2 = \int_{-L_2/2}^{L_2/2} \exp\left(ik\eta_2\left[\sin\gamma_2-\sin\beta_2\right]\right)\cos\beta_1\,\mathrm{sinc}\left[\frac{kL_1}{2}\left(\sin\gamma_1-\sin\beta_1\right)\right]d\eta_2$$

$$\cong \cos\beta_{10}\,\mathrm{sinc}\left[\frac{kL_1}{2}\left(\sin\gamma_1-\sin\beta_{10}\right)\right] L_2\,\mathrm{sinc}\left[\frac{L_2}{2}k\left(\sin\gamma_2-\sin\beta_2\right)\right] \tag{B.8}$$

The scattered electric field at the receiver from the second wall is then given by

$$\vec{E}_s \cong -i\vec{R}_3 x\hat{k}\,\frac{k^2}{\pi^2}L_1L_2h_1E_o f(\psi)\frac{\exp\left(ik\left[R_1+D_{p20}+R_3\right]\right)}{R_1D_{p20}R_3}\cos\beta_2$$

$$\cdot\ \cos\beta_{10}\,\mathrm{sinc}\left[\frac{L_2}{2}k(\sin\gamma_2-\sin\beta_2)\right]\mathrm{sinc}\left[\frac{L_1}{2}k(\sin\gamma_1-\sin\beta_{10})\right]$$

$$\cdot\left\{\frac{\sin(AC)}{2B}\left[\int_{C-h_2}^{C+h_2}\frac{\sin(A+B)x}{x}dx-\int_{C-h_2}^{C+h_2}\frac{\sin(A-B)x}{x}dx\right]\right.$$

$$\left.+\ \frac{\cos(AC)}{2B}\left[\int_{C-h_2}^{C+h_2}\frac{\cos(A+B)x}{x}dx-\int_{C-h_2}^{C+h_2}\frac{\cos(A-B)x}{x}dx\right]\right\} \tag{B.9}$$

where

$$A = kz_3/R_3, \qquad B = \frac{kh_1}{D_{p2}} \cong \frac{kh_1}{D_{p20}}, \qquad C = \frac{D_{p20}H}{D_{p1}} \tag{B.10}$$

and where

$$\int\frac{\sin ax}{x}dx = ax - \frac{(ax)^3}{3\cdot 3!} + \frac{(ax)^5}{5\cdot 5!} - \ldots \tag{B.11}$$

and

$$\int\frac{\cos ax}{x}dx = \log(ax) - \frac{(ax)^2}{2\cdot 2!} + \frac{(ax)^4}{4\cdot 4!} - \ldots \tag{B.12}$$

Combinations of reflections from walls with the lower edge flush against the ground plane can be used to compute the reflection from walls whose lower edges are at a height above the ground plane. The following figures show schematically such a procedure.

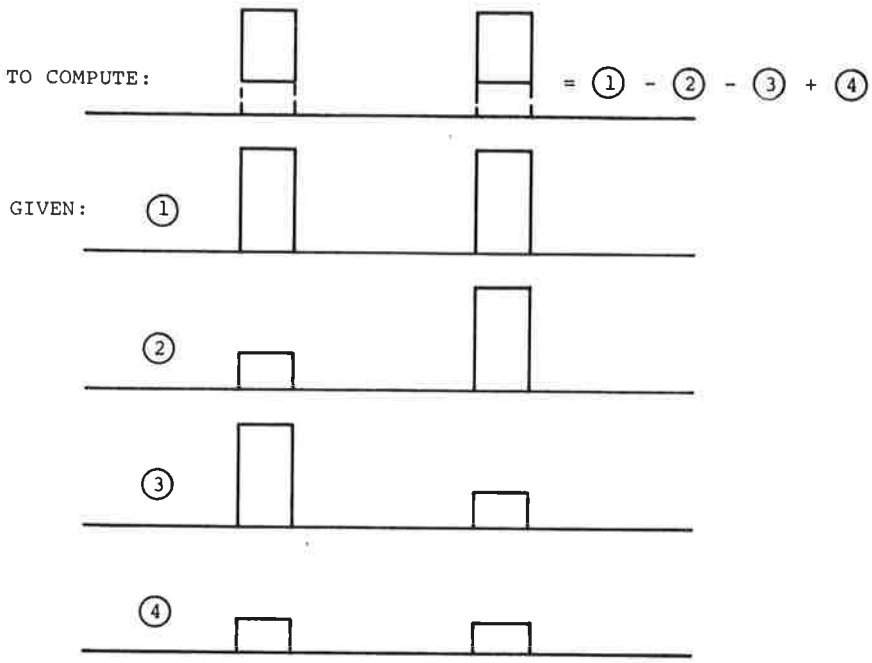

Figure B-3. Elevated Structures

SYMBOLS

R_1 from antenna to reference point on ground plane at 1st wall.

D_{p1} from foot of antenna to reference point at 1st wall.

$f(\psi)$ antenna gain factor.

h_1 height of 1st wall.

L_1 width of 1st wall.

γ_1 angle of incidence at 1st wall.

β_1 look angle from reference point on 1st wall to element of integration on 2nd wall.

β_{1o} look angle from reference point on 1st wall to reference point on 2nd wall.

$\hat{n}_1$ normal vector at 1st wall.

$\vec{R}_2$ vector from reference point on 1st wall to element of integration on 2nd wall.

D_{p20} reference point on 1st wall to reference point on 2nd wall.

D_{p2} reference point on 1st wall to fort of element of integration on 2nd wall.

L_2 width of 2nd wall.

h_2 height of 2nd wall.

$\hat{n}_2$ normal vector at 2nd wall.

$\hat{k}$ unit vector normal to ground plane.

k 2π divided by wavelength.

$\hat{\eta}_2$ unit vector along horizontal direction tangent to wall surface at 2nd wall.

$\vec{\rho}$ vector from reference point on 2nd wall to the element of integration

γ_2 angle of incidence at 2nd wall.

β_2 look angle from 2nd wall to receiver.

$\vec{R}_3$ vector from reference point on 2nd wall to aircraft receiver.

APPENDIX C

DERIVATION OF GAIN VECTOR FOR
SMALL CIRCULAR LOOP RECEIVING ANTENNA

We consider a linearly polarized plane wave given by $\vec{E} = \vec{E}_o e^{i(\vec{k}\cdot\vec{r}-\omega t)}$ incident on a perfectly conducting circular loop of radius a which is connected to a receiver input impedance Z_L (Fig. C-1). The current generated in the load impedance Z_L can be written as

$$I = V/(Z_L + Z_a), \tag{C.1}$$

where Z_a is the antenna radiation impedance and V is the net electromotive force (E.M.F. developed in the loop by the incident field). The E.M.F. is given by the following development of the basic line integral of E around the loop:

$$\begin{aligned} V &= \oint \vec{E} \cdot \vec{dl} \\ &= \iint dA\ \hat{n} \cdot \vec{\nabla}\times\vec{E} \\ &= i\vec{E}_o \cdot (\hat{n}\times\vec{k}) \iint r\ dr\ d\phi\ e^{i\vec{k}\cdot\vec{r}} \end{aligned} \tag{C.2}$$

Here the vector r lies in the plane of the loop and is perpendicular to the unit vector $\hat{n}$. We may replace the scalar product in the exponential by

$$\vec{k} \cdot \vec{r} = k\ r \sin\theta \cos\phi$$

with the result that the integral reduces to[7]

$$\begin{aligned} &\int_0^a r\ dr \int_{-\pi}^{\pi} d\phi\ e^{2kr \sin\theta \cos\phi} \\ &\qquad = 2\pi \int r\ dr\ J_o(kr\sin\theta) \\ &\qquad = 2\pi a^2\ J_1(ka \sin\theta)/(ka \sin\theta) \\ &\qquad \simeq \pi a^2 \end{aligned} \tag{C.3}$$

The latter approximation is valid whenever $a << \lambda/2\pi$. Using this result we find that the current delivered to the receiver can be expressed as

$$I = \frac{i\pi a^2 (\hat{n}\times\vec{k})\cdot\vec{E}_o}{Z_L + Z_a} \tag{C.4}$$

Thus the gain-polarization vector of Equation (C.1) takes the form

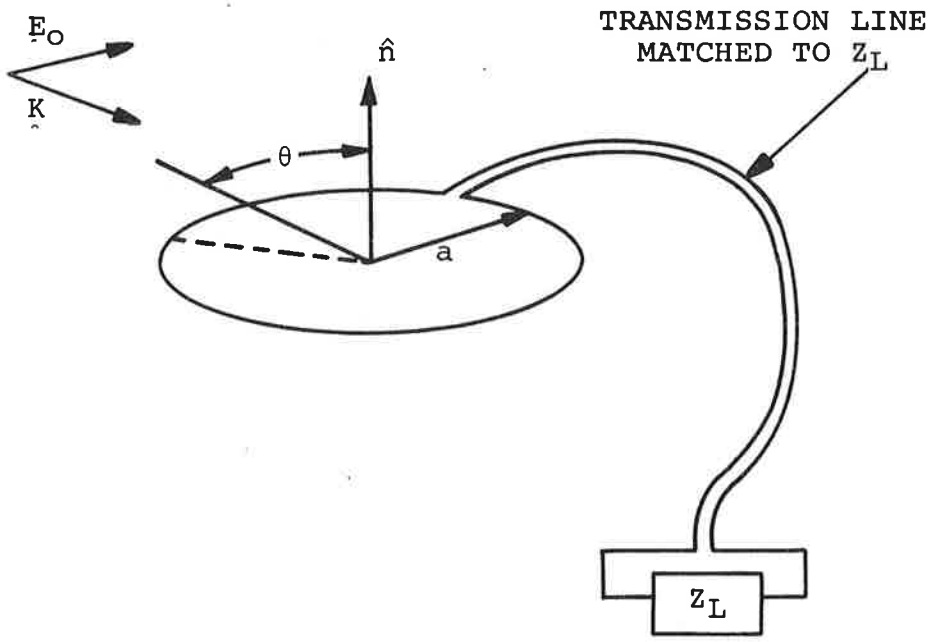

Figure C-1. Illustration of Circular Loop Receiving Antenna Problem

$$\vec{g}(\hat{k}) = C_a \hat{n} \times \hat{k} \qquad \text{(C.5)}$$

This vector selects the component of $\vec{E}$ normal to the vertical plane of incidence and applies a factor of $\sin\theta$.

APPENDIX D

INVESTIGATION OF DEPOLARIZATION
WITH A DIPOLE ANTENNA:

Calculation of the Polarization of the Electro-Magnetic Field Due to a Dipole Antenna with Inclusion of Image Reflection from an Infinitely Conducting Ground Plane

A horizontally polarized electric field vector will remain horizontally polarized when the observation point is restricted to lie on the vertical plane through the runway; however, whenever the field point is to the side of the runway, the electric vector develops a tilt, exhibiting a vertical as well as a horizontal component with a resultant depolarization.

Figure D-1 shows the geometric relationship for the e-m field radiated from the dipole antenna situated at a height H above the conductive ground plane. The axis of the dipole current is along the y direction while the runway is along the z direction. The electric vector at the field point F is perpendicular to the radial line r_1 and lies in the plane through F and the antenna, namely in the direction FO_1'.

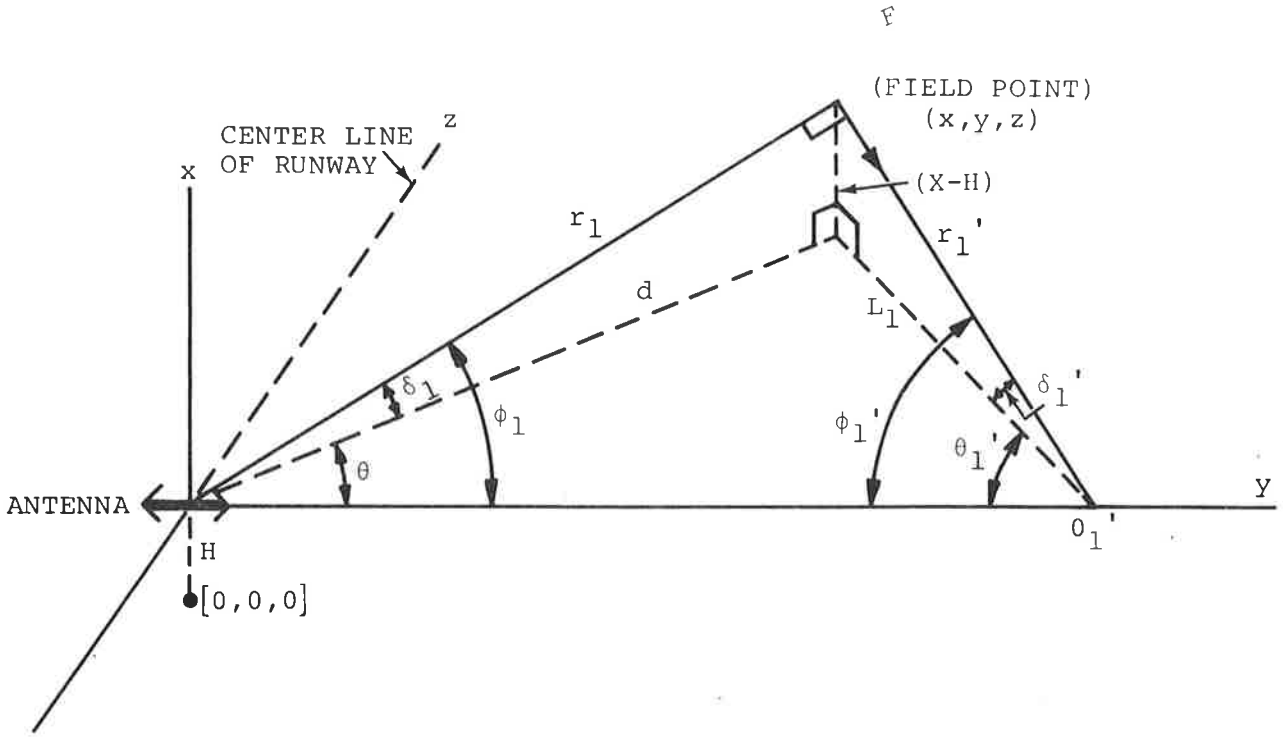

Figure D.1. Geometric Relationship for Radiation from Dipole Antenna which is at a Height H above the Ground Plane

Given δ_1, θ and d then ϕ_1 is determined by

$$\cos \phi_1 = \cos \delta_1 \cos \theta \tag{D.1}$$

When E_d is the magnitude of the direct electric field at F then the electric field vector $\vec{E}_d$ is given by

$$\vec{E}_d = E_d \left[-\sin\delta_1'\hat{x}+\cos\delta_1'\cos\theta_1'\hat{y}-\cos\delta_1'\sin\theta_1'\hat{z}\right] \tag{D.2}$$

The relations

$$\begin{aligned} r_1 &= \sqrt{d^2 + (X-H)^2} \\ r_1' &= r_1 \tan \phi_1 \\ L_1 &= \sqrt{r_1'^2 - (X-H)^2} \\ \cos \delta_1' &= L_1/r_1' \end{aligned} \tag{D.3}$$

can be used to calculate cos δ_1'. Also cos θ_1' can be calculated from the relation

$$\cos \theta_1' = \cos \phi_1' / \cos \delta_1' \tag{D.4}$$

where

$$\phi_1' = 90° - \phi_1 \tag{D.4}$$

Similarly the field from the antenna image can be obtained (Fig. D.2):

$$\vec{E}_{im} = E_{im} \left[-\sin\delta_2'\hat{x}+\cos\delta_2'\cos\theta_2'\hat{y}-\cos\delta_2'\sin\theta_2'\hat{z}\right] \tag{D.5}$$

The combined field may be written as

$$\begin{aligned} \vec{E} &= \frac{p(\phi_1)}{r_1} e^{-i\beta r_1} \hat{E}_d - \frac{p(\phi_2)}{r_2} e^{-i\beta r_2} \hat{E}_{im} \\ &\cong \frac{p(\phi)}{r} \left[e^{-i\beta r_1} \hat{E}_d - e^{-i\beta r_2} \hat{E}_{im}\right] \end{aligned} \tag{D.6}$$

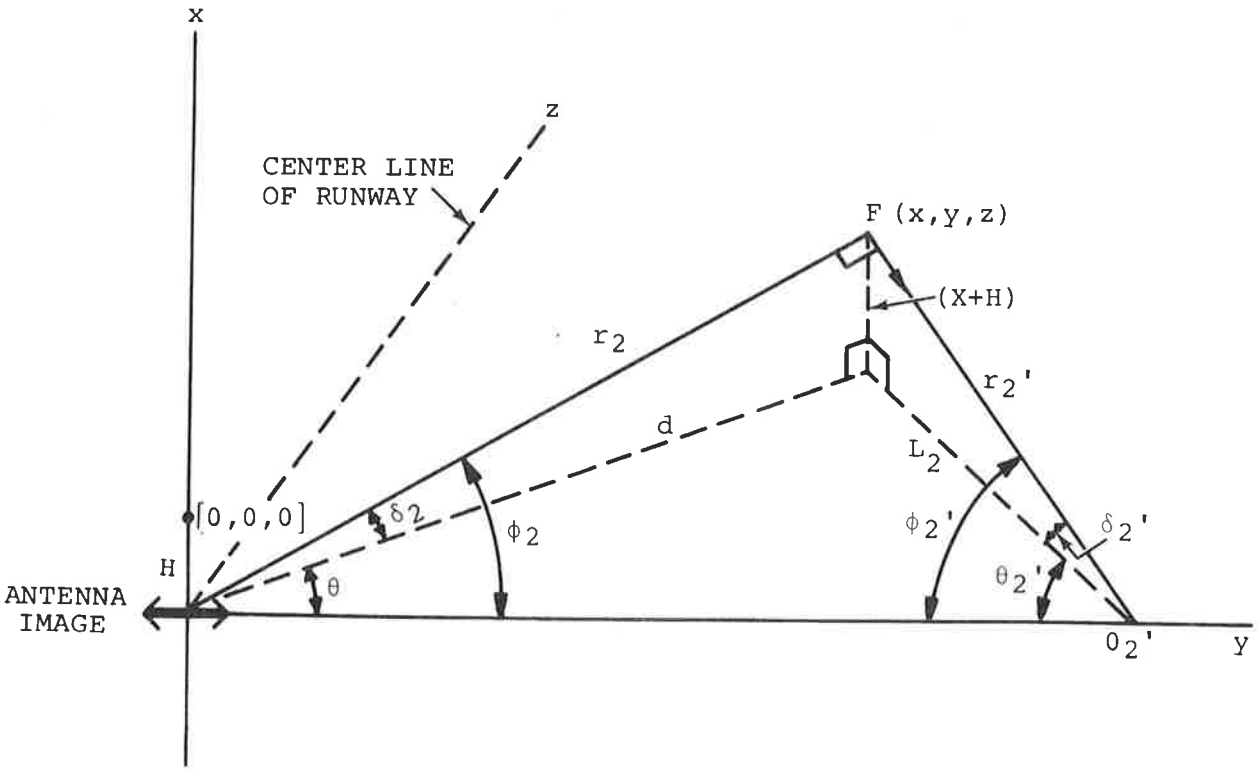

Figure D.2. Geometric Relationship for Radiation from Image

In making this approximation for the radiation field we may imagine that a fictitious antenna is located at the origin midway between the actual antenna and its image. Geometric relationships similar to those in Figures D.1 and D.2 would then yield the interpretation of the quantities: ϕ, δ, r, r', ϕ' etc. (Fig. D.3) as mean values.

Utilizing the previous expressions for $\vec{E}_d$ and $\vec{E}_{im}$ we have

$$\vec{E} = \frac{p}{r} e^{-i\beta(r+\frac{1}{2}H^2/r)}$$

$$\cdot\Big\{\hat{x}\left[-e^{i\beta HX/r}\sin\delta_1' + e^{-i\beta HX/r}\sin\delta_2'\right]$$

$$+ \hat{y}\left[e^{i\beta HX/r}\cos\delta_1'\cos\theta_1' - e^{-i\beta HX/r}\cos\delta_2'\cos\theta_2'\right]$$

$$+ \hat{z}\left[-e^{i\beta HX/r}\cos\delta_1'\sin\theta_1' + e^{-i\beta HX/r}\cos\delta_2'\sin\theta_2'\right] \tag{D.7}$$

Since $\sin\delta_1' = (X-H)/r_1'$, and $\sin\delta_2' = (X+H)/r_2'$, approximating r_1' and r_2' by r' we obtain for the perpendicular component of $\vec{E}$

$$E_\perp \cong \frac{p}{r} e^{-i\beta(r+\frac{1}{2}H^2/r)}$$

$$\cdot 2\left[-i(X/r')\sin(\beta HX/r) + (H/r')\cos(\beta HX/r)\right] \tag{D.8}$$

Likewise the other components of the electric field and the components of the magnetic field are obtained by a similar approximation. Using

$$\alpha_o = \frac{p(\phi)}{r} e^{-i\beta(r+\frac{1}{2}H^2/r)} \tag{D.9}$$

the result is:

$$\vec{E} \cong 2\alpha_o\Big\{\left[-i(X/r')\sin(\beta HX/r) + (H/r')\cos(\beta HX/r')\right]\hat{x}$$

$$+ i\cos\delta'\sin(\beta HX/r)\,\hat{U}_1\Big\} \tag{D.10}$$

where

$$\hat{U}_1 = \cos\theta'\,\hat{y} - \sin\theta'\,\hat{z}\,. \tag{D.11}$$

(Fig. D.3)

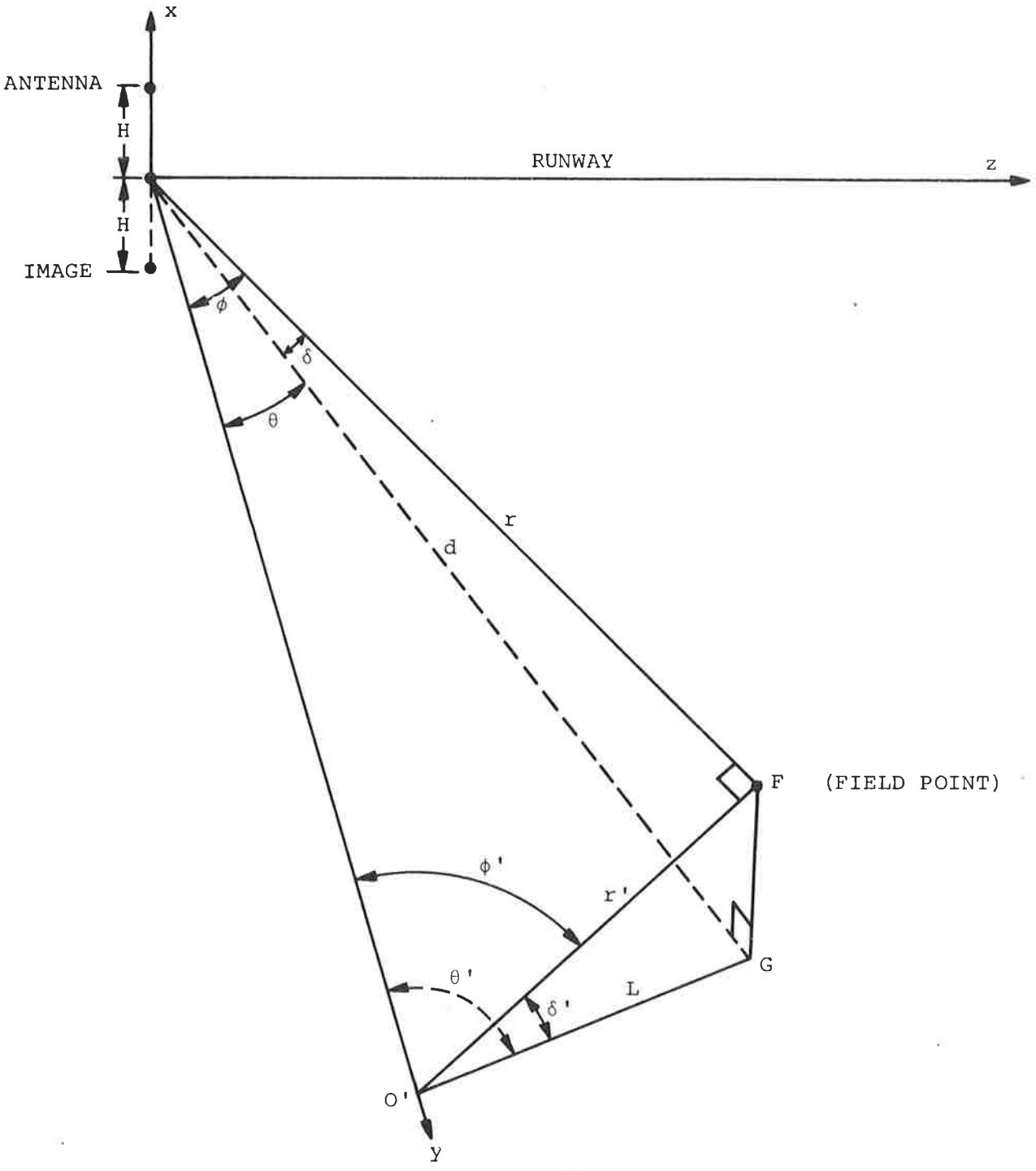

Figure D.3. Geometric Scheme for the Approximation of a Fictitious Antenna Located at Origin

The approximations of $\cos\delta_1'$ and $\cos\delta_2'$ by $\cos\delta'$ and $\cos\theta_1'$ and $\cos\theta_2'$ by $\cos\theta'$ were used in computing the previous expression, Equation D.10.

The magnetic field at the field point F can be calculated from the equation

$$\vec{H} = \frac{-\alpha_o}{\sqrt{\mu/\epsilon}} \left[e^{i\beta HX/r} (\hat{E}_d x \hat{r}_1) - e^{-i\beta HX/r} (\hat{E}_{im} x \hat{r}_2) \right] \qquad (D.12)$$

where

$$\hat{r}_1 = \sin\delta_1 \hat{x} + \cos\delta_1 \cos\theta_1 \hat{y} + \cos\delta_1 \sin\theta_1 \hat{z} \qquad (D.13)$$

and an analogous expression exists for $\hat{r}_2$. Carrying out the calculations and using the equations

$$\sin\delta_1' = \frac{X-H}{r_1'} \simeq \frac{X-H}{r'}$$

$$\text{and} \quad \sin\delta_2' = \frac{X+H}{r_2'} \simeq \frac{X+H}{r'}$$

$$\text{and} \quad \cos\delta_1 = \frac{d}{r_1} \simeq \frac{d}{r}$$

$$\cos\delta_2 = \frac{d}{r_2} \simeq \frac{d}{r} \qquad \text{etc.} \qquad (D.14)$$

we obtain

$$\vec{H} \cong \frac{2\alpha_o}{\sqrt{\mu/\epsilon}} \left\{ \left[-\cos\delta' \cos\delta \sin(\theta'+\theta)\, i \sin(\beta HX/r) \right] \hat{x} \right.$$
$$+\cos\delta \left[-i(X/r')\sin(\beta HX/r) + (H/r')\cos(\beta HX/r) \right] \hat{U}_2$$
$$\left. +\cos\delta' \left[i(X/r)\sin(\beta HX/r) - (H/r)\cos(\beta HX/r) \right] \hat{U}_L \right\} \qquad (D.15)$$

where

$$\hat{U}_2 = \sin\theta\ \hat{y} - \cos\theta\ \hat{z}$$

$$\hat{U}_L = \sin\theta'\hat{y} + \cos\theta'\hat{z} \qquad \text{(D.16)}$$

$\hat{U}_2 \cong \hat{U}_1$ is in the general direction from G to o' a horizontal transverse component; $\sin(\theta'+\theta) \cong 1$. $\hat{U}_L$ is approximately along the line d, that is, a horizontal longitudinal component.

These expressions for the electric and magnetic fields are now compared with those given by Ohio University[8]. The electric field obtained by Ohio University is

$$\vec{E} = \hat{U}_1 \frac{2pe^{-i\beta r}}{r}\left(i\frac{\beta HX}{r}\right), \qquad \text{(D.17)}$$

which corresponds to the transverse term in our Equation (D.10) though we do have an additional vertical component (Eq. (D.10). The magnetic field term given by Ohio University is

$$\vec{H} = \frac{2pe^{-i\beta r}}{\sqrt{\mu/\varepsilon}\ r}\left[\hat{x}\left(-i\beta\frac{HX}{r}\right) + \hat{U}_L\ \left(-\frac{H}{r}\right)\right] \qquad \text{(D.18)}$$

The vertical term is the same as that calculated in our Equation D.15, except for a factor $\cos\delta'\ \cos\delta$. The longitudinal term in Equation D.18 corresponds to the real part of the $\hat{U}_L$ term in our Equation D.15, but we have an additional imaginary part to this term. Also there is an additional complex horizontal component $\hat{U}_2$ in our Equation D.15.

In order to test the effect of these additional terms, numerical computation was made for the ratio of the vertical component to the horizontal component of the electric field for the following localizer geometric imputs:

H = 10' - antenna height

X = 100' - vertical distance of observation point

λ = 10' - wavelength

d = 1000' - horizontal distance to observation point

The following table gives the results for several values of the angle ϕ (between the antenna axis and the radius to the field point). (The antenna axis is perpendicular to the runway.)

TABLE D.1.

ϕ (DEG)	VERTICAL / HORIZONTAL
20	0.293
30	0.175
45	0.1
60	0.058
90	0

We also considered a set of possible numerical parameters for the case of the glide slope dipole antenna:

$H = 30'$

$X = 50'$

$\lambda = 3'$

$d = 500'$.

With the above inputs we calculated the ratio of the vertical component of the electric vector to the horizontal component as a function of the angle θ for both the field radiated from the antenna and that from the antenna image.* Our results are below:

TABLE D.2.

	VERTICAL / HORIZONTAL	
θ (DEG)	REAL ANTENNA	IMAGE ANTENNA
20	.11	.43
30	.07	.28
45	.04	.16
60	.02	.09

We see that a dipole localizer, (Table D.1), would lead to significant depolarization. For $\phi = 20°$ we see that the ratio of the vertical to horizontal component of electric field

*θ and ϕ are the angles as shown in Figure D.3.

reaches 30%, a non-negligible depolarization.

For a glide slope dipole, (Table D.2), we likewise see possibly significant depolarizations. For $\theta = 30°$. The ratio of the vertical to horizontal component of the electric field for the image antenna is 28%, again a non-negligible amount of depolarization.

Of course, for any real case, the actual antenna pattern must be used to determine the magnitude of the effect. What this analysis has shown, is that potentially serious depolarizations may occur with dipole antennas.

APPENDIX E

ADDITIONAL COMMENTS ON PREVIOUS ILS
MATH MODELLING WORK

INTRODUCTION

Our main critique of previous ILS mathematical models is contained in the body of this report as part of the analysis and development of an ILS scattering and signal detection model. Here we append several additional comments on previous ILS work which, collected in one section, should help highlight some additional limitations of the models.

LOCALIZER

Two localizer problems have been treated by Ohio University 1) the reflection from large hangers, and 2) reflection from large aircraft. Computer programs were written for these two cases to predict the course bending of the localizer signal (these computer programs, however, are not in as convenient a form as those of I.B.M.).

In deriving the scattered field from a hanger the following assumptions were made by Ohio University (as clearly stated by them)

1. Flat perfectly conducting terrain
2. Small elevation angles
3. The hanger wall as part of an infinite wall
4. Localizer field fully focused at hanger wall

With these assumptions, Ohio University derived the scattered field by calculating the current density distribution on the wall, as discussed previously in Section 2. The current density $\vec{J}$ is given by

$$\vec{J} = \hat{n} \times \vec{H} \qquad \text{(E.1)}$$

where $\hat{n}$ = unit vector normal to the wall

$\vec{H}$ = total magnetic field at the wall

= $\vec{H}_i + \vec{H}_r$ the vector sum of incident and reflected magnetic fields.

Their application of assumption (2) leads to course bending predictions which are independent of the height of the receiving aircraft. This assumption may yield erroneous results. For

example, from equations 1 and 3 (Ref.8) the factors $2\beta yd/r_1$ and $2\beta yh/r_2$ were evidently obtained by power series expansions of the exponential. The complete expression in fact would lead to the factors:

$$2 \sin(\beta yd/r_1) \text{ and } 2 \sin(\beta yh/r_2)$$

respectively, as shown in Section 2 Equation 2.71, and discussed in Section 2.6. The variation of derogation with receiver height which follows from retention of the complete sine functions has been confirmed in experimental data taken by IBM at NAFEC.

Another limitation of the Ohio University calculation is that a definition of DDM is used which is strictly valid only when the received direct and scattered carriers are in phase and the amplitude of the derogating component is relatively small. This was mentioned in Section 3 and it is perhaps worthwhile to discuss this in greater detail here.

The difficulty in properly treating DDM arises from a misconception about the meaning of "depth of modulalation" in the general case where carrier and sideband signals are combined with arbitrary relative phase. For a carefully adjusted antenna array, the transmitted carrier and sideband signals are always nearly perfectly "in phase" or "out of phase", i.e. the amplitude peaks of the unmodulated carrier occur simultaneously with peaks or minima of the sideband signal. For such a case, the maximum amplitude of the combined signal can be expressed as the sum of the average carrier amplitude and the peak sideband amplitude C+S, while the minimum is expressed by the difference C-S (assuming C > S). The depth of modulation can be given an obvious definition

$$\begin{aligned} DM &= 1/2(\text{Maximum}-\text{Minimum})/\text{Average} \\ &= S/C \end{aligned} \qquad \text{(E-2)}$$

and where modulations at 90 Hz and 150 Hz are being compared, the "difference in depth of modulation" is simply

$$DDM = (S_{150}-S_{90})/C \qquad \text{(E-3)}$$

In terms of the usual notation for the carrier signal modulation component E_c and the "sidebands only" amplitude E_s, we have for a null reference signal system

$$\begin{aligned} C &= E_c/m \\ m &= \text{modulation factor (= .2 for N.R. localizers)} \end{aligned}$$

$$S_{150} = E_c + E_s$$

$$S_{90} = E_c - E_s$$

$$DDM = 2m\, E_s/E_c\ , \qquad \text{(E-4)}$$

which is applicable when the total carrier and sideband signals are exactly in phase or out of phase.

However, for an aircraft exactly on the center of the glidepath any difference in amplitude of the 90 Hz and 150 Hz modulations comes from the scattered component of the radiation received. This component varies through all possible relative phases with the direct signal as the aircraft proceeds along its trajectory. In this situation a generalization of our above definition of depth of modulation is

$$DM = 1/2\ \big||C+S| - |C-S|\big|/|C| \qquad \text{(E-5)}$$

where now C and S are complex signal amplitudes with arbitrary relative phase. (This is not quite the operational definition implied by our analysis in Section 3, but it would lead to the same final approximate results.) For example, the DM value for 150 Hz modulation is

$$DM_{150} = 1/2\ \big|\,|E_c+m(E_c+E_s)| - |E_c-m(E_c+E_s)|\,\big|/|E_c|\ , \qquad \text{(E-6)}$$

while the value for 90 Hz is

$$DM_{90} = 1/2\ \big|\,|E_c+m(E_c-E_s)| - |E_c-m(E_c-E_s)|\,\big|/|E_c| \qquad \text{(E-7)}$$

Here E_c and E_s are complex sums of direct and scattered amplitudes, i.e.

$$E_c = E_{cd} + E_{cs}$$

$$E_s = E_{sd} + E_{ss} \qquad \text{(E-8)}$$

The difference DM_{150}-DM_{90} is an appropriate definition of DDM.

This difference is to be compared with

$$DDM_0 = m(|E_c+E_s| - |E_c-E_s|)/|E_c| \qquad \text{(E-9)}$$

which has been adopted by both IBM and Ohio. In order to further reduce the expression, Ohio makes the following assumptions:

1. $E_{cs} = 0$

2. $|E_c+E_{cs}+E_s+E_{ss}| = |E_c+E_{cs}| + |E_s+E_{ss}|$

3. $|E_s+E_{ss}| = |E_s| + |E_{ss}|$ (E-10)

which, in general, are not valid. Assumption 1 implies no scattered field from the carrier signal. Assumptions 2 and 3 imply that direct and scattered fields have identical phase, which is not true. By this stratagem they are able to obtain a relation for DDM equivalent to the "in phase" definition

$$DDM = 2m\ |E_s|/|E_c| \qquad \text{(E-11)}$$

TERRAIN (Refs. 12, 13, 14, 15)

In the past several years, derogation of the glide slope due to different terrain problems has been studied by the Ohio group. In calculating the reflected field from the ground, Ohio University considered an element of area of ground and related the reflected fields to both the electric and magnetic current sheets, $\vec{J}$ and $\vec{M}$ by

$$\vec{J} = \hat{n} \times \vec{H}_r$$

$$\vec{M} = -\hat{n} \times \vec{E}_r \qquad \text{(E-12)}$$

where $\vec{J}$ = electric current sheet

$\vec{M}$ = magnetic current sheet

$\hat{n}$ = unit vector normal to the surface

$\vec{H}_r$ = reflected magnetic field

$\vec{E}_r$ = reflected electric field.

The radiated fields at the observation point are thus determined by both the electric and the magnetic currents, with the reflected fields related to the incident fields by

$$H_r = R_h\ H_i$$

$$E_r = R_h\ E_i \qquad \text{(E-13)}$$

where R_h is the reflection coefficient.

The resultant scattered field at the observation point is the sum of the contributions from all elementary ground areas. Two major computer programs were written. One determines the Fresnel zone sizes providing the size of the elemental reflecting area for integration purposes while the other computes the DDM readings for the following types of terrain:

1. Flat terrain: Flat terrain extended beyond the first Fresnel zone. The computation time for this type of terrain is very short.

2. Limited flat terrain: The extent of the flat terrain falls short of the first Fresnel zone. Integration time is long.

3. Hillside: The terrain in front of the glide slope is non-flat.

There are two sub-groups:

1. Uniform terrain: The contour of the hillside runs perpendicular to the runway center line.

2. Non-uniform terrain: The contour of the hillside runs non-perpendicular to the runway center line.

Both 1 and 2 require long computer runs.

In general, it takes hours to compute the DDM whenever a fairly complex terrain exists. Additionally, verification of the program (Reference 12) has not been good. Much additional work is needed in developing a useful mathematical model of terrain scattering.

DIFFRACTION

Diffraction effects are best treated with Keller's geometrical theory of diffraction as I.B.M. has, in fact, done. However, a few cautionary remarks are in order.

Since diffraction effects to some degree are already taken into account in the iterative solution used for the scattered field, it is not clear that it is correct to simply add this field to the Keller field to obtain the correct total scattered field.

Further, a singularity appears in the asymptotic solutions of the Keller theory when applied to the transition between the illuminated and un-illuminated regions. The effects of this singularity on the validity of the solutions near the geometric

shadow must be investigated in order to determine the limits of validity of the solutions to the ILS scattering problem. This has yet to be done.

EXPERIMENTAL VERIFICATION

The math model computes the DDM on the centerline of the runway. However, experimentally, the DDM is obtained off the centerline. This is so because the pilot flies the DDM = 0 path which would coincide with the runway centerline only in the absence of derogation. Because of derogation, the DDM = 0 path is off the centerline of the runway.

In order to relate the math model's prediction of DDM over the centerline of the runway with experiment, a theodolite tracking is performed which gives the distance between the aircrafts actual path and the runway centerline. However, in order to make the comparison, the theodolite distance measurements must be related to the slope of the DDM, that is, to the variation of DDM with distance off the centerline. Since the DDM = 0 flight path which the pilot takes may often require excessive flight maneuvers, the resulting actual flight path either might not coincide with a DDM = 0 path or may make a valid determination of the slope impossible.

In order to compare theory and experiment, it would be better to obtain the DDM on the centerline directly. This can be done by flying directly over the centerline as guided by the theodolite. In this way, DDM readings from the aircraft's instruments could be compared directly with the math model's prediction of DDM over the runway centerline.